Cold sensitive engrams control whole-body thermoregulatory responses

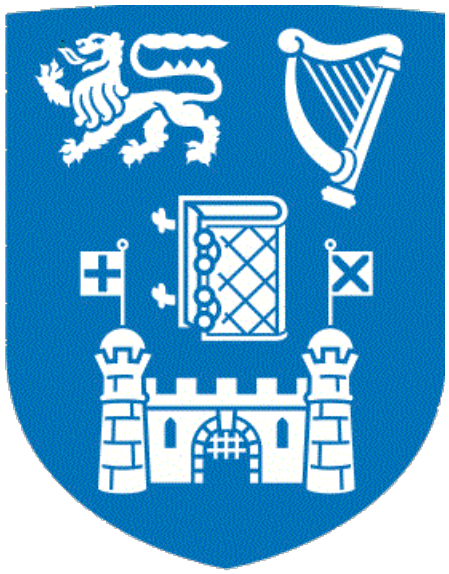

A dissertation submitted to Trinity College Dublin in candidature for the degree of Doctor of Philosophy

School of Biochemistry and Immunology
Trinity Biomedical Sciences Institute
Trinity College, Dublin

2024

By Andrea Muñoz Zamora

Under the supervision of Dr. Tomás Ryan

DECLARATION

I declare that this thesis has not been submitted as an exercise for a degree at this or any other university and it is entirely my own work unless otherwise stated in the figure legends.

I agree to deposit this thesis in the University's open access institutional repository or allow the library to do so on my behalf, subject to Irish Copyright Legislation and Trinity College Library conditions of use and acknowledgement.

I consent to the examiner retaining a copy of the thesis beyond the examining period, should they so wish (EU GDPR May 2018).

X

Andrea Muñoz Zamora

For mis abuelitos,
For my parents,
For Laura and Noa,
For Aaron,

I would not be me without you

ABSTRACT

Environmental thermal challenges trigger the brain to coordinate both autonomic and behavioral responses to maintain optimal body temperature. It is unknown how temperature information is precisely stored and retrieved in the brain, and how it is converted into a physiological response. Here, we investigated whether memories could control whole-body metabolism by training mice to remember a thermal challenge. Mice were conditioned to associate a context with a specific temperature, by combining thermoregulatory Pavlovian conditioning with engram labeling technology and optogenetics. We report that if mice are returned to an environment where they previously experienced a 4°C cold challenge, they increase their metabolic rates regardless of the actual environmental temperature. Additionally, we show increased hypothalamic activity when animals are exposed to the cold, and that a specific network emerges between the hippocampus and the hypothalamus during the recall of a cold memory. Moreover, both natural retrieval and artificial reactivation of cold-sensitive memory engrams in the hippocampus mimic the physiological responses that are seen during a cold-challenge. These results show that retrieval of a cold memory causes whole-body autonomic and behavioral responses that enable animals to maintain thermal homeostasis.

ACKNOWLEDGEMENTS

Four years ago, I arrived in Ireland, in the middle of a global pandemic to start my PhD. To put it mildly, starting your PhD in a pandemic is not ideal, and in the first few months there were many times that I contemplated leaving. Looking back at it now, I can honestly say that I am happy that I didn't. Although completing the PhD was challenging, I look back at this time as incredibly fulfilling and happy years, during which I got to meet some phenomenal people. It takes a village to raise a PhD student, and I have grown so much as a scientist and as a person thanks to the people around me.

First and foremost, I would like to thank my supervisor Tomás Ryan for giving me the opportunity to complete a PhD. You have always allowed me to freely explore my scientific interests, which led us to engrams and whole-body processes, something that neither of us expected. I also really appreciated that that you encouraged me to present my work at conferences in various amazing locations such as Bordeaux, Verona and Washington DC. Thank you for allowing me to be the unofficial Ryan lab party planner, we had some excellent dinners and celebrations together. Finally, I am thankful that at times you put up with my Dutch directness, as I often like to say things as they are.

To Clara, who has been my guiding light during this PhD. Clara, you are one of the most incredible scientists and humans I have met. If I had a problem (and I had many) you had the solution. I have learned so much from you, and I truly hope to be like you as a Postdoc in the future. Your efficiency is both amazing and hilarious to me, I don't think I will ever meet a speedy Gonzalez like you again. I cannot wait so see all the amazing thing you do with your own lab.

To Livia, who's positivity and voice notes cheered me up at all times. Having you to party with was an essential feature of my PhD. I especially cherish our time in Verona, where I felt like I was living an alternative live with my Italian sister. I loved our chats and laughs there, and in Dublin. I cannot wait to continue those in Paris and NYC in the coming years.

To Paul, for always being there with a dad joke when I needed some cheering up. Thank you so much for showing me around in Ireland and working on my Irish bucket list with me. Even though I at times could not understand what you were saying, you have always been patient with me. I am so happy that we got to share this PhD journey together since day one.

To Louisa, my office buddy since the day that she arrived. Thank you, Louisa, for always having time for a chat, even though I probably distracted you a lot. Thank you for reading papers with me, discussing experiments at crazy hours and most of all laughing with me in the office. I am excited to see where you end up going.

To James, who always had time to chat with me. Thank you, James, for always doing surgeries with me and having deep life conversations. Thank you for always being up for a party, a beer or even some dancing. You made me laugh a lot and made the PhD journey a lot more fun as a result.

To Esteban, my Mexican bestie. From day one we got on like a house on fire. Even though you don't like coriander or the sun, you are still a piece of home in the lab for me. Thank you for enduring all my bad jokes, for going to all the art exhibitions with me and being an amazing friend. I am excited for you to start as a PhD student and for you to follow your dreams.

To Erika, who has been an incredible friend. Thank you, Erika for listening to all me on all the good and bad days. This journey would have not been the same without you. Thank you for the endless coffee and food dates, the dancing at concerts and parties and the laughs we've shared. Thank you for making all my milestones so special whenever you could. I am so happy that I will be able to take you with me to NYC.

To Sebastian, Sofia and Michelle, my sweet NYC friends. Thank you for being incredible humans who have supported me at all times. I am so grateful for your friendship, the many phone calls we have had and the reunions that we planned. Meeting you all in NYC remains one of my biggest achievements, and I cannot wait to be back with you all.

To Danny, Bodil and Akira, my oldest and dearest friends. Thank you for being you and always having my back no matter where I go. Thank you for all the amazing conversations and the time that we spent together, you guys are truly special. I have grown to be the person that I am thanks to you.

To Mami, the strongest and most attentive woman I know. Thank you for always being there for me, for talking and texting with me daily and for all the sacrifices that you have made for me to be able to follow my dreams. Words cannot describe how important you are to me, how much I look up to you and how much I appreciate you.

To Papi, the most loyal and hardworking dad anyone could ever have. Thank you for simply being you. Your patience and kindness inspire me every day. I truly do not know what I would do without you. Thank you for always believing in me, helping me achieve my dreams and always having some great dad advice ready.

To Laura, my amazing sister. Thank you for being the funny, supportive and sweet little sister that you are. Thank you for making me get a tattoo with you and for always being up for anything I propose. You are one of the best parts of my life.

To Noa, my baby sister. Thank you for being the small miracle that you are. You're the light of my life, always cheer me up and above all make me feel so loved. I can't wait to see you conquer the world my tiny little boss.

To Aaron, the love of my life. Asking you out is by far the biggest achievement of my PhD. I adore everything about you. Thank you for being the most supportive, kind and patient partner I could have wished for. You are one of the most talented people I have ever met, and you inspire me every day. Thank you for making me laugh every single day, for listening to my endless chatting and for embracing all the Latin craziness that comes with me. I cannot wait for our next chapter together.

TABLE OF CONTENTS

LIST OF FIGURES

CHAPTER 1 INTRODUCTION

CHAPTER 1 RESULTS

CHAPTER 2 INTRODUCTION

CHAPTER 2 RESULTS

PUBLICATIONS

Cold sensitive engrams control whole-body thermoregulatory responses.

Andrea Muñoz Zamora, Aaron Douglas, Esteban Urrieta, Paul B. Conway, Taylor Moniz, James D. O'Leary, Lydia Marks, Clara Ortega-de San Luis, Christine A. Denny, Lydia Lynch and Tomás J. Ryan.

Nature, in review. Submitted February 2024.

Extinction and reinstatement of a looming stimulus fear response, replaces a midbrain-dependent circuit with a hippocampus-dependent circuit.

Coauthor, in preparation.

ABBREVIATIONS

CNS	Central nervous system
PNS	Peripheral nervous system
MDD	Major depressive disorder
DRG	Dorsal root ganglia
VTA	Ventral tegmental area
PTSD	Post-traumatic stress disorder
BAT	Brown adipose tissue
VO_2	Oxygen consumption
CO_2	Carbon dioxide production
EE	Energy expenditure
CS	Conditioned stimulus
US	Unconditioned stimulus
UR	Unconditioned response
CPP	Conditioned place preference
SEM	Standard errors of the mean
BL2	Baseline day 2
IEG	Immediate early gene
PKA	Protein kinase A
CaMKII	Ca^{2+}/CaM-dependent protein kinase II
RTF	Regulatory transcription factor
DG	Dentate gyrus
CA3	*Cornu ammonis* 3
CA1	*Cornu ammonis* 1
POA	Preoptic area
DMH	Dorsomedial hypothalamus
rRPA	Rostral raphe pallidus
LHA	Lateral hypothalamus
PFA	Paraformaldehyde
PBS	Phosphate buffered saline
PBST	PBS with TritonX-100
DMSO	Dimethyl sulfoxide
NGS	Normal goat serum

PTwH	PBS with 0.2% Tween-20 and 10 μg/ml heparin
CL1	Cold training day 1
T1	Test day 1
MPO	Medial preoptic area
LPO	Lateral preoptic area
PVi	Periventricular hypothalamic nucleus
ARH	Arcuate hypothalamic nucleus
VMH	Ventromedial hypothalamic nucleus
AI	Agranular insular cortex
SSp	Primary somatosensory cortex
BST	Bed nucleus of the stria terminalis
CeA	Central amygdalar nucleus
BLA	Basolateral amygdalar nucleus
BMA	Basomedial amygdalar nucleus
ChR2	Channelrhodopsin 2
RSC	Retrosplenial cortex
Dox	Doxycycline
tTa	Tetracycline transactivator
TRE	Tetracycline response element
RAM	Robust Activity Marker
4-OHT	4-Hydroxytamoxifen
PRAM	Promoter Robust Activity Marker
eYFP	Enhanced yellow fluorescent protein
NpHR	Halorhodopsin
CNO	Clozapine N-oxide
DV	Dorsoventral
AP	Anteroposterior
ML	Mediolateral
WAT	White adipose tissue
AR-β3	β3-adrenergic receptor
cAMP	Cyclic adenosine monophosphate
ATGL	Adipose triglyceride lipase
HSL	Hormone sensitive lipase

FFA	Free fatty acids
CPT1	Carnitine palmitoyltransferase 1
UCP-1	Uncoupling protein-1
ETC	Electron transport chain
ATP	Adenosine triphosphate
T_{BAT}	Temperature of interscapular BAT
IL6	Interleukin-6
TMT	Trimethylthiazoline
DREAD	Designer Receptors Exclusively Activated by Designer Drugs

General Introduction

The field of neuroscience has traditionally focused on investigating the central nervous system (CNS) in health and disease. Interactionism, the theory that the mind and body are two distinct independent systems that interact with one another, is a philosophical theory that was coined in the seventeenth century by Descartes. However, only recently have scientists started to investigate how the CNS directly interacts with the peripheral nervous system (PNS) in a bidirectional manner. Indeed, there has been a growing understanding that psychological states can have an impact on physiological processes in the body, and that somatic states can in turn influence the CNS, and as a result, the organisms behavior. One example of how mental state can influence bodily functions is the impact of stress on biological mechanisms and overall health. Psychological stress has been extensively shown to have a negative effect on blood pressure, heart rate, and overall longevity [1]. Moreover, stress-related disorders such as major depressive disorder (MDD) have been reported to have a high comorbidity with immune and inflammatory conditions [2-4]. For instance, a recent study found elevated expression of a circulating myeloid cell-specific proteinase in the serum of depressed humans and mice, suggesting increased interactions between immune cells and the brain during depressive episodes [5].

Pain, a mental state that is physically experienced and that involves neuroimmune crosstalk in the skin and dorsal root ganglia (DRG), is another example of how the body and brain interact. A recent study showed that the brain is able to encode pain-state-specific immune responses in the spleen, suggesting that the brain is able to control immunity in response to distinct pain states [6]. Several additional studies have now also linked the brain with immune responses in healthy and diseased states [7-9]. For example, Kayama and colleagues showed that there is a direct link between dopaminergic phasic firing in the ventral tegmental area (VTA) and peripheral immunity [9]. Interestingly, the VTA has also been shown to modulate anti-tumor immune responses, as chemogenetic activation of this area resulted in reduced tumor growth, suggesting that this area could be a promising target for cancer therapy [7]. In general, this growing body of research has unequivocally shown that mental state can affect physiological function, and that specific neurons in the brain can influence immune responses.

Most recent brain-body studies show that top-down signaling from the brain can alter responses in the periphery. However, growing evidence now suggests a reciprocal signaling pathway, with bottom-up physiological processes from the periphery affecting brain function, with knock-on effects in organismal behavior. Prolonged or severe immune activation during neurodevelopmental has been shown to increase the risk of developing psychiatric illnesses such as depression, schizophrenia and autism spectrum disorder [10]. Moreover, physiological theories from over a century ago proposed that there could be a dominant flow of information from the body to the brain that has a direct influence on emotional state [11]. This theory has been validated by a recent study, where optically induced tachycardia increased anxiety-like behavior in mice [12]. Interestingly, the increase in anxiety-like behavior was only seen in risky contexts, indicating that both central and peripheral processes are necessary in the generation of emotional states.

A big question that remains in the body-brain field is how memories interact with peripheral physiological processes. Memories play an essential role in mental state and adaptive behavior, yet it remains unclear whether memories also have a direct influence on peripheral function. For example, patients that are diagnosed with post-traumatic stress disorder (PTSD) re-experience traumatic life events in the form of memory flashbacks that are accompanied with physical sensations such as pain, smell, and taste. As such, remembering a traumatic event triggers the bodily sensations that were experienced during the original event. Clinicians have additionally argued that certain mental health problems could be driven by bodily experiences that are stored in the form of memories [13]. Therefore, understanding the mechanisms behind the storage and retrieval of memories associated with bodily experiences might provide insight into how memories impact physiology in health and disease.

Previous studies have demonstrated that memories are stored in the brain in the form of engram cells. Engram cells can be operationally defined as neuronal ensembles that are activated by learning, undergo physical changes, and whose reactivation leads to the retrieval of the target memory [14-17]. By leveraging engram labelling technology, we aimed to investigate whether memories control whole-body responses. To do so, we focused on thermoregulation, a behavior that relies on various behavioral

and physiological components. Our goal was to label a memory of a cold-context with engram labelling technology and determine whether cold-engrams control whole-body responses. Here, we show that there are cold-sensitive memory engrams in the hippocampus and specific regions of the hypothalamus, and that both natural retrieval and artificial reactivation of these engrams mimic the physiological responses that are seen during a cold-challenge. These results highlight that cold-sensitive engrams control whole-body autonomic and behavioral responses that enable animals to maintain thermal homeostasis.

The following chapters will aim to demonstrate that:

1. A cold-paired contextual memory increases metabolic rate and causes avoidance behavior.
2. Retrieval of a contextual cold memory increases neural activity in the hippocampus and hypothalamus.
3. Cold-sensitive memory ensembles are located in the DG, LHA, and MPO, which correlate with metabolic rate.
4. Artificially manipulating cold engrams alters whole-body metabolism.
5. Natural and artificial reactivation of cold memories upregulates thermogenesis genes in brown adipose tissue.

Chapter 1:

A cold-paired contextual memory increases metabolic rate and causes avoidance behavior.

INTRODUCTION

1.1.1 Behavioral and physiological thermoregulation.

One of the most crucial functions of the nervous system is the regulation of body temperature, known as thermoregulation, which is observed across the animal kingdom from behavioral changes in reptiles to autonomic shivering in mammals. Homeothermy is defined as the ability of organisms to maintain their body temperature within a narrow range. Homeothermy, and therefore thermoregulation, are necessary for critical cellular function and survival [18, 19]. When animals are exposed to an environmental thermal challenge, the brain will trigger several thermoregulatory responses to preserve homeostatic body temperature. As a result, animals are able to maintain a constant body temperature of approximately 37°C, despite changes in their external environment (Figure 1.1.1) [20-22].

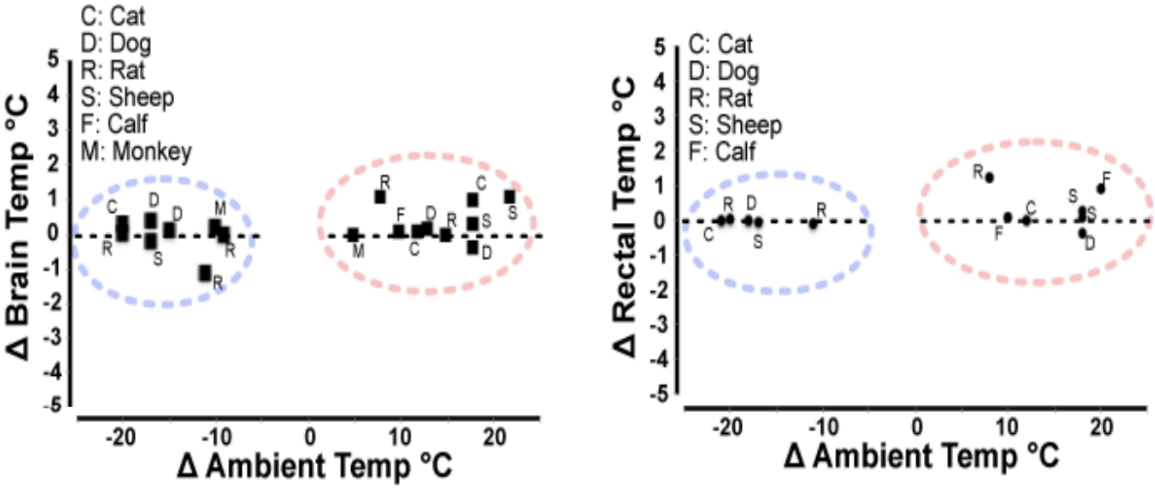

Figure 1.1.1 Core temperature during environmental challenges. Changes in brain (left) or rectal (right) temperatures are small during temperature challenges in a variety of mammals. *Adapted from Tan & Knight, 2018 [20].*

The responses that are triggered by the brain can be subdivided into motivated, goal-directed behavioral responses, and autonomic physiological mechanisms (Figure 1.1.2). Some of the most basic behavioral responses are cold and warm- seeking behaviors, where animals move from one microenvironment to another within their habitat. Various studies have shown that when given the choice, mice prefer to spend more time in a warmer environment compared to a colder one [23, 24]. Moreover, mice that are trained on a self-heating operant task, where a nose poke turns on a heat

lamp, will increase the amount of nose pokes in colder environments [23, 25]. More complex thermoregulatory behaviors include nest building, and social behaviors such as huddling, which are conscious, and goal orientated behaviors with the ultimate aim of decreasing the difference in temperature between the animal and the environment, in order to reduce the temperature gradient between internal and external components [26]. Eventually, this strategy results in limited metabolic costs in adult individuals.

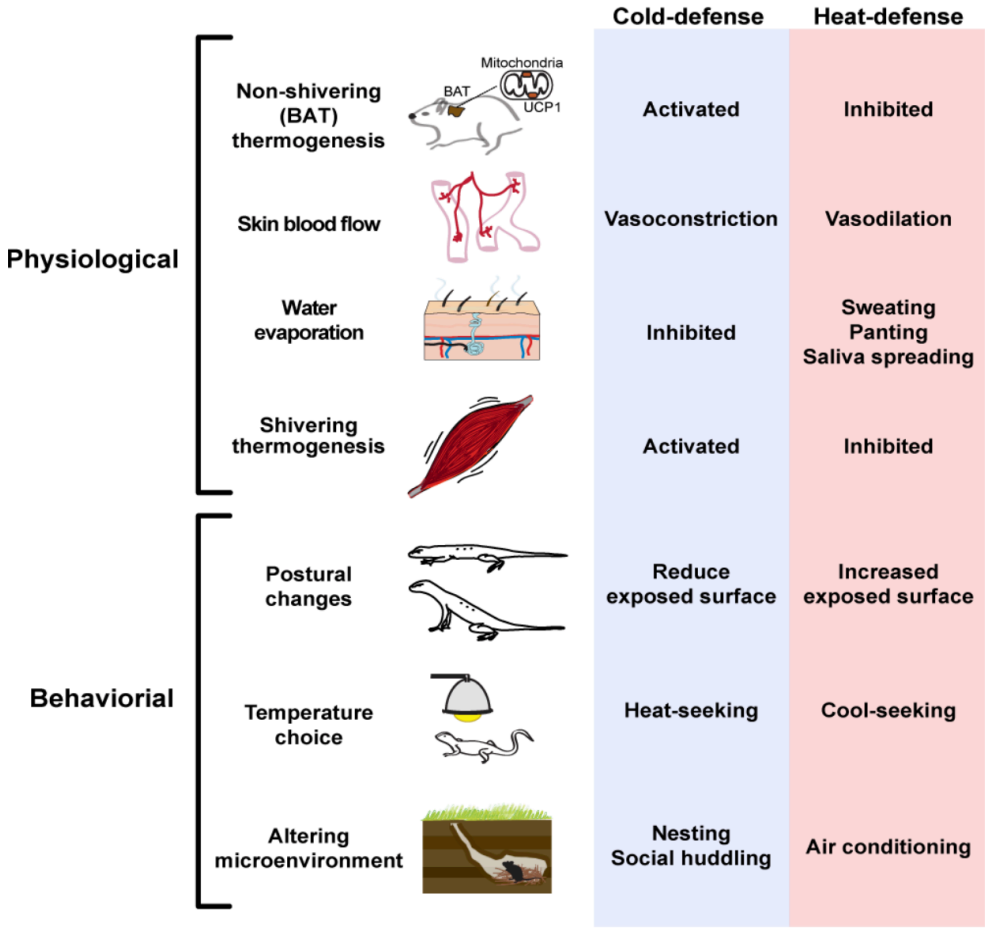

Figure 1.1.2 Types of thermoregulatory responses. Examples of the different physiological and behavioral responses used to maintain body temperature. *Adapted from Tan & Knight, 2018 [20].*

Thermoregulatory mechanisms are thought to be hierarchical, with different mechanisms being activated at different temperature thresholds. Typically, behavioral responses will precede physiological responses, as they generally are more cost-effective in terms of energy. Automated physiological responses are also thought to be activated in a specific order. For example, cold challenges will trigger vasoconstriction, before shivering and non-shivering thermogenesis [20]. Shivering thermogenesis in

skeletal muscles is used to produce heat through the contractile ability of myocytes, whereas non-shivering thermogenesis is a neuronal regulated metabolic process that contributes to the production of heat and the maintenance of core body temperature, and is largely influenced by altered metabolism in brown adipose tissue (BAT) [27, 28]. BAT thermogenesis is seen as an essential component of the homeostatic repertoire to maintain body temperature when animals are exposed to a cold environment. Taken together, these mechanisms ensure that animals maintain a constant body temperature in order to sustain crucial cellular processes.

1.1.2 Whole-body metabolism during cold challenges.

Animals that are exposed to a cold environment will maintain their heat through thermogenesis. Thermogenesis is a metabolically costly process, which is reflected in an increase in metabolic rates such as oxygen consumption (VO_2), carbon dioxide emission (CO_2) and energy expenditure (EE). Indeed, there is a direct inverse correlation between metabolic rate and environmental temperature. Mice incrementally increase the amount of oxygen they consume during cold adaptation, as the temperature decreases from 28°C to 4°C (Figure 1.1.3)[29].

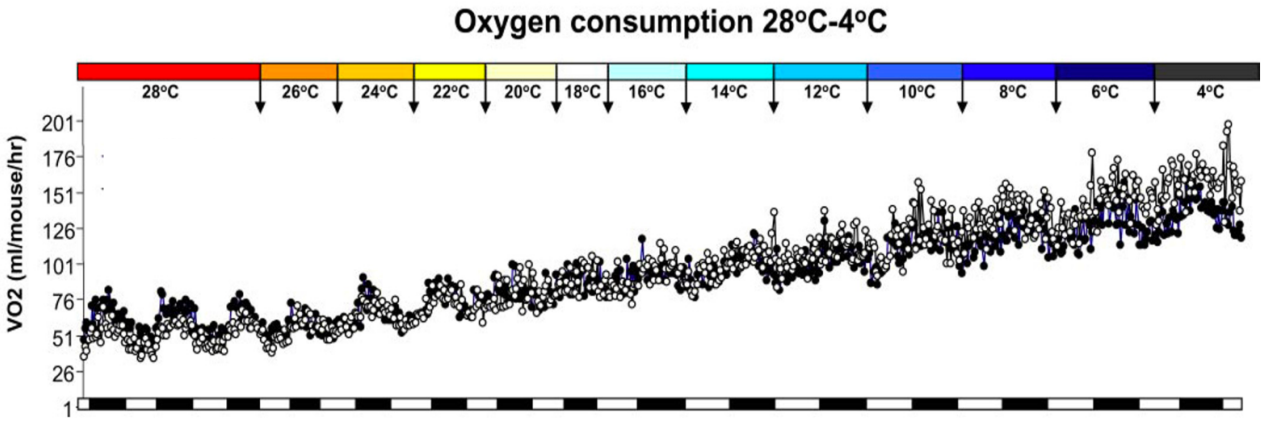

Figure 1.1.3 Metabolic rate during cold adaptation. Oxygen consumption increases incrementally with decreasing temperatures. *Adapted from Ukropec et al., 2006 [29].*

Similar increases have been found for EE, where the variation in EE could largely be attributed to temperature changes, and not to fat mass, sex or physical activity [30]. Moreover, the inverse correlation between metabolic rate and temperature has been reported in mice, in addition to humans [31]. In cold environments, animals will additionally increase their food consumption and physical activity [29, 32]. These

behavioral and cellular adaptions are directed at releasing cellular energy that is necessary for adaptive thermogenesis. In summary, decreasing environmental temperatures will increase metabolic rates in animals to fuel physiological responses such as shivering and non-shivering thermogenesis (Figure 1.1.4), which will in turn enable animals to maintain their body temperature at a constant temperature [33, 34].

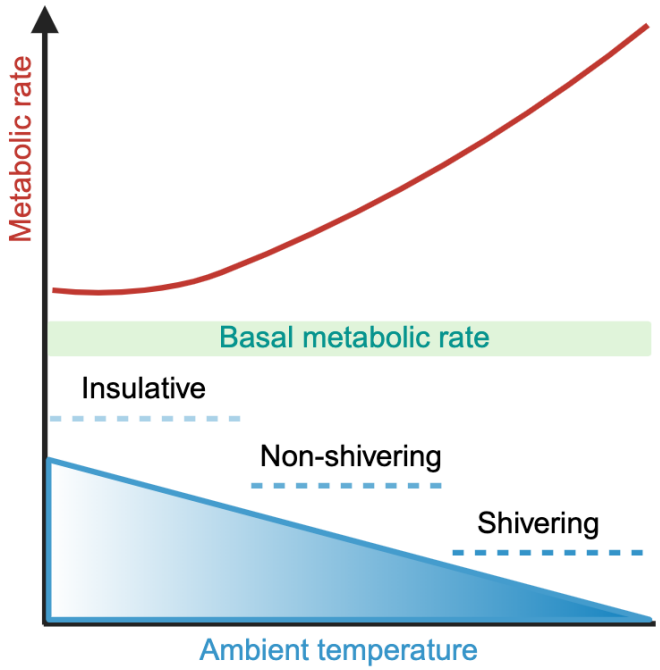

Figure 1.1.4. Adaptive thermogenesis model. When environmental temperature decreases the adaptive thermogenic responses move from insulative to non-shivering and finally shivering thermogenesis. This process is accompanied by an increase in metabolic rate. *Adapted from Celi, 2018 [34].*

1.1.3 Temperature information in the form of memories.

Thermal challenges require animals to evaluate temperature information and to efficiently adapt to the changes in their environment. Whether temperature information about a given environment can also be stored in the brain in the form of a memory, has yet to be determined. The storage of temperature-based memories could enable animals to anticipate thermal challenges based on previous experience and allow them to respond in an energy-efficient manner. However, this would require the storage, retrieval, and conversion of temperature information into behavioral and physiological responses. Up until now, no studies have shown that animals can remember that a specific environment is associated with a particular temperature. As such, we set out to design a pavlovian thermoregulatory paradigm.

Pavlovian training was first described by the neurologist Ivan Pavlov in 1927 [35]. In his original experiments Pavlov presented an untrained dog with a bell as the conditioned stimulus (CS) and showed that the dog had no specific response to the CS. Next, the dog was presented with food as the unconditioned stimulus (US) which resulted in an unconditioned response (UR) in the form of salivation. The dog was then put through a training phase, where the dog was presented with food while the bell was rung. As such, in the training phase the US and the CS were paired. Finally, in the testing phase Pavlov showed that the bell (the CS) on its own triggered the UR, as the dog started salivating without any food being present. With these experiments, Pavlov showed that animals can learn to associate two previously unrelated stimuli with each other [35, 36]. Although usually not emphasized, through these experiments Pavlov also showed that memories can trigger bodily responses such as salivation.

With the original Pavlovian experiments in mind, we set out to design a thermoregulatory pavlovian paradigm where mice would learn to associate a specific context (the CS) with a cold environmental temperature (the US). We hypothesized that by doing so, we would trigger an increase in metabolic rate (the UR) when animals are presented with the original context (the CS) where the cold was initially encountered. As such, this chapter's research question aims to answer whether a context can be paired with a specific temperature, and whether this association can trigger a whole-body metabolic response.

METHODS

1.2.1 Mice

All experiments were performed with C57BL/6J mice. Male mice were used in all experiments. All mice were group-housed in a 12:12-h (07:00-19:00) light-dark colony room at 22°C. Food and water were provided *ad libitum*, and all testing was performed during the light phase. Mice used for experiments were approximately 8-12 weeks of age. All experiments were conducted in accordance with the European Directive 2010/63/EU, under an authorization issued by the Health Products Regulatory Authority Ireland and approved by the Animal Ethics Committee of Trinity College Dublin.

1.2.2 Metabolic Cages

To capture metabolic and behavioral information, mice were singly housed in metabolic cages for a duration of 8 hours per day. These cages were chosen as they are specifically designed for high resolution metabolic and behavioral phenotyping (Promethion, Sable Systems). Each cage included a ceiling-mounted food hopper, water bottle and house, all attached to a mass monitor. Mice had *ad libitum* access to food and water throughout the entire 8 hours. VO_2, CO_2, EE, body weight, food and water intake, and locomotor activity were monitored throughout the session. Briefly, respiratory gasses were measured with an integrated fuel cell oxygen analyzer, a spectrophotometric CO_2 analyzer, and a water vapor pressure analyzer (GA3m1, Sable Systems) [37]. Before each run, gas sensors were calibrated with 100% N_2 as zero reference and with a span gas containing a known concentration of 0.933% CO_2. Air flow was measured and controlled with the multichannel mass flow generator (FR8-1, Sable Systems). Flow rate was set at 2000 mL/min. VO_2 and CO_2 were measured for each mouse at 3-4 min intervals. Energy expenditure was calculated using the following equation: $Kcal/h = 60 * (0.0003941 * VO_2 + 0.001106 * VCO_2)$ [38].

1.2.3 Cold Training Schedule

Male mice were taken from their home cage each morning and individually housed in the Promethion cages for a maximum of eight hours. On day one and two, mice were placed into the Promethion cages at 21°C to allow them to habituate to the machine. On day three, mice were put into the Promethion cages at 21°C while metabolic and behavioral data were simultaneously recorded in order to establish baseline

measurements (Context A). On day four, the cages were changed before the mice were placed inside. Contextual cues were added to the chambers, including wall and floor patterns, brighter lights, different bedding and 3 drops of acetic acid odor (Context B). Once the mice were placed into the cages, the temperature decreased in increments of ~10 degrees per hour. As such, the mice spent a total of 6 hours in the altered context at a temperature of 4°C. This was repeated for a total of three days, with metabolic and behavioral data recorded throughout. Mice were then returned and kept in their home cages for a two-day break period. Next, on day nine, mice were put back into the Promethion cages without any of the additional cues at 21°C to allow for a second baseline measurement (Context A). Finally, on day ten all the additional context cues were added back in before the mice were put into the cages (Context B, Figure 1.3.1a-b). Temperature was kept at 21°C and metabolic and behavioral data was simultaneously recorded to establish the test day measurements.

1.2.4 No Cold Training Schedule

Mice were run through the exact same behavioral timeline as described above. However, in this training schedule the temperature was kept at 21°C throughout the entire experiment. As such, mice were exposed to the context changes as described above but were never exposed to any cold (Figure 1.3.6a-b).

1.2.5 Conditioned Cold Aversion

The conditioned place preference (CPP) apparatus consisted of two separate chambers. Each chamber had different wall and floor cues (Black and white pattern). Mice could freely enter both chambers through an opening in the wall in the middle of the apparatus. On day one, mice were taken from their home cage and placed inside the apparatus where they could freely explore both sides of the apparatus for a total of 20 minutes. The entire apparatus was kept at 21°C. On day two, the opening in the middle wall of the apparatus was closed. During the morning sessions, mice were exposed to one side of the apparatus at 21°C for a duration of two hours. Mice were then returned to their home cage for a two-hour break. In the afternoon sessions, mice were then exposed to the other side of the apparatus at 4°C for a duration of two hours. This was subsequently repeated for a total of three days. On day five, the opening in the middle wall of the apparatus was re-opened before mice were placed back into the apparatus. Mice could freely explore both chambers again for a total of 20 minutes,

while the entire apparatus was kept at 21°C. All behavior was videotaped and subsequently hand scored. Time spent in each chamber in seconds was measured on day one (pre-test) and day five (test). The time spent in each chamber was normalized using the following formula (test phase duration spent in the cold-paired chamber/ time spent there in the pre-test phase), to account for any pre-existing preferences [39]. Both time of day and side of apparatus were counterbalanced across all mice.

1.2.6 Statistics

All data were analyzed using Prism 10. All data were graphed as means ± Standard errors of the mean (SEM). An alpha level of 0.05 was used as a criterion for statistical significance. The results of figures 1.3.1, 1.3.2, 1.3.3, 1.3.4, 1.3.5 and 1.3.7 were analyzed using repeated measure one-way ANOVAS and Tukey's multiple comparison test. Figure 1.3.6 was analyzed using two-way ANOVAS and unpaired t-tests. Figure 1.3.8 was analyzed with unpaired t-tests.

1.2.7 Figure design and visualization

Figures and graphical illustrations were created with Biorender (Biorender.com).

RESULTS

1.3.1 Cold exposure upregulates whole-body metabolic rate and alters behavior.

To determine whether mice can store and retrieve temperature information, we designed a thermoregulatory Pavlovian conditioning paradigm where mice were trained in Context A at 21°C and in Context B at 4°C (Figure 1.3.1a). First, we aimed at establishing the effects of cold exposure on whole-body metabolic rate. To achieve this, we measured and compared the metabolic rates of mice during baseline day 1 at 21°C with cold training days at 4°C. As described above, cold exposure stimulates thermogenesis by increasing lipid and glucose metabolism in BAT, which in turn upregulates whole-body metabolic rate [40-42]. As such, we hypothesized that the metabolic rates measured during the cold training days would be significantly higher than the rates measured on baseline day 1. In agreement with this, our results show that mice increased their oxygen consumption (VO_2; Figure 1.3.1b), energy expenditure (EE; Figure 3.1c) and carbon dioxide production (VCO_2; Figure 1.3.1d) when exposed to a 4°C environment compared to a 21°C environment. Additionally, we found that this increase in metabolic rate and energy expenditure persisted across all three cold training days (Figure 1.3.1b-d). Next, to better understand whether mice also behave differently in a cold environment, we tracked movement and the amount of food that the mice consumed at baseline and during the training days. Interestingly, we found that mice moved significantly more in the 4°C environment than in the 21°C environment on the third cold training day (Figure 1.3.2a-b). No differences were found with regards to food consumption as the mice ate similar amounts of food during all four days (Figure 1.3.2c). Taken together, these data show that, in response to a cold environment, mice increase their metabolic rate and alter their behavior.

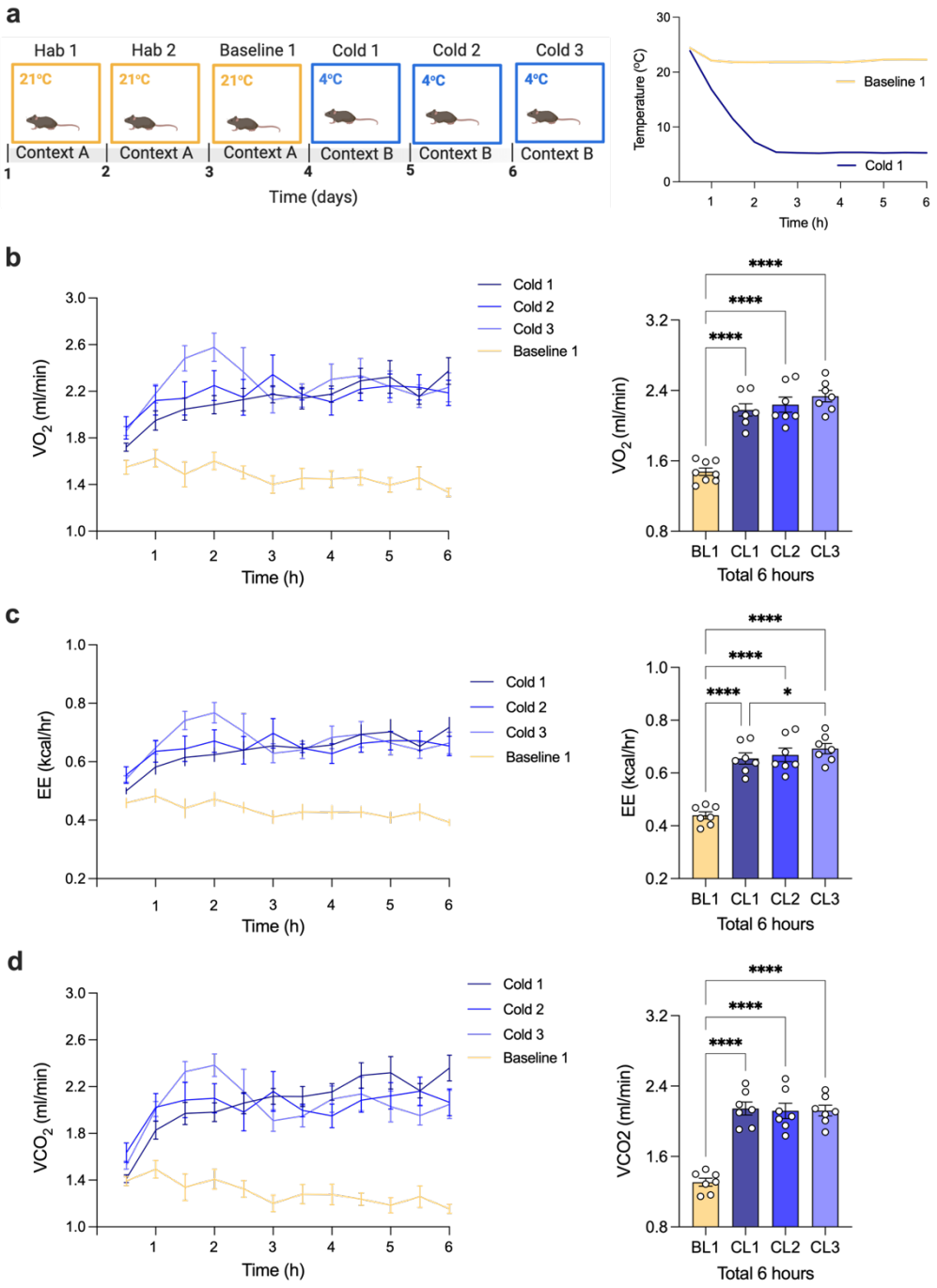

Figure 1.3.1 Cold exposure increases metabolic rate.

(a) Diagrammatic representation of experimental timeline for Pavlovian conditioning to a cold-paired context (left). Environmental temperature during Baseline 1 and Cold 1 (right). **(b)** Time plot of oxygen consumption between mice during Baseline 1, Cold 1, Cold 2, and Cold 3 (left), with comparisons of total time averaged in metabolic cages (right). **(c)** Time plot of energy expenditure between mice during Baseline 1, Cold 1, Cold 2, and Cold 3 (left), with comparisons of total time averaged in metabolic cages (right). **(d)** Time plot of carbon dioxide production between mice during Baseline 1, Cold 1, Cold 2, and Cold 3 (left), with comparisons of total time averaged in metabolic cages (right). Data shown as mean ± SEM, *n* = 7-8 mice per group. * $p < 0.05$, ** $p < 0.01$, *** $p < 0.001$, **** $p < 0.0001$. BL1, baseline 1; CL1, cold 1; CL2, cold 2; CL3, cold 3; VO_2, oxygen consumption; VCO_2, carbon dioxide emission; EE, energy expenditure; h, hour.

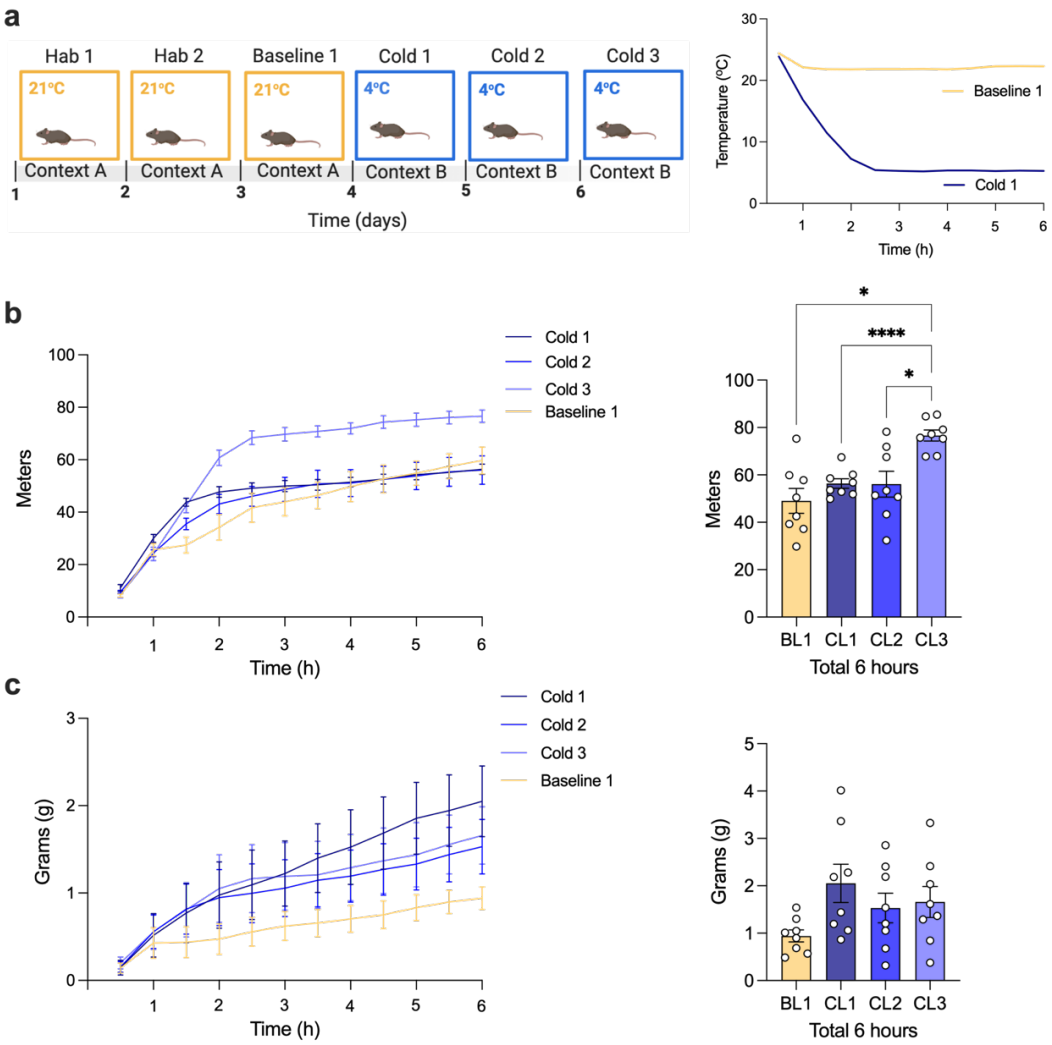

Figure 1.3.2 Cold exposure alters behavior.
(a) Diagrammatic representation of experimental timeline for Pavlovian conditioning to a cold-paired context (left). Environmental temperature during Baseline 1 and Cold 1 (right). **(b)** Time plot of movement between mice during Baseline 1, Cold 1, Cold 2, and Cold 3 (left), with comparisons of total time averaged in metabolic cages (right). **(c)** Time plot of food consumption between mice during Baseline 1, Cold 1, Cold 2, and Cold 3 (left), with comparisons of total time averaged in metabolic cages (right). Data shown as mean ± SEM, *n* = 7-8 mice per group. * $p < 0.05$, ** $p < 0.01$, *** $p < 0.001$, **** $p < 0.0001$. BL1, baseline 1; CL1, cold 1; CL2, cold 2; CL3, cold 3; h, hour; g, grams.

1.3.2 A cold-paired contextual memory increases metabolic rate.

To establish whether mice can associate a specific context with a given temperature, we trained mice to associate Context A with 21°C and Context B with 4°C (Figure 1.3.3a). After training, mice were tested in Context B at 21°C. We hypothesized that if mice associated Context B with 4°C, their metabolic rates and behavior would be similar to that observed during training days. Here, we found an increase in metabolic rate when mice were returned to the cold-paired context, irrespective of the actual temperature of that context (Figure 1.3.3b-d), suggesting that mice can learn to associate a specific context with a particular temperature. Moreover, we found a temporal dynamic on test day, as the metabolic rates resembled cold day 1 during the first few hours and came closer to baseline levels after 6 hours (Figure 1.3.3b-d). Additionally, mice showed significantly increased movement when returned to the cold-paired context, but no differences in food consumption compared to baseline day (Figure 1.3.4b-c). These results suggests that in addition to increasing their metabolic rates, mice also adjust their behavior in the cold-paired context on test day, similarly to what was observed during the 4°C training days. Finally, to confirm that these effects were specifically induced by the contextual cues associated with cold training, and not just exposure to a neutral context, we also compared the test day measurement to a second baseline (BL2). We find that the observed effects can be attributed to test day specifically, as we find significantly higher metabolic rates during test day compared to both baseline 1 and baseline 2 (Figure 1.3.5). Together, these data suggest that mice can learn and recall a cold-paired contextual memory, and that the recall of a cold memory will increase their whole-body metabolic rate.

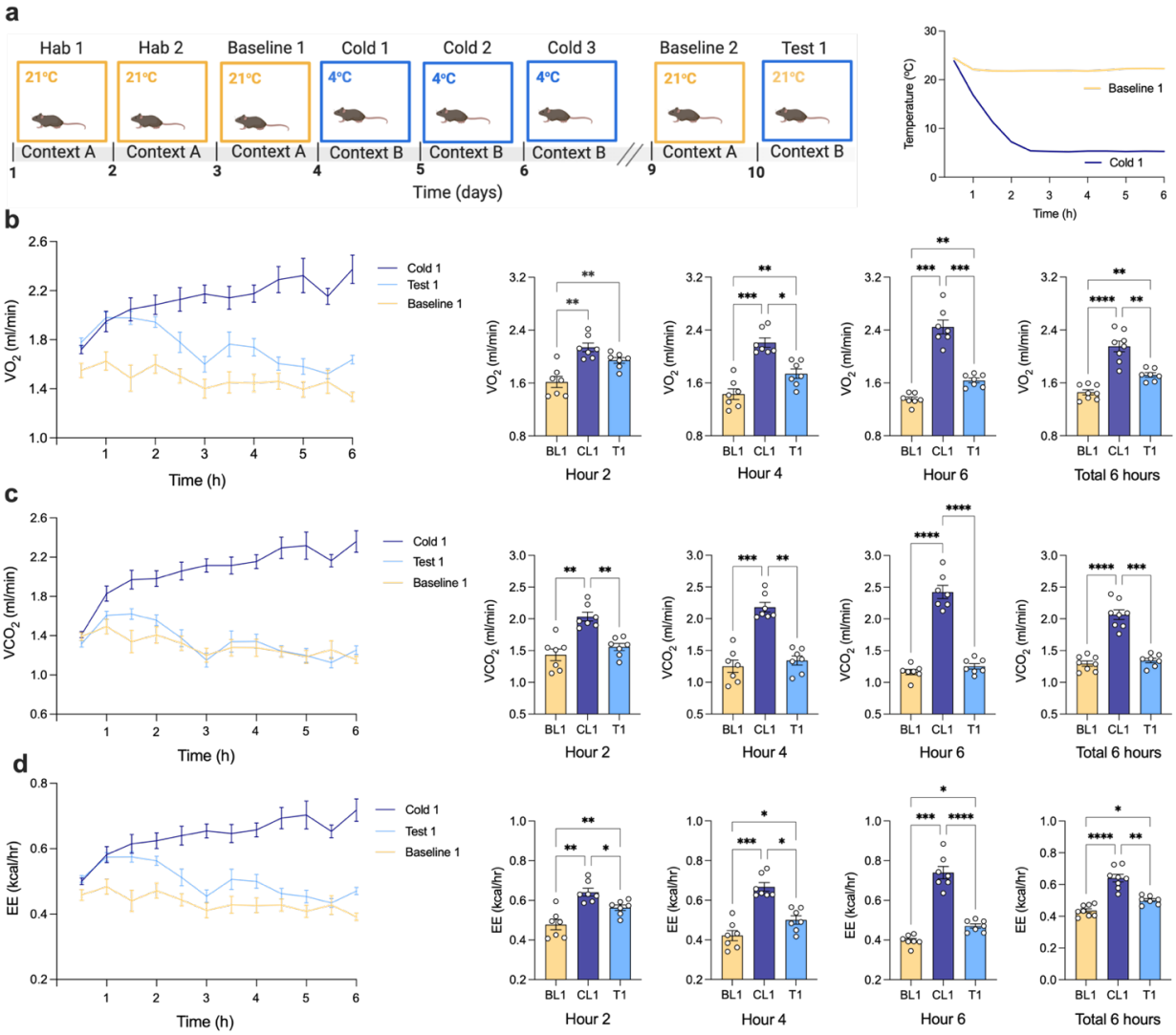

Figure 1.3.3 Mice increase their metabolic rate in the cold-paired context. **(a)** Diagrammatic representation of experimental timeline for Pavlovian conditioning to a cold-paired context (left). Environmental temperature during Baseline 1 and Cold 1 (right). **(b)** Time plot of oxygen consumption between mice during Baseline 1, Test 1 and Cold 1 (left). Comparison of oxygen consumption between mice during Baseline 1, Test 1 and Cold 1 at hour 2, hour 4, hour 6 and, total time averaged in metabolic cages (right). **(c)** Time plot of carbon dioxide production between mice during Baseline 1, Test 1 and Cold 1 (left). Comparison of carbon dioxide production between mice during Baseline 1, Test 1 and Cold 1 at hour 2, hour 4, hour 6 and, total time averaged in metabolic cages (right). **(d)** Time plot of energy expenditure between mice during Baseline 1, Test 1 and Cold 1 (left). Comparison of energy expenditure between mice during Baseline 1, Test 1 and Cold 1 at hour 2, hour 4, hour 6 and, total time averaged in metabolic cages (right). Data shown as mean ± SEM, *n* = 7-8 mice per group.* p < 0.05, ** p < 0.01, *** p < 0.001, **** p < 0.0001. BL1, baseline 1; BL2, baseline 2; T1, Test 1; CL1, cold 1; CL2, cold 2; CL3, cold 3; VO_2, oxygen consumption; VCO_2, carbon dioxide emission; EE, energy expenditure; h, hour.

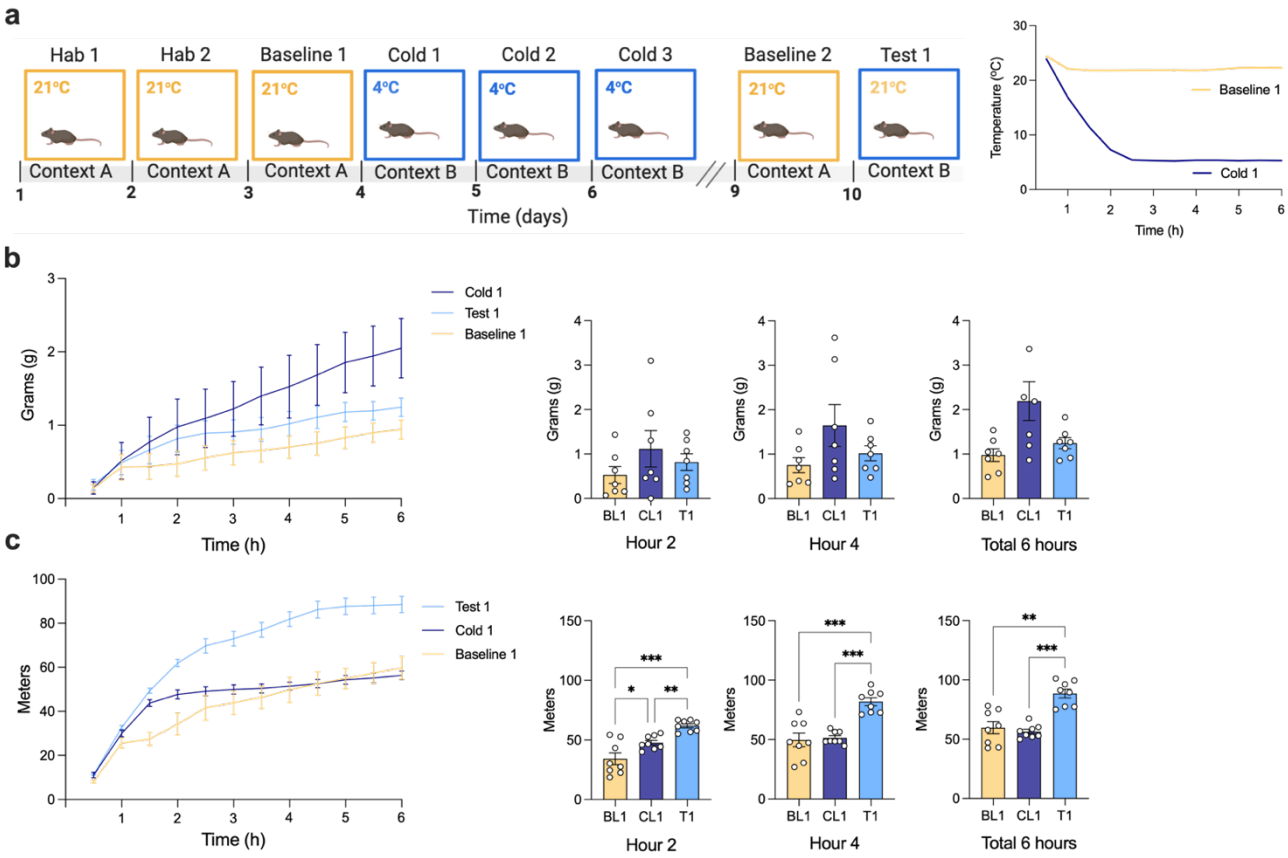

Figure 1.3.4 Mice show increased movement when returned to the cold-paired context. (a) Diagrammatic representation of experimental timeline for Pavlovian conditioning to a cold-paired context (left). Environmental temperature during Baseline 1 and Cold 1 (right). **(b)** Time plot of food consumption between mice during Baseline 1, Test 1 and Cold 1 (left). Comparison of food consumption between mice during Baseline 1, Test 1 and Cold 1 at hour 2, hour 4, hour 6 and, total time averaged in metabolic cages (right). **(c)** Time plot of movement between mice during Baseline 1, Test 1 and Cold 1 (left). Comparison of movement between mice during Baseline 1, Test 1 and Cold 1 at hour 2, hour 4, hour 6 and, total time averaged in metabolic cages (right). Data shown as mean ± SEM, *n* = 7-8 mice per group. * p < 0.05, ** p < 0.01, *** p < 0.001, **** p < 0.0001. BL1, baseline 1; BL2, baseline 2; T1, Test 1; CL1, cold 1; CL2, cold 2; CL3, cold 3; h, hour; g, grams.

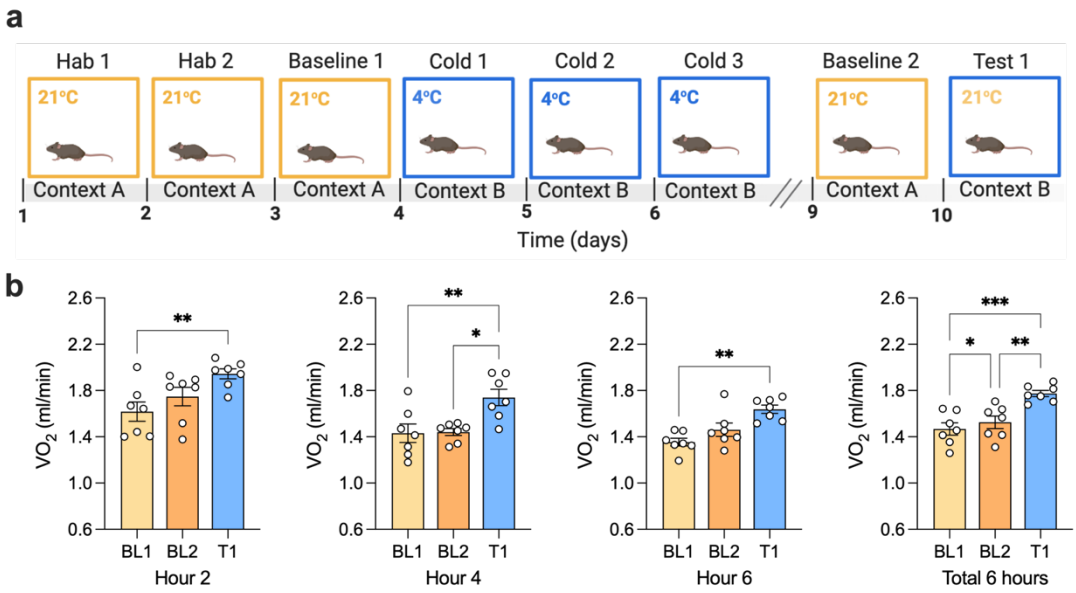

Figure 1.3.5 Metabolic rate increases specifically on test day 1 as a result of cold memory recall. (a) Diagrammatic representation of experimental timeline for Pavlovian conditioning to a cold-paired context. **(b)** Comparison of oxygen consumption between mice during Baseline 1, Baseline 2 and Test 1 at hour 2, hour 4, hour 6 and, total time averaged in metabolic cages. Data shown as mean ± SEM, *n* = 7-8 mice per group. * $p < 0.05$, ** $p < 0.01$, *** $p < 0.001$. VO_2, oxygen consumption; BL1, baseline 1; BL2, baseline 2; T1, Test 1.

1.3.3 Increased metabolic rates are not caused by extended cold effects or novelty.

To confirm that the upregulation of metabolic rate on test day was due to the pairing of 4°C with Context B, and not due to novelty of the context, we trained mice in the same Pavlovian timeline without deviating the temperature from 21°C (Figure 1.3.6a). As such, these mice were never exposed to 4°C. We found that, although the novelty of Context B caused an increase in metabolic rate in the initial 2 hours of the no-cold training and test days, there were no differences in metabolic rate between baseline, no-cold training, and test after two hours (Figure 1.3.6b), suggesting that novelty does not affect metabolic rate beyond two hours. Next, we directly compared mice that underwent 4°C cold training in Context B with mice that underwent the 21°C no-cold training in Context B. Our results demonstrate that cold training at 4°C in Context B significantly increased metabolic rate on test day 1 compared to 21°C no-cold training (Figure 1.3.6c). Moreover, these effects were not due to initial differences between the two groups, as they did not significantly differ in metabolic rate on baseline day (Figure 1.3.6d). These data suggest that the increase in metabolic rate was not caused by the novelty of Context B, but rather by the association of 4°C with Context B.

Finally, to rule out that the increase in metabolic rate was not due to prolonged effects of long-term cold exposure, a separate cohort of mice was allowed to recover in their home cage for four consecutive days instead of two after cold training (Figure 1.3.7a). We found that the increase in metabolic rate persisted even after a prolonged recovery break, indicating that the observed increase in whole-body metabolism was not due to prolonged cold effects, but rather to the recall of the cold-paired contextual memory (Figure 1.3.7b-d). Taken together, these data suggest that neither novelty nor extended cold effects were causing the above reported increases in metabolic rate.

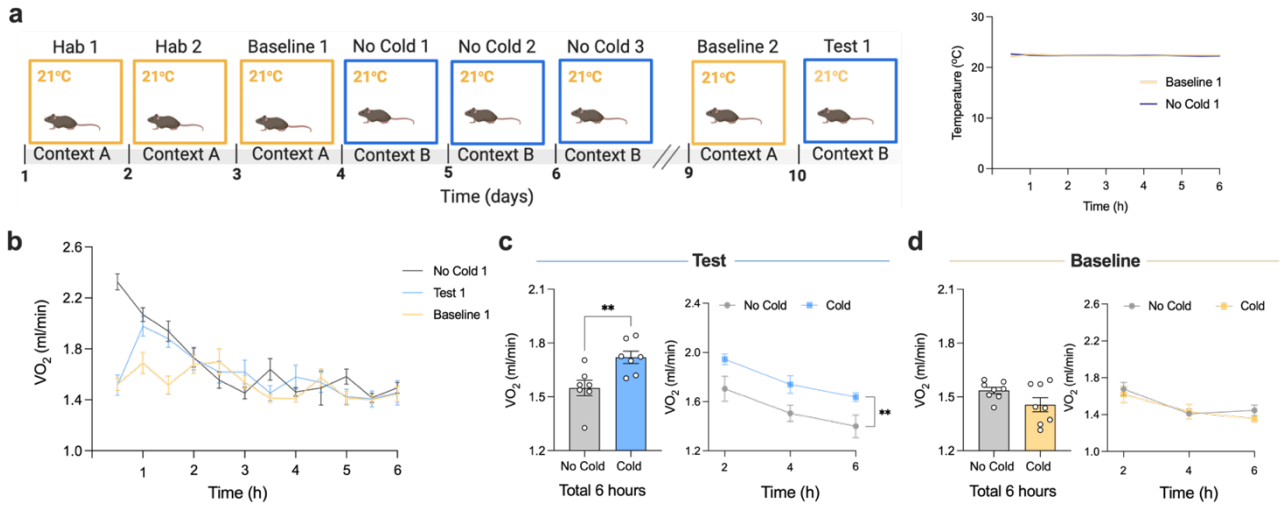

Figure 1.3.6 Novelty does not increase metabolic rate.
(a) Diagrammatic representation of experimental timeline for no cold-paired context control (left). Environmental temperature during Baseline 1 and No Cold 1 (right). **(b)** Time plot of oxygen consumption between mice during Baseline 1, Test 1 and No Cold 1 **(c)** Comparison of oxygen consumption between the cold-paired and no-cold paired cohorts on test day (6 hours averaged; left), and at hours 2, 4 and 6 (right). **(d)** Comparison of oxygen consumption between the cold-paired and no-cold paired cohorts on Baseline 1 (6 hours averaged; left), and at hours 2, 4 and 6 (right). Data shown as mean ± SEM, *n* = 7-8 mice per group. ** p < 0.01, ***. BL1, baseline 1; BL2, baseline 2; T1, Test 1; CL1, cold 1; CL2, cold 2; CL3, cold 3; VO_2, oxygen consumption; h, hour.

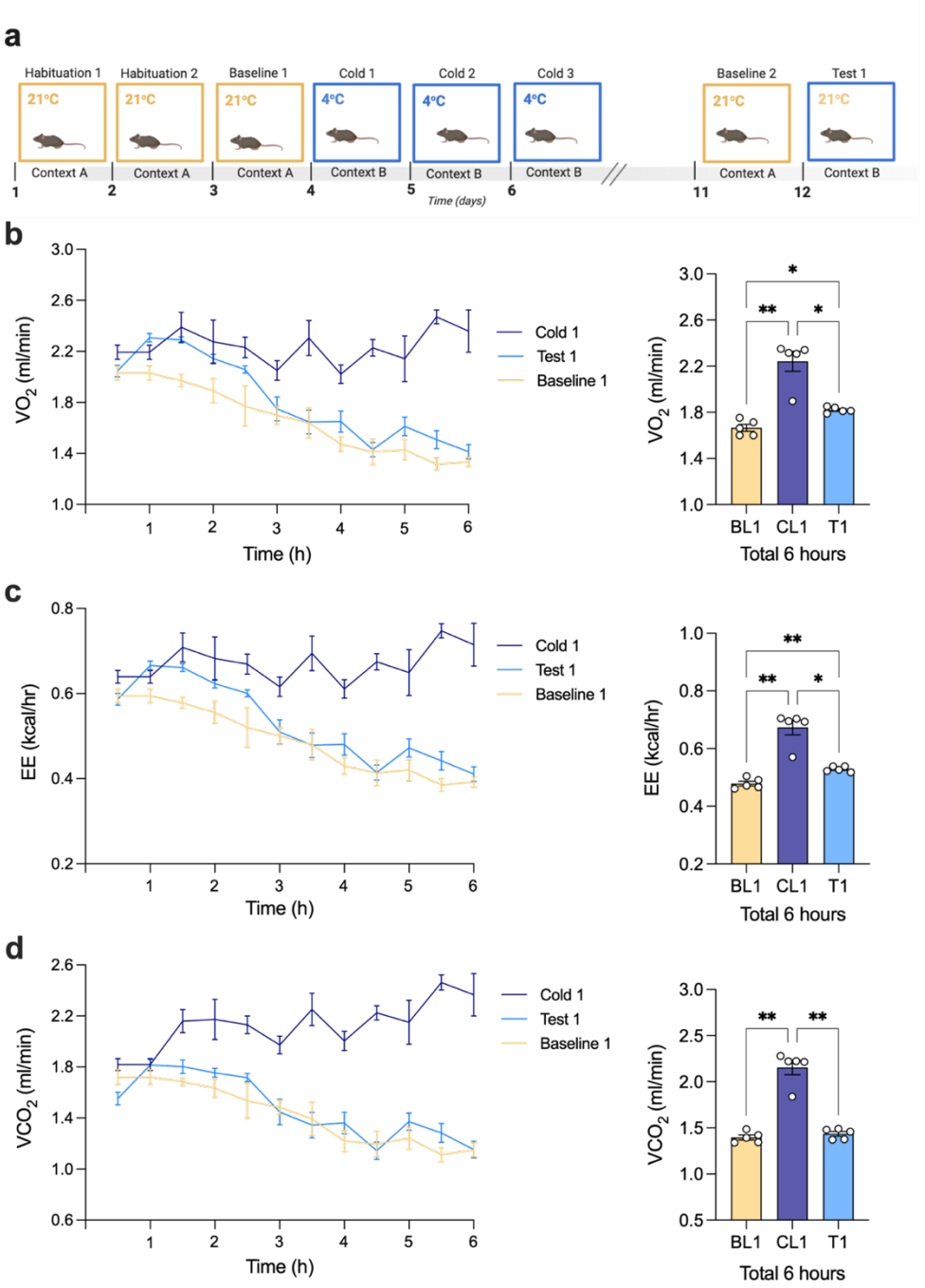

Figure 1.3.7 Metabolic rates do no increase due to extended cold effects. **(a)** Diagrammatic representation of experimental timeline for Pavlovian conditioning to a cold-paired context with an extended (4 day) break. **(b)** Time plot of oxygen consumption between mice during Baseline 1, Test 1 and Cold 1 following an extended (4 day) break (left), with comparisons of total time averaged in metabolic cages (right). **(c)** Time plot of energy expenditure between mice during Baseline 1, Test 1 and Cold 1 following an extended (4 day) break (left), with comparisons of total time averaged in metabolic cages (right). **(d)** Time plot of carbon dioxide production between mice during Baseline 1, Test 1 and Cold 1 following an extended (4 day) break (left), with comparisons of total time averaged in metabolic cages (right). Data shown as mean ± SEM, *n* = 5 mice per group. * $p < 0.05$, ** $p < 0.01$. BL1, baseline 1; T1, Test 1; CL1, cold 1; VO_2, oxygen consumption; EE, energy expenditure; VCO_2, carbon dioxide emission; h, hour.

1.3.4 A cold-paired contextual memory causes avoidance behavior.

In the above-described Pavlovian timelines, mice were not able to escape the cold-context due to being locked into the metabolic cages to allow for continuous metabolic rate measurements. However, to further demonstrate the behavioral expression of a cold memory, we investigated whether mice developed a conditioned cold aversion due to training at 4°C in a CPP apparatus (Figure 1.3.8a). We show that mice had no preference for either side of the apparatus during the pre-test day at 21°C (Figure 1.3.8b); however, mice trained at 4°C displayed a conditioned place aversion to the cold-paired side of the CPP apparatus, but not to the 21°C paired side (Figure 1.3.8c). These data show that not only do mice form a contextual memory for a cold environment, but that they will avoid the cold-paired context if given the choice.

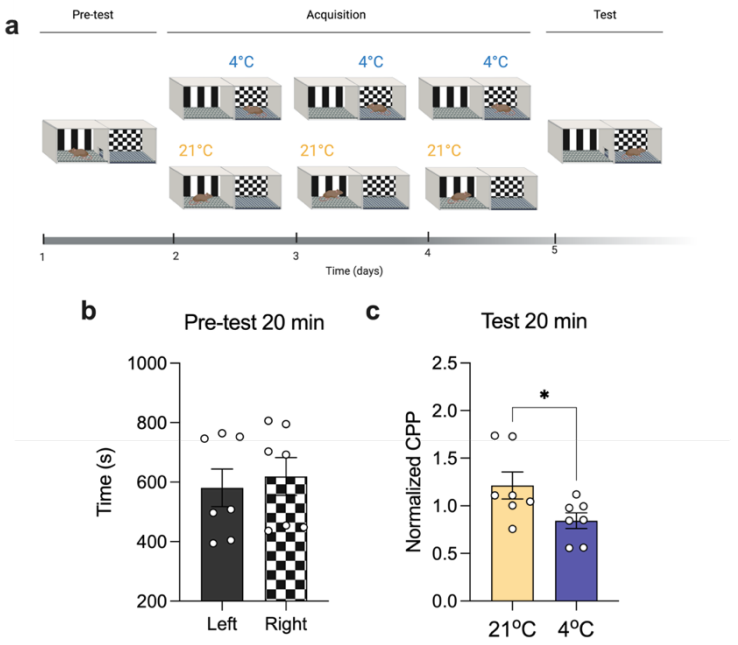

Figure 1.3.8 A memory of a cold-paired context causes avoidance behavior. **(a)** Diagrammatic representation of experimental timeline for Pavlovian conditioning to the cold-paired side, or no cold paired side, of a CPP apparatus. **(b)** Time spent in each chamber of the CPP apparatus during pre-test. **(c)** Place preference for the no cold paired side of the CPP apparatus compared to the cold-paired side, time spent in either the cold-paired side, or no cold paired side was divided by the time spent in the same chamber during pre-test (Test/Pre-test). Data shown as mean ± SEM, *n* = 7 mice per group. * p < 0.05. s, seconds; CPP, conditioned place preference.

DISCUSSION

In this chapter, we showed that when mice were exposed to a cold environment, they increased their metabolic rates. These results are in line with previous studies showing that increases in metabolic rate are necessary to maintain body temperature at a constant rate during cold adaptation [29, 31, 34]. Next, we showed that mice increased their metabolic rates when recalling a cold environment, indicating that mice can store and recall temperature information. Moreover, we showed that mice adjust their behavior accordingly, as they avoided the cold-paired context when given the choice. To our knowledge, this is the first study showing that mice can store and recall temperature information and that cold memories increase whole-body metabolism.

The increase in metabolic rates that were observed on test day lasted six hours yet showed a temporal decrease. Indeed, the test day metabolic rates resembled cold day 1 during the first few hours and leveled off over the course of the six testing hours. As such, one question that remains is how long a cold memory lasts. As animals are tested at 21°C, it is possible that at the end of the testing day animals have updated the original memory and no longer associate Context B with a cold environment. Future studies are needed to establish exactly how long cold memories last, and whether there are any extinction effects on subsequent testing days. Moreover, in the above-described experiments, mice were trained at 4°C for three consecutive days. Future experiments are needed to establish whether fewer training days result in shorter memory effects on metabolic rates.

We found no differences in food consumption during cold exposure or cold memory recall, suggesting that six hours of cold exposure is not long enough to cause changes in feeding behavior, in line with previously reported studies [43]. Interestingly, we found that animals increased their movement across training days and when recalling the cold, indicating that previous experience and expectations cause adaptive behavioral responses in mice. It is therefore possible that mice would increase their food consumption as well upon recall of a cold memory. To determine whether a cold memory leads to an increase in food consumption, more long-term experiments are needed where mice are tested for more than six hours.

During the 4°C training days, we chose to expose animals gradually to a cold environment. As such, the temperature decreased in increments of ~10 degrees per hour. The gradual decrease of temperature was chosen to avoid any cold shock effects, as sudden exposure to 4°C could potentially result in high stress levels in mice. Recent studies have shown that other stressful experiences, such as exposure to a predator odor, do not increase metabolic rate [44]. Thus, the reported increase in metabolic rate during training and test days can be attributed to the cold specifically and not to a general stress response.

The results presented in this chapter show that Pavlovian conditioning can be used to demonstrate that memories not only elicit a behavioral response, but that they can also trigger a whole-body reaction. More studies are necessary to explore what bodily responses are triggered by the recall of certain memories. For example, PTSD patients often report traumatic physical sensations that are triggered by memory flashbacks of a traumatic event, yet few studies have explored how these sensations are exactly triggered by the memories. Further understanding of the connection between memories and whole-body responses will allow us to design better treatment strategies for these patients in the future.

Chapter 2:

Retrieval of a contextual cold memory increases neural activity in the hippocampus and hypothalamus.

INTRODUCTION

2.1.1 Immediate early genes as a proxy for neuronal activity

Immediate-early genes (IEGs) are the most extensively used activity markers to dissect the neuronal circuits that are involved in specific behaviors across species [45]. IEG expression increases rapidly following neural activity, is associated with the induction of synaptic plasticity (Figure 2.1.1) and with neural encoding processes [46, 47].

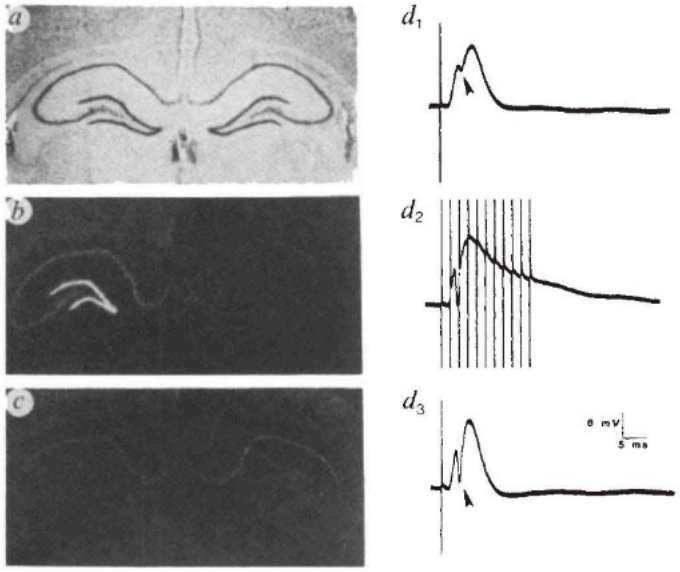

Figure 2.1.1 Neural activity rapidly increases IEG expression. Induction of LTP increases zif268 mRNA levels in granule cell neurons of the dentate gyrus. *Adapted from Cole et al., 1989 [46].*

Different stages of neuronal activation can be distinguished that lead to the induction of the intracellular cascade of IEGs. The first responses to neuronal stimulation include the activation of voltage dependent Ca^{2+} channels or membrane receptors that respond to neurotransmitters and growth factors (Figure 2.1.2). This activation triggers intracellular secondary messenger pathways such as protein kinase A (PKA) and $Ca^{2+/}$CaM-dependent protein kinase II (CaMKII). The activity of these kinases modifies the function of ion channels and the expression of constitutive transcription factors such as cAMP and CREB, and eventually cause the expression of IEGs. Generally, IEGs are subdivided into two functional classes: regulatory transcription factors (RTFs) and effector proteins. RTFs such as c-Fos, zif268 and c-Jun broadly influence cell function depending on the downstream genes that they regulate [48, 49]. Effector proteins such as Arc and Homer directly modulate specific cellular functioning and are

involved in processes such as receptor modulation, vesicle storage and synaptic trafficking [49]. It is estimated that the IEG response in neurons is limited to 30-40 genes, of which 10-15 are RTFs [50].

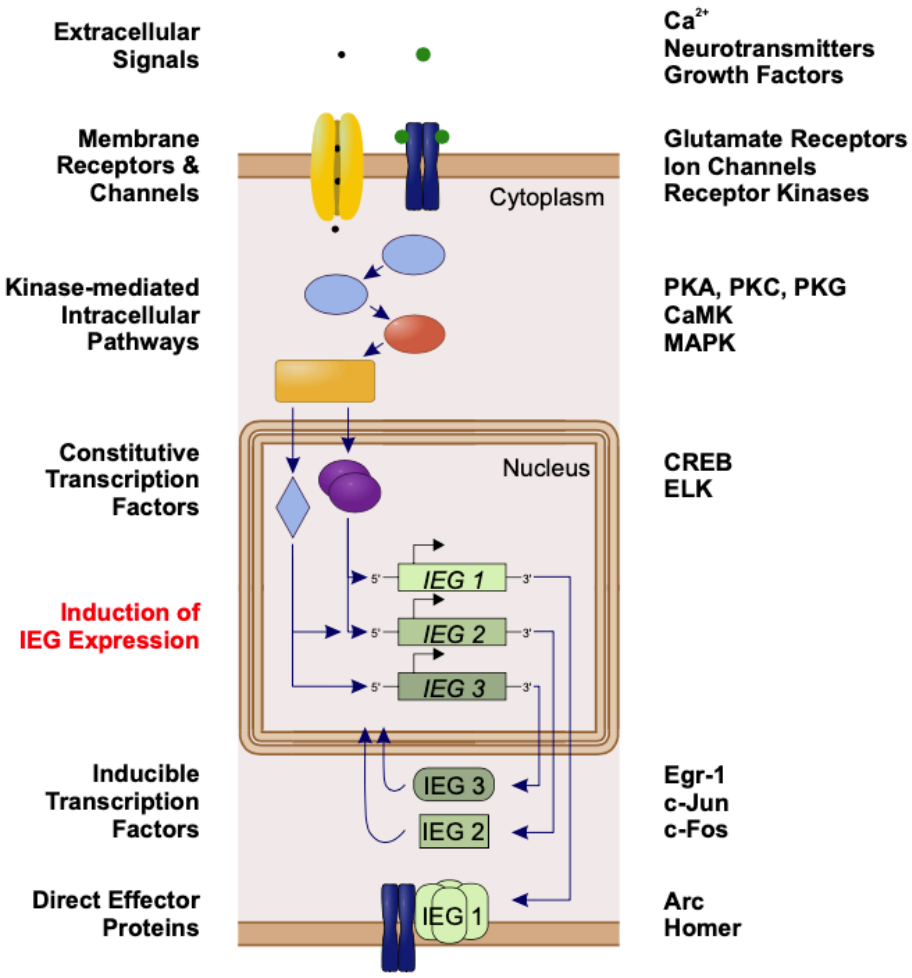

Figure 2.1.2 The intracellular pathways of IEG activation. Extracellular signals activate channels and receptors that will in turn trigger a variety of intracellular pathways. Kinases mediate the expression of the constitutive transcription factors, whose activation will lead to the expression of IEGs. Protein products from these IEGs will act as inducible transcription factors or direct effector proteins. *Adapted from Sommerlandt et al., 2019 [49].*

IEGs expression is rapid and transient in nature and are expressed at low levels in the absence of sensory stimulation. This makes them ideal markers to study neuronal activation and circuitry in healthy and diseased states. Indeed, IEGs are most commonly used to further understand which brain regions are important for specific behaviors, and to create a roadmap regarding the functional construction of the brain [45].

2.1.2 Hippocampal circuitry and memory.

For many decades, the hippocampus has been associated with memory. Early human studies have shown that bilateral damage of the hippocampus causes anterograde amnesia [51]. Similar results have been found in monkeys, where damage to the hippocampus and its connections resulted in impaired object location memories [52]. At a systems level, the hippocampus receives inputs from a variety of different association areas in the cortex (Figure 2.1.3). This cortical information is relayed to the hippocampus through both the parahippocampal gyrus and the entorhinal cortex. As a result, the hippocampus has access to multimodal information that has previously been processed by different interconnected sensory pathways [52].

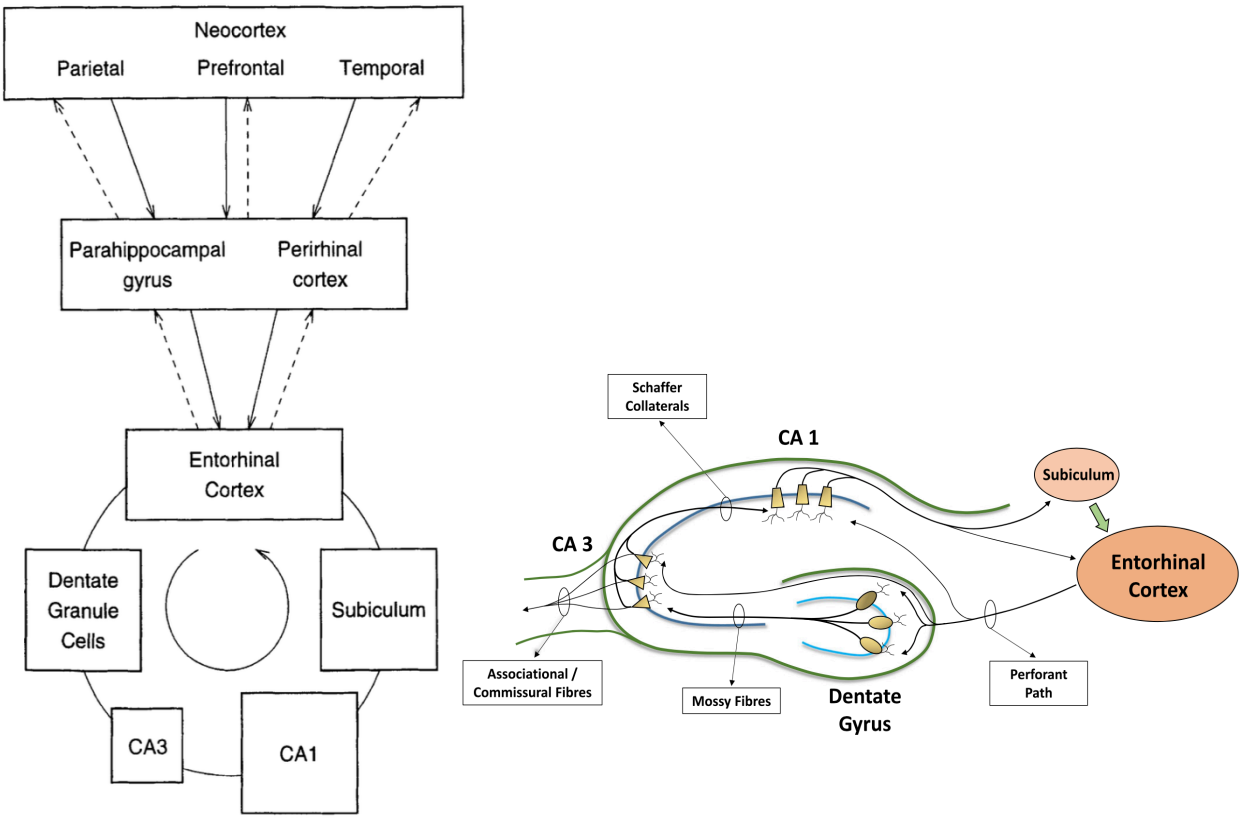

Figure 2.1.3 Systems-level model of hippocampal circuitry. Information is processed in cortical areas and relayed to the hippocampus through the parahippocampal gyrus, perirhinal and entorhinal cortex. From here, information reaches the dentate gyrus granule cells, before being projected to CA3 and CA1 pyramidal neurons. The CA1 then communicates back to the entorhinal cortex through the subiculum, making the circuitry come full circle again. *Adapted from Rolls, 1996 [51] and from Mancini et al., 2017 [53].*

From the entorhinal cortex, information reaches the dentate gyrus (DG) granule cells trough projections in the perforant path. The DG granule cells then project to *Cornu Ammonis* 3 (CA3) and *Cornu Ammonis* 1 (CA1) cells through mossy fibers, providing a powerful connection between the DG, CA3 and CA1 [52]. CA3 pyramidal cells additionally project to ipsilateral CA1 pyramidal neurons directly, through connecting fibers called Schaffer Collaterals [53]. Finally, CA1 axons communicate directly and indirectly with the entorhinal cortex through projections that cross the subiculum [52, 53]. Many different types of memory have been shown to rely on this hippocampal circuitry and it is now accepted that this circuitry is essential for the encoding and retrieval of memories in general [54-57].

2.1.3 Hypothalamic circuitry and thermoregulation.

It is currently understood that the hypothalamus is a key structure that integrates temperature information and coordinates both the behavioral and autonomic responses that are necessary to maintain homeostasis [20]. The primary input into the thermoregulatory circuitry comes from the sensory neurons that have cell bodies in peripheral ganglia and axons in tissues such as the skin and spinal cord. Additionally, there are sensory neurons located within the brain that measure the temperature of the hypothalamus specifically. Within the hypothalamus, several regions have been identified that are essential for thermoregulatory responses (Figure 2.1.4). For example, the preoptic area (POA) has been shown to have thermosensitive neurons which induce BAT thermogenesis [58, 59]. However, the POA does not seem to be necessary for all types of thermoregulatory responses, as lesions to the rat POA were shown to have no effect on behavioral thermoregulatory responses [60, 61].

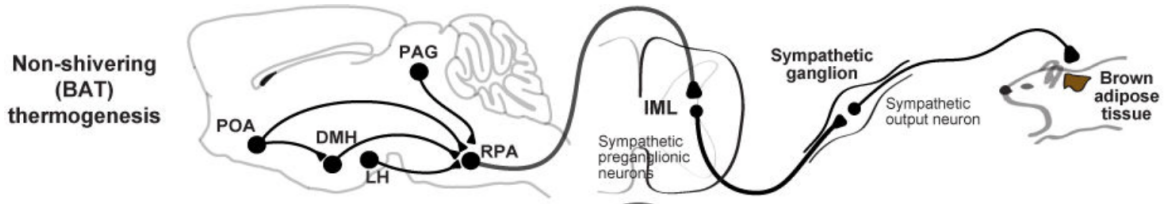

Figure 2.1.4 Hypothalamic circuitry underlying behavioral and autonomic thermoregulatory responses. The brain regions that have been found to be involved in various thermoregulatory processes and their proposed pathway to brown adipose tissue. *Adapted from Tan & Knight, 2018 [20].*

Thermal information that is received in the POA is subsequently communicated to downstream structures such as the dorsomedial hypothalamus (DMH) and the rostral raphe pallidus (rRPA). These regions have been established as key regions for several physiological responses that are important for thermoregulation. For example, chemical stimulation of the DMH was shown to increase BAT thermogenesis, whereas silencing the DMH prevented it [62, 63]. Moreover, optogenetically stimulating the DMH resulted in an increase of heart rate and energy expenditure [64]. Although many regions within the hypothalamus have been shown to be important for thermoregulation in general, there have been few regions associated with both the physiological and behavioral aspects of thermoregulation. However, an exception to this seems to be the lateral hypothalamus (LHA). In recent studies, LHA neurons have been shown to be necessary for diverse thermoregulatory behaviors and for the control of energy homeostasis [23, 65]. On top of this, neurons that express orexins in the LHA have been shown to promote BAT thermogenesis [66]. Therefore, the LHA may be a crucial and essential region that is involved in both the physiological and the behavioral aspects of thermoregulation.

2.1.4 Brain-wide mapping of cFos$^+$ cells.

Up until the 19th century the predominant view was that specific brain regions were responsible for certain cognitive functions [67]. However, recent studies have been shifting away from this, by adapting a more brain-wide approach to understand the underlying circuitry of complex behaviors. This novel framework suggests that cognitive functions are supported by the coordinated activity, or networks, of multiple brain regions. With these network-based approaches have been able to identify large-scale anatomical and functional connections in the brain across species [68-71]. Moreover, multiple studies investigating how memories are stored in the brain have now leveraged these network-based approaches and quantified IEG activity throughout the entire brain [72-75]. To quantify IEG activity reliably throughout multiple regions, different tissue clearing techniques have been employed to facilitate maximum IEG visibility in different brain structures. Popular clearing techniques include, iDISCO, CLARITY and CUBIC [76-78]. All clearing techniques aim at making tissue transparent by minimizing light scattering and light absorption to allow for the imaging of large samples (Figure 2.1.5).

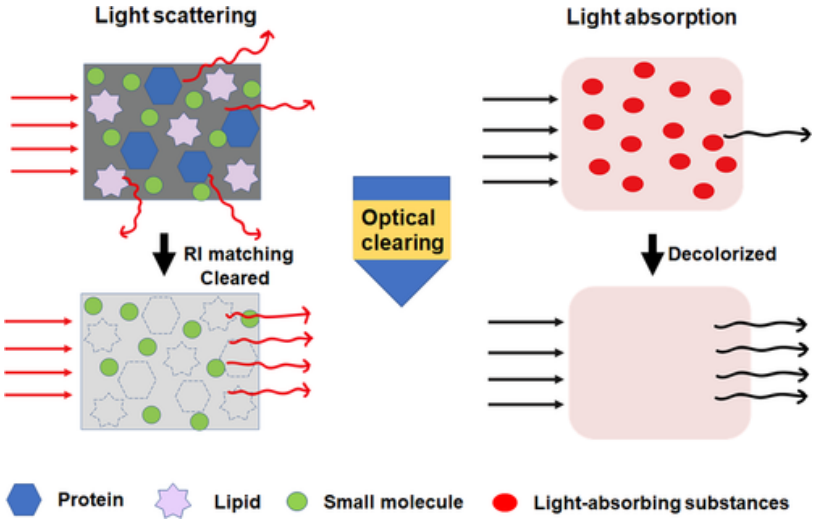

Figure 2.1.5 Principles of tissue clearing. Heterogenous substances such as proteins and lipids with different optical properties cause light scattering. Light scattering is caused by light absorbing components such as hemoglobin and melanin. Both light scattering and absorption cause tissue opacity. Tissue clearing techniques aim at making tissue optically transparent by reducing light scattering and absorption. *Adapted from Tian et al., 2021 [79].*

Finally, when these clearing techniques are combined with molecular labeling methods they enable for brain-wide imaging at cellular resolution [79]. With the advancement of these techniques, studies have been able to perform brain-wide analysis of neuronal activity and identify the functional connectivity between multiple brain regions. For example, previous studies have found the brain networks underlying contextual fear memory in mice and showed that a single memory is distributed across multiple brain regions, rather than just the amygdala and hippocampus [72, 75].

This chapter's research question aims at examining the underlying circuitry that is activated during the encoding and retrieval of a contextual cold experience. Moreover, we aimed at understanding the underlying brain networks of cold memories by analyzing the functional connectivity between multiple regions. Here, we designed a brain-wide c-Fos detection pipeline to be able to simultaneously count c-Fos$^+$ neurons in hippocampal, hypothalamic, and cortical regions from animals that were encoding and recalling a cold experience.

METHODS

2.2.1 Mice

All experiments were performed with C57BL/6J mice. Male mice were used in all experiments. All mice were group-housed in a 12:12-h (07:00-19:00) light-dark colony room at 22°C. Food and water were provided *ad libitum*, and all testing was performed during the light phase. Mice used for experiments were approximately 8-12 weeks of age. All experiments were conducted in accordance with the European Directive 2010/63/EU, under an authorization issued by the Health Products Regulatory Authority Ireland and approved by the Animal Ethics Committee of Trinity College Dublin.

2.2.2 Brain Harvest

Brains were harvested from mice that went through the above-described Cold Memory Schedule (methods chapter 1). All brains were harvested on baseline day 1, cold day 1, baseline day 2 and test day 1. To ensure that the differences seen were due to the differences in conditions and not time of day, all brains were harvested exactly 3 hours after the mice were put inside the Promethion cages.

2.2.3 Brain Tissue Preparation

Mice were transcardially perfused with 4% paraformaldehyde (PFA), and brains were fixed in 4% PFA overnight. The next day, brains were transferred into phosphate buffered saline (PBS) and kept at 4°C. They were subsequently sliced in 100 μm coronal sections with a vibratome (Leica VT1200 S) and collected in PBS.

2.2.4 Immunohistochemistry

To get clear immunolabeling we utilized the previously described iDISCO-based immunohistochemistry protocol [76, 80]. Sections were rinsed 3 times in 1X (PBS) before subsequently being dehydrated in 50% MeOH/ PBS at room temperature for 2.5 hours. Sections were then rinsed 3 times in 0.2% PBS with TritonX-100 (PBST) and blocked in 0.2% PBST with 10% dimethyl sulfoxide (DMSO) and 6% normal goat serum (NGS) for two hours at room temperature. After blocking, they were washed 3 times in PBS with 0.2% Tween-20 and 10 μg/ml heparin (PTwH). Sections were then incubated with primary antibody rabbit polyclonal IgG anti-c-Fos (1:1000) Invitrogen,

Waltham, MA) at 4°C on a shaker for 3 days in PTwH with 5% DMSO and 3% NGS. On day 4, sections were washed 3 times in PTwH and incubated with a secondary antibody Alexa 568 Anti-Rabbit IgG (1:500, Invitrogen, Waltham, MA) overnight at 4°C. The next day, sections were washed three times in PTwH, followed by 3 washes in PBS at room temperature. Finally, sections were stained with DAPI in PBS for 10 minutes followed by a final wash in PBS. Sections were then mounted on superfrost slides using Vectashield-DAPI, cover slipped and sealed.

2.2.5 Confocal Imaging

All images were taken on a confocal scanning microscope (Leica TCS SP8, Leica Microsystems Inc.). Fluorescence from DAPI was detected at 417–488 nm, and Alexa Fluor 568 was detected at 595–650 nm. Sections were imaged with a dry 20x objective (NA 0.70, working distance 0.5 mm), with a pixel size of 1.14 x 1.14 μm^2, a z step of 3 μm, and a z-stack of approximately 25 μm. Fields of view were stitched together to form tiled images by using an automated stage and the algorithm of the LAS X software.

2.2.6 Automated Cell Counting

To perform automatic brain wide analysis of c-Fos+ cells we used the NeuroInfo software (MBF Bioscience). Briefly, immunohistochemistry-labelled whole brain sections were aligned to the Allen Mouse Brain Atlas using the registration tool within the program [81]. Here, brain sections were matched to the most closely corresponding atlas plate. All sections were manually adjusted where necessary, to ensure accurate fit. After the correct atlas plate was identified, all anatomical regions of interest were delineated and measured for size in μm^2. Next, c-Fos+ cells were identified using the cell detection workflow. Throughout all sections, only cells between 7 μm and 19 μm were counted for size consistency. These parameters where then combined with a deep learning algorithm to successfully identify c-Fos+ cells. Counts were then checked for accuracy and adjusted were necessary. Finally, detected cells were mapped to the Allen Mouse Brain Atlas and tallied in the corresponding anatomical brain structure. Normalized counts (cells per μm^2) were subsequently plotted into Prism 10.0 for further analysis.

2.2.7 Network Analysis

Cross-correlations between all pairs of regions were calculated in R as previously reported [74]. Pearson's correlations were computed in all cases after which networks were created using the igraph package. To be able to interpret the networks, correlations with an absolute value below 0.5 were not included. Both positive and negative correlations were included in the networks.

2.2.8 Statistics

All data were analyzed using Prism 10. All data were graphed as means ± Standard errors of the mean (SEM). An alpha level of 0.05 was used as a criterion for statistical significance. The results of figures 2.3.1, 2.3.2, 2.3.3 and 2.3.4 were analyzed using repeated measure one-way ANOVAS with Tukey's multiple comparison tests. Figures 2.3.1 and 2.3.2 were furthermore analyzed with simple linear regressions. Figure 2.3.5 was analyzed using unpaired t-tests. Figures 2.3.7 and 2.3.8 were made using Pearson's correlations.

2.2.9 Figure design and visualization

Figures and graphical illustrations were created with Biorender (Biorender.com).

RESULTS

2.3.1 Retrieval of a cold memory increases neural activity in the hippocampus.

To identify the neuronal activity patterns underlying cold memory encoding and retrieval, we examined c-Fos expression throughout multiple brain regions. Here, we compared c-Fos activity during baseline (BL1), cold training day 1 (CL1) and test day (T1), to determine which regions were active during specific conditions (Figure 2.3.1a). To enable automated c-Fos detection in various hippocampal regions, all brains were run through an automated brain-wide counting pipeline (Figure 2.3.1b-c). Our results show no differences in the number of c-Fos$^+$ cells in the DG between the BL1, CL1 and T1 day conditions (Figure 2.3.1d). However, increased c-Fos activity was found in the CA3 and CA1 subregions of the hippocampus at CL1 and T1, compared to BL1, suggesting that CA3 and CA1 are important areas that are involved in contextual cold memories (Figure 2.3.1e-f). Although no raw differences in c-Fos$^+$ cells were found in the DG between the three conditions, we hypothesized that there may be differences in how this region interacts with whole-body metabolism. As such, we correlated c-Fos activity in the DG with oxygen consumption (VO_2) at BL1, CL1, or T1 (Figure 2.3.1g). Our results show that at BL1, there is no correlation between c-Fos activity in the DG and metabolic rate. At CL1, there is a significant negative correlation between VO_2 and DG activity. However, at T1, there is a significant positive correlation between VO_2 and DG activity (Figure 2.3.1g). A similar correlation pattern was observed in CA1 but not in CA3 (Figure 2.3.1h-i). We conclude that various subregions of the hippocampus are involved in the encoding or retrieval of contextual cold memories, and that the DG and CA1 play a role on T1 in regulating whole-body metabolism.

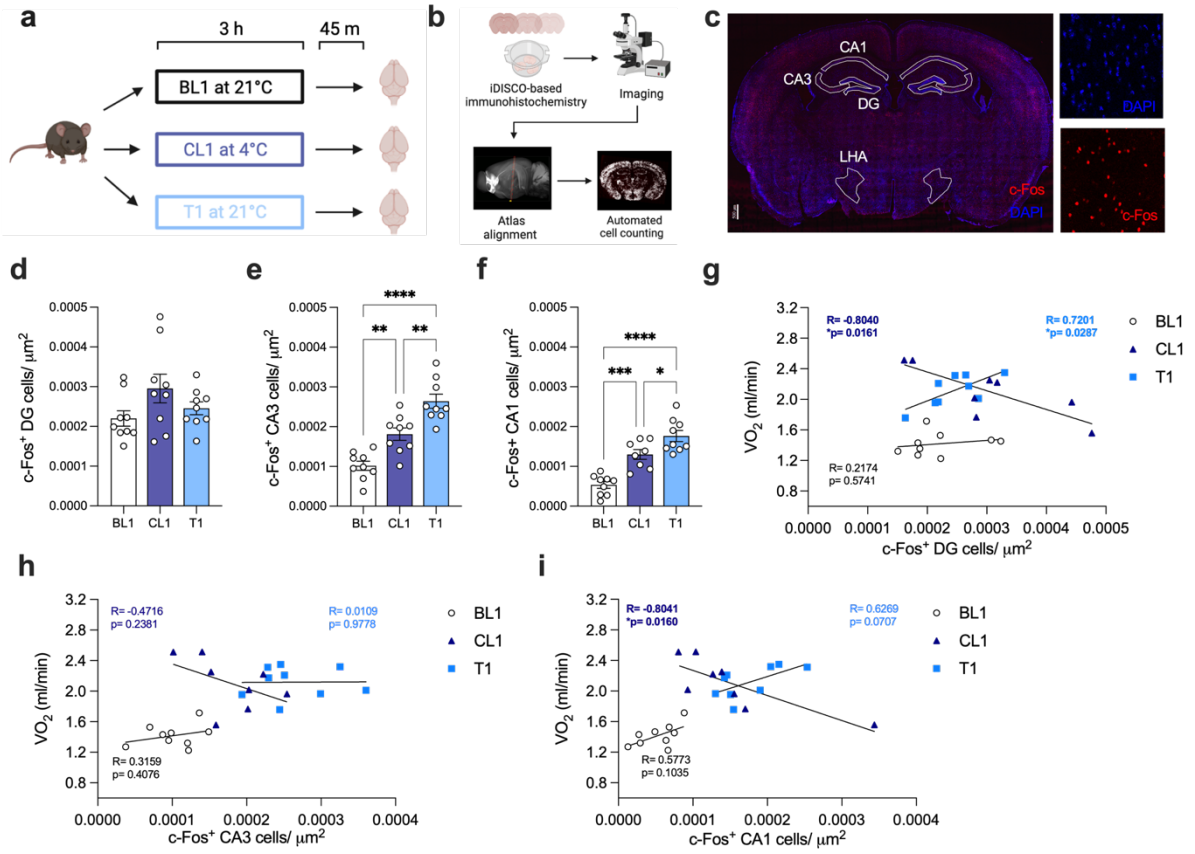

Figure 2.3.1 Neural activity in the hippocampus increases during the retrieval of a cold memory. **(a)** Diagrammatic representation of experimental timeline for tissue collection. **(b)** Diagrammatic representation of the automated brain-wide c-Fos detection pipeline used to identify c-Fos$^+$ cells in multiple brain regions simultaneously. (**c)** Representative image of hippocampal slice (left) with c-Fos$^+$ cells (red; bottom-right) and DAPI$^+$ cells (blue; top-right). Comparison of c-Fos$^+$ neurons normalized to area in the **(d)** DG **(e)** CA3 and **(f)** CA1 between mice housed during BL1, CL1 and T1. **(g)** Correlation between c-Fos$^+$ cells in the DG and oxygen consumption between mice housed during BL1, CL1 and T1. **(h)** Correlation between c-Fos$^+$ cells in the CA3 and oxygen consumption between mice housed during BL1, CL1 and T1. **(i)** Correlation between c-Fos$^+$ cells in the CA1 and oxygen consumption between mice housed during BL1, CL1 and T1. Data shown as mean ± SEM, *n* = 7-10 mice per group.* $p < 0.05$, ** $p < 0.01$, *** $p < 0.001$, **** $p < 0.0001$. BL1, baseline 1; T1, Test 1; CL1, cold 1; DG, dentate gyrus; CA3, cornu ammonis 3; CA1, cornu ammonis 1; VO_2, oxygen consumption.

2.3.2 The hypothalamus is important for the encoding and retrieval of a cold memory.
Previous studies have identified the lateral hypothalamic area (LHA), medial preoptic area (MPO), and lateral preoptic area (LPO) as key regions involved in thermoregulation [82]. Therefore, we aimed at comparing c-Fos activity in these regions at BL1, CL1 and T1 (Figure 2.3.2a). In line with previous studies, we show that c-Fos activity in the LHA is upregulated when mice are exposed to the cold during CL1 (Figure 2.3.2b). Interestingly, we found similar levels of activity in this area when mice were retrieving a cold memory on T1 compared to that on CL1. Although we also observed increased activity in the MPO and LPO during cold exposure (Figure 2.3.2c-d), we found no increases in c-Fos activity in these areas on T1. Next, we analyzed c-Fos activity in four additional hypothalamic regions to determine whether hypothalamic activity generally increased after cold exposure and cold memory retrieval (Figure 2.3.2e-h). We found no significant differences in activity between BL1, CL1 or T1 in the periventricular hypothalamic nucleus (PVi), arcuate hypothalamic nucleus (ARH), ventromedial hypothalamic nucleus (VMH) or dorsomedial nucleus of the hypothalamus (DMH). This suggests that only certain subregions of the hypothalamus are important for the encoding and retrieval of a contextual cold memory. Finally, we tested whether the LHA, MPO and LPO correlated with metabolic rate. We found that mice that were exposed to the cold on CL1 showed a positive correlative trend between c-Fos activity in the LHA and oxygen consumption (Figure 2.3.2i). This trend was not found in any other condition or hypothalamic region (Figure 2.3.2j-k). These findings suggest that the LHA is important during encoding and retrieval of a cold memory, and that it correlates with metabolic rate during a cold experience.

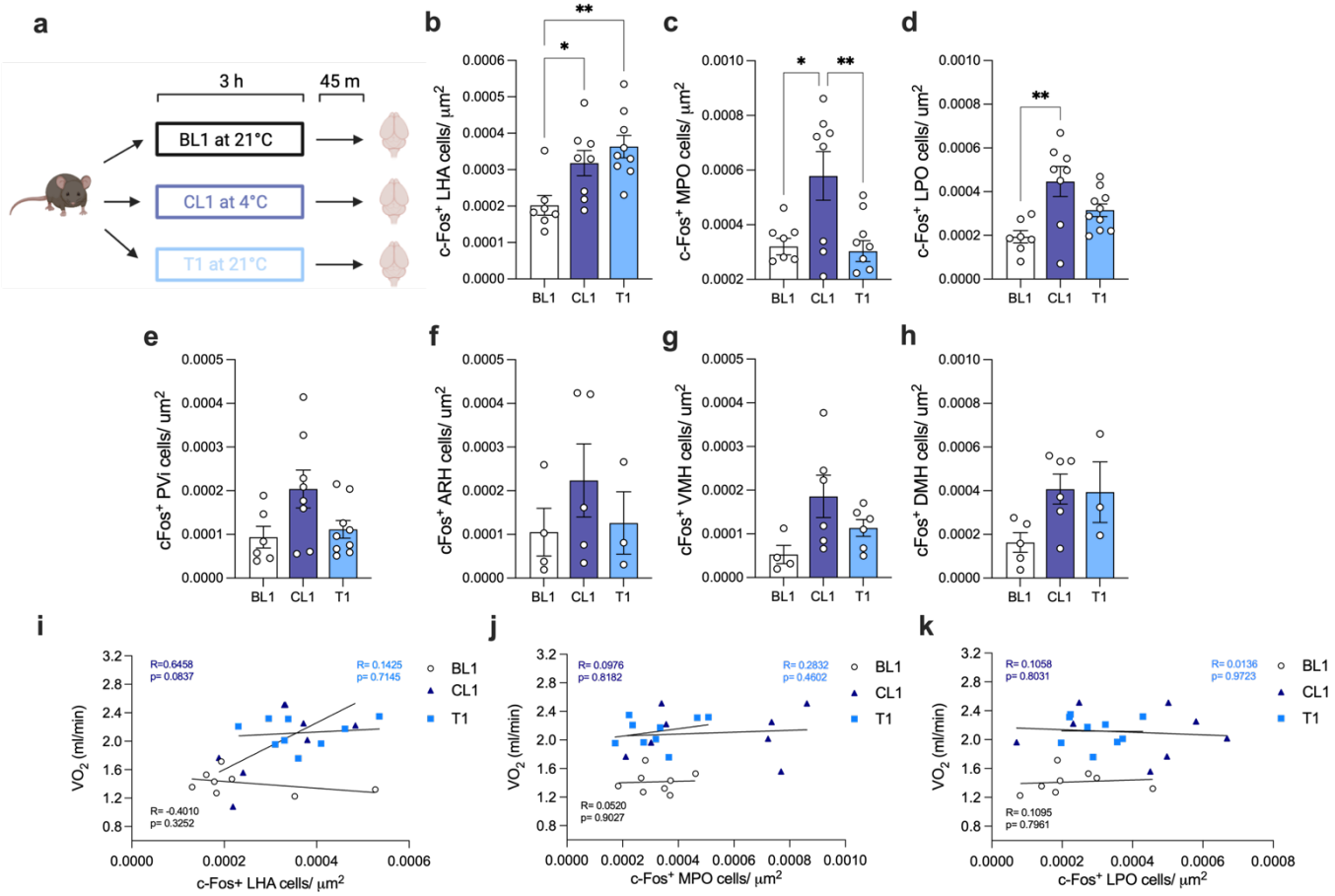

Figure 2.3.2 Retrieval of a contextual cold memory increases neural activity in specific regions of the hypothalamus. (a) Diagrammatic representation of experimental timeline for tissue collection. Comparison of c-Fos$^+$ neurons normalized to area in the **(b)** LHA **(c)** MPO **(d)** LPO **(e)** PVi **(f)** ARH **(g)** VMH and **(h)** DMH between mice housed during BL1, CL1 and T1. **(i)** Correlation between c-Fos$^+$ cells in the LHA and oxygen consumption between mice housed during BL1, CL1 and T1. **(j)** Correlation between c-Fos$^+$ cells in the MPO and oxygen consumption between mice housed during BL1, CL1 and T1. **(k)** Correlation between c-Fos$^+$ cells in the LPO and oxygen consumption between mice housed during BL1, CL1 and T1. Data shown as mean ± SEM, *n* = 3-10 mice per group.* $p < 0.05$, ** $p < 0.01$. BL1, baseline 1; T1, Test 1; CL1, cold 1; LHA, lateral hypothalamic area; MPO, medial preoptic area; LPO, lateral preoptic area; PVi, periventricular hypothalamic nucleus, intermediate part; ARH, arcuate hypothalamic nucleus; VMH, ventromedial hypothalamic nucleus; DMH, dorsomedial nucleus of the hypothalamus; VO_2, oxygen consumption.

2.3.3 Encoding and retrieval of a cold memory increases activity in the insular and somatosensory cortex.

The agranular insular cortex (AI) was recently been found to be involved in body-brain interactions, whereas the primary somatosensory cortex (SSp) has been shown to be a part of the neural circuitry underlying cold perception [8, 83]. Therefore, to further understand what brain regions are involved when mice encode and retrieve a cold experience, we quantified c-Fos activity in the insular and somatosensory cortex (Figure 2.3.3a). We found that both the AI and the SSp were highly activated when mice were exposed to a cold environment at CL1 (Figure 2.3.3b-c). In line with previous literature, this suggests that both cortical regions are important for thermal perception specifically and that they are part of the multimodal sensory input system. Interestingly, we found that the AI and SSp were also highly active when mice were retrieving a cold memory at T1 (Figure 2.3.3b-c). As such, we conclude that the AI and the SSp are important for both the encoding and the retrieval of cold memories.

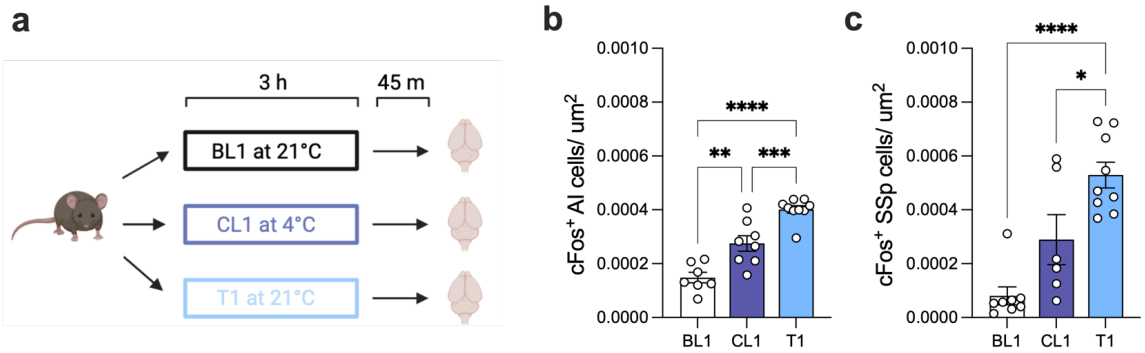

Figure 2.3.3 The insular and somatosensory cortex are important for the encoding and retrieval of cold memories. (a) Diagrammatic representation of experimental timeline for tissue collection. Comparison of c-Fos$^+$ neurons normalized to area in the **(b)** AI and **(c)** SSp between mice housed during BL1, CL1 and T1. Data shown as mean ± SEM, *n* = 6-9 mice per group.* $p < 0.05$, ** $p < 0.01$, *** $p < 0.001$, **** $p < 0.0001$. BL1, baseline 1; T1, Test 1; CL1, cold 1; AI, agranular insular area; SSp, primary somatosensory area; VO_2, oxygen consumption.

2.3.4 The amygdala is not important for the retrieval of a cold memory.

Previously, we have shown that mice avoid a cold-paired context if given the option (Chapter 1). Therefore, we hypothesized that a cold experience is associated with a negative valence, and that this experience is potentially linked to stress. Previous studies have extensively shown that stress exposure can induce amygdala activation and that this area is involved in the processing of emotionally arousing events [84]. Moreover, the bed nucleus of the stria terminalis (BST), has been identified as a potentially important area that mediates longer lasting responses to sustained stressful events [85]. To exclude the possibility that the above-described results are solely due to stress, we quantified c-Fos activity throughout multiple amygdalar regions and in the BST during BL1, CL1 and T1 (Figure 2.3.4a). In line with previous literature, we found that the BST and the central amygdalar nucleus (CeA) were significantly more activated during CL1 compared to BL1 (Figure 2.3.4b-e). No differences were found in the basolateral amygdalar nucleus (BLA) or the basomedial amygdalar nucleus (BMA). Moreover, we found no significant increases in any region during the retrieval of a cold memory on T1. These data suggest that being exposed to a cold environment is potentially stressful, yet retrieving a contextual cold memory is not stress dependent. As such, we conclude that although some stress is involved with real time cold exposure, our previously established effects on T1 are not specifically caused by stress.

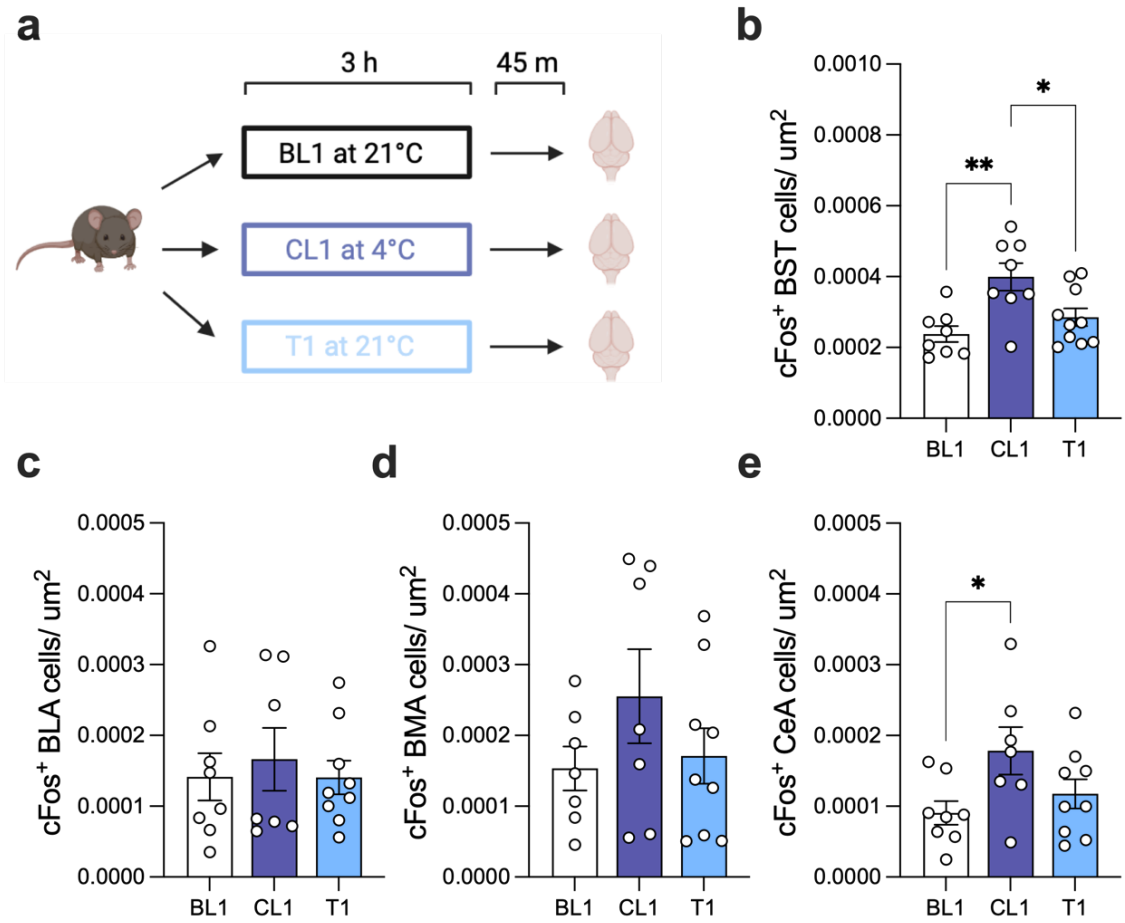

Figure 2.3.4 The amygdala is not activated during the retrieval of cold memories. (a) Diagrammatic representation of experimental timeline for tissue collection. Comparison of c-Fos$^+$ neurons normalized to area in the **(b)** BST **(c)** BLA **(d)** BMA and **(e)** CeA between mice housed during BL1, CL1 and T1. Data shown as mean ± SEM, *n* = 7-10 mice per group. * $p < 0.05$, ** $p < 0.01$. BL1, baseline 1; T1, Test 1; CL1, cold 1; BST, bed nuclei of stria terminalis; BLA, basolateral amygdalar nucleus; BMA, basomedial amygdalar nucleus; CeA; central amygdalar nucleus; VO_2, oxygen consumption.

2.3.5 Increases in neural activity are specific to the cold context.

To confirm that the previously found increases in c-Fos activity were specifically due to the cold-paired context, we compared raw differences in c-Fos$^+$ cells between BL2 and T1 (Figure 2.3.5a). This enabled us to compare neural activity caused by re-exposure to a cold-paired context with neural activity caused by re-exposure to a neutral context. Our results showed no differences in c-Fos activity between BL2 and T1 in the DG or CA3 (Figure 2.3.5b-c). However, increased neural activity was found in the CA1 on T1 compared to BL2 (Figure 2.3.5d), suggesting that the CA1 may have a unique role with regards to context specificity of cold memories. Although we found no significant differences between the BL2 and T1 in the LHA, there was a trending increase in c-Fos$^+$ cells at T1 compared to at BL2 (Figure 2.3.5e). No differences were found in the MPO; however, a significant increase was found in the LPO (Figure 2.3.5f-g). These data suggest, in line with our previous results, that the lateral sections of the hypothalamus are important for the retrieval of contextual cold memories. Next, we compared BL2 neural activity with T1 in the BST and found no differences between the two conditions, potentially suggesting that re-exposure to the cold context is not more or less stressful than re-exposure to a neutral context (Figure 2.3.5h). Finally, we found a large difference in neural activity in the AI at T1 compared to BL2 (Figure 2.3.5i). Taken together, these data suggest that the increases in c-Fos$^+$ cell activity found in the CA1, LHA, LPO and AI on T1 are context specific and important for the retrieval of a cold memory.

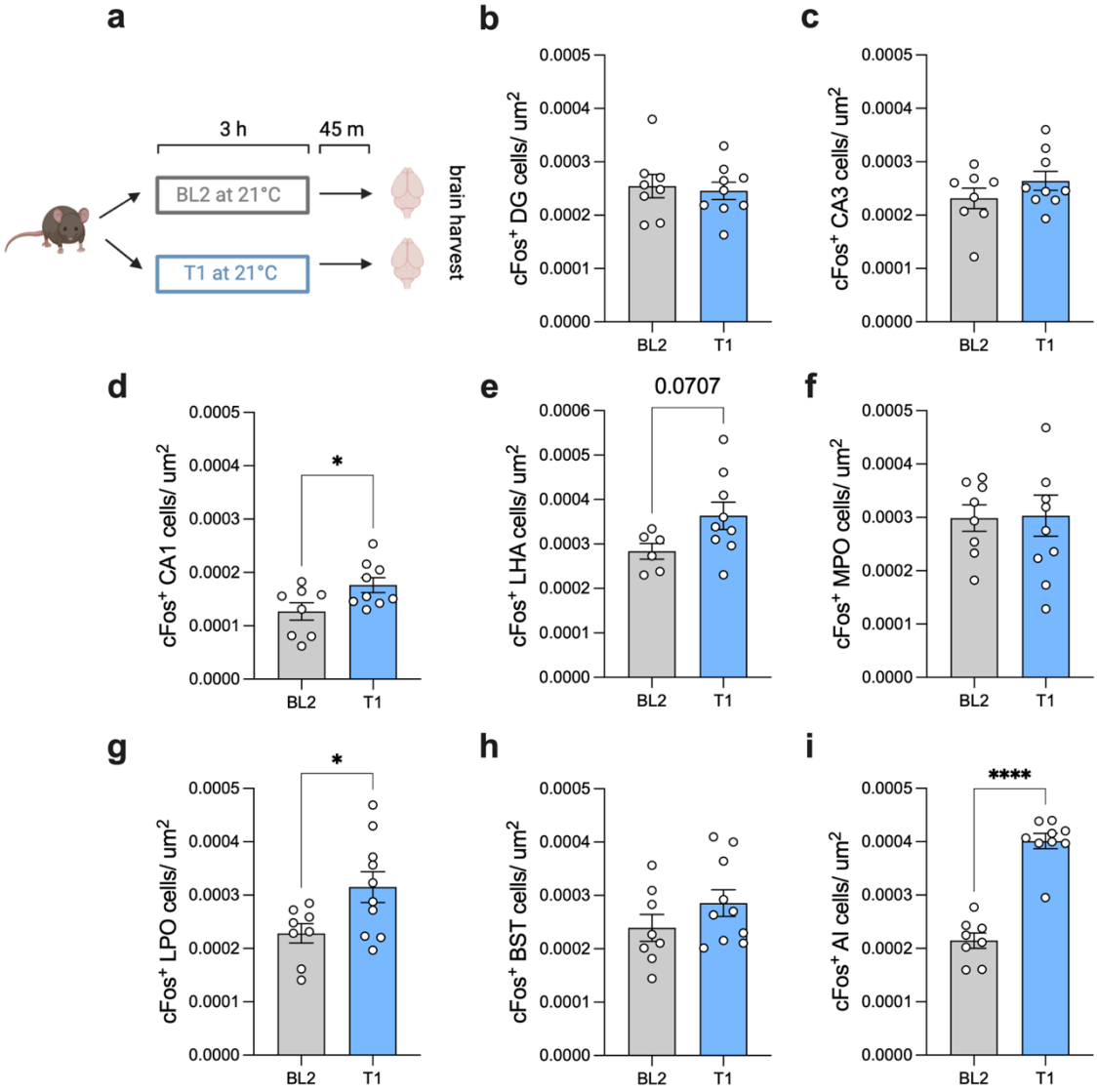

Figure 2.3.5 Increases in neural activity are specific to the cold context.
(a) Diagrammatic representation of experimental timeline for tissue collection. Comparison of c-Fos$^+$ neurons normalized to area in the **(b)** DG **(c)** CA3 **(d)** CA1 **(e)** LHA **(f)** MPO **(g)** LPO **(h)** BST and **(i)** AI between mice housed during BL1, CL1 and T1. Data shown as mean ± SEM, *n* = 6-10 mice per group. * $p < 0.05$, **** $p < 0.0001$. BL2, baseline 2; T1, Test 1; BST, bed nuclei of stria terminalis; DG, dentate gyrus; CA3, cornu ammonis 3; CA1, cornu ammonis 1; LHA, lateral hypothalamic area; MPO, medial preoptic area; LPO, lateral preoptic area; BST, bed nuclei of stria terminalis; AI, agranular insular area; VO_2, oxygen consumption.

2.3.6 Functional connectivity between the hippocampus and the hypothalamus increases during cold retrieval.

To understand how functional connectivity between brain regions is altered during cold exposure and cold memory retrieval, we performed further correlational analyses of c-Fos activity across brain regions (Figure 2.3.6a-c). From this, we built correlational networks that corresponded to BL1, CL1, and T1 to further visualize changes in functional connectivity (Figure 2.3.7a-c). We found that, compared to the baseline network, there was increased functional connectivity between hypothalamic regions when mice are exposed to the cold (Figure 2.3.7a-b). Moreover, we found an increase in functional connectivity between the hippocampus and the hypothalamus when mice are recalling the cold, compared to when they are experiencing the cold, which is not observed in the baseline network (Figure 2.3.7a-c). These data suggest that this is a plasticity feature that only forms after mice encode a cold contextual memory.

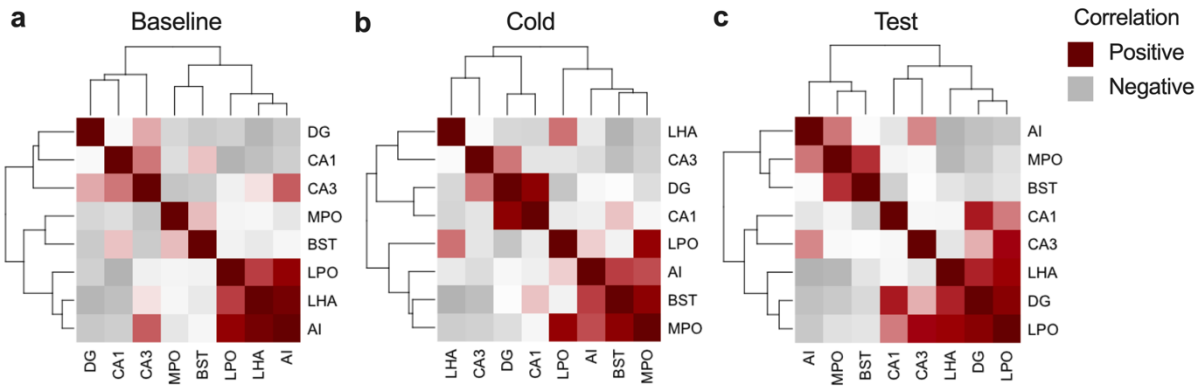

Figure 2.3.6 Functional connectivity between the hippocampus and hypothalamus increases during cold recall. (a) Correlation matrix of c-Fos$^+$ cells normalized to area during baseline day (BL1), with positive (red) and negative (grey) correlations. **(b)** Correlation matrix of c-Fos$^+$ cells normalized to area during cold training day (CL1), with positive (red) and negative (grey) correlations. **(c)** Correlation matrix of c-Fos$^+$ cells normalized to area during the recall of a contextual cold memory on test day, with positive (red) and negative (grey) correlations. *n* = 7-9 mice per group. DG, dentate gyrus; CA3, cornu ammonis 3; CA1, cornu ammonis 1; LHA, lateral hypothalamic area; MPO, medial preoptic area; LPO, lateral preoptic area; BST, bed nuclei of the stria terminalis; AI, agranular insular area.

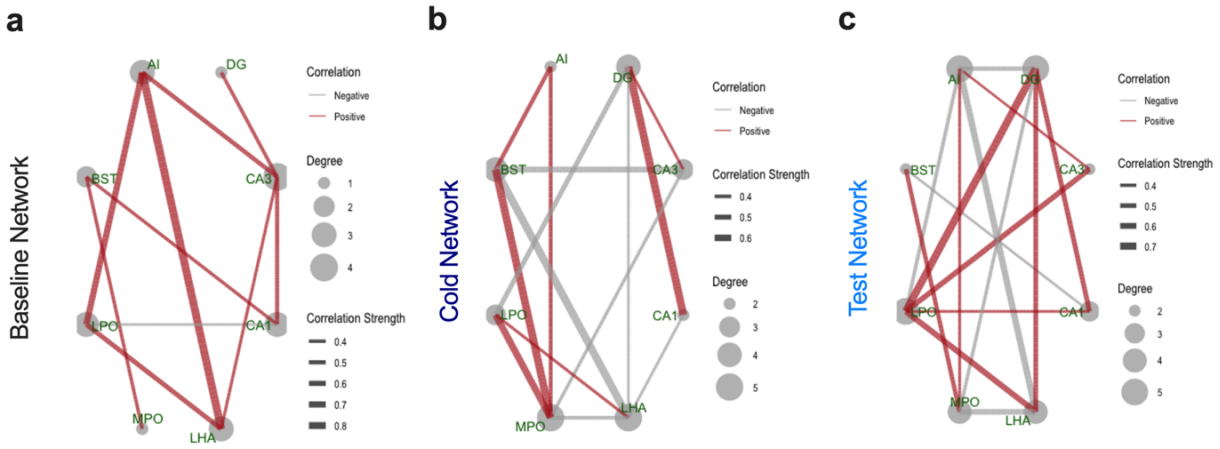

Figure 2.3.7 Functional connectivity between the hippocampus and the hypothalamus is important for the retrieval of a cold memory. Correlation analysis of c-Fos^{+} cells between brain regions at **(a),** baseline (BL1), **(b),** cold exposure (CL1), and **(c),** cold recall (T1). Correlations with R>.5 are displayed in red. Correlations with R<.5 are displayed in grey. Line thickness is proportional to the strength of the correlation (R value). *n* = 7-10 mice per group. DG, dentate gyrus; CA3, cornu ammonis 3; CA1, cornu ammonis 1; LHA, lateral hypothalamic area; MPO, medial preoptic area; LPO, lateral preoptic area; BST, bed nuclei of the stria terminalis; AI, agranular insular area.

DISCUSSION

In this chapter, we used an automated brain-wide detection protocol to determine which brain regions are important for encoding and retrieval of a cold experience. With this protocol, we found an increase in c-Fos$^+$ cell activity in specific hippocampal, hypothalamic, and cortical regions. Moreover, we showed that the c-Fos activity in the DG, CA1 and LHA correlated with whole-body metabolism during the encoding and retrieval of cold memories. By analyzing several amygdalar regions, we also found that although a cold experience may be stressful, retrieving a cold memory is not. Finally, we showed that the retrieval of a cold memory resulted in increased functional connectivity between the hippocampus and the hypothalamus.

The development of clearing techniques and molecular labeling methods that allow for brain-wide imaging at cellular resolution has revolutionized the way brain activity is analyzed. With these techniques, we were able to simultaneously assess IEG activity in multiple brain regions and determine how the activity in these regions correlate with one another. By doing so, we aimed at obtaining a more accurate representation of neural activity following the retrieval of a cold memory. However, in this study we only analyzed c-Fos activity. To further understand the role that different IEGs play in the encoding and retrieval of contextual cold experiences, future studies are necessary that perform brain-wide analyses with other IEGs such as Arc, for example. Indeed, recent studies have shown low overlap between ensembles labeled by both Arc and c-Fos, despite them labeling the same experience [86].

When analyzing the neural activity of the DG, we found no differences between any of the conditions that were quantified. The DG has previously been shown to be crucial for the formation of contextual representations, pattern separation and encoding of spatial information [87-89]. In general, all four of the investigated conditions (BL1, CL1, BL2 and T1) were highly contextual experiences. As such, the similar levels of c-Fos$^+$ cell activity that were observed between conditions are in line with published literature [87, 88]. Interestingly, both the CA3 and CA1 showed increased activity after cold exposure during CL1. This raises the question of whether there are innate cold-sensing cells present in these areas. The hippocampus has been found to hold warm-sensitive cells, as exposure to warm temperatures resulted in increased c-Fos expression in the DG [90]. To our knowledge, innate cold-sensitive cells have not been

identified in the hippocampus specifically. As such, future follow up studies will be necessary to determine whether the CA3 and CA1 do indeed contain such cells. In this study, we analyzed neural activity during CL1, to prevent confounding memory effects that might be present during CL2 and CL3. Future comparisons of c-Fos activity between the three cold training days may give us more insight as to what regions hold innate cold-sensing cells in general, in addition to how a memory representation might change throughout repeated exposure to the same contextual experience.

As described above, many studies have previously linked the hypothalamus with the coordination of thermoregulatory responses. In alignment with this, we found that the LHA, MPO and LPO are activated when mice are exposed to a cold environment. We also found that this increase does not happen throughout the entire hypothalamus, suggesting that cold experiences activate specific hypothalamic subregions. Interestingly, we found that from all the regions examined, only the LHA is activated when mice retrieve a cold memory. This finding fits with the idea that the LHA may act as an integrator of metabolic and environmental needs [91]. Indeed, it has been suggested that LHA neurons can sense glucose, leptin, and CO_2, and that this structure is essential for metabolic function in general [92]. Future studies are needed to investigate how the LHA exerts its effects on whole-body metabolism in general and during cold challenges specifically.

Our results indicated that cortical regions are involved when mice are exposed to a cold environment, as both the AI and SSp showed increased c-Fos activity at CL1. In humans, insular infarctions have been shown to result in the loss of cold- and cold pain perception, and in rodents a secondary somatosensory representation has been found to be located in the AI [93-95]. The AI might therefore be involved in cold-perception, in addition to being important for body-brain interactions. Interestingly, both the SSp and the AI showed increased activity when mice retrieved a contextual cold memory at T1. This raises the question of whether mice also perceive or ‘feel’ cold when they retrieve a cold memory. For example, it is possible that mice perceive the environment as actual cold when they recall a contextual memory, and that this is due to increased activity in cortical regions.

Finally, by analyzing the BST and amygdalar regions, we attempted to determine whether a cold experience and a cold memory are associated with stress. We found increased activity in the BST and CeA during CL1 but not during T1. This suggests that being exposed to a cold environment causes some stress, but that remembering a cold environment does not. However, it remains complicated to disentangle the exact effects that stress and cold have on different brain regions, as cold exposure will inevitably be a negative and stressful experience. It is therefore likely that mice remember that a specific context is associated with the cold because the original cold experience became salient due to it being stressful or negative. We therefore conclude that stress is involved during cold exposure, but that our findings during memory retrieval are not due to stress only.

In this chapter we aimed at furthering our understanding into the brain circuitry that underlies cold exposure and the retrieval of a cold memory. Taken together, we show that specific hippocampal and hypothalamic regions are involved in the encoding and retrieval of a cold memory. These findings were then used as a guide in subsequent chapters. Although we quantified many different regions, we were not able to analyze the entire brain. Future studies will be necessary where intact brains are cleared and analyzed for IEG activity to get a complete picture regarding the underlying whole-brain networks that are important for the encoding and retrieval of temperature memories.

Chapter 3:

Cold-sensitive memory ensembles are located in the DG, LHA, and MPO which correlate with metabolic rate.

INTRODUCTION

3.1.1 Past and present definitions of the engram.

Memory is defined as the ability to encode, store, and retrieve information [96]. Indeed, in order to develop adaptive behavior to survive, animals encode information through learning processes and store this information in the form of memories [97]. In 1904, Richard Semon introduced the term ‘engram’ for the first time to describe how memories are represented in the brain [98, 99]. Semon described the engram as ‘’the enduring though primarily latent modification in the irritable substance produced by a stimulus’’ [98, 99]. Essentially, Richard Semon considered the engram to be the equivalent of a memory trace. Years after this conceptualization, the psychologist Karl Lashley attempted to systematically locate an engram in the rodent brain [100-102]. In his studies, Lashley trained animals on a memory task and subsequently removed cortical tissue from different locations and in varying sizes (Figure 3.1.1). He would then observe how these lesions would affect the behavior of animals on the memory task. Lashley concluded that the behavioral impairments he subsequently found mostly correlated with the size off the lesion, and not with the location. His final conclusion therefore was that engrams cells were not located in the cortex specifically, and that they were too difficult to find in general [103].

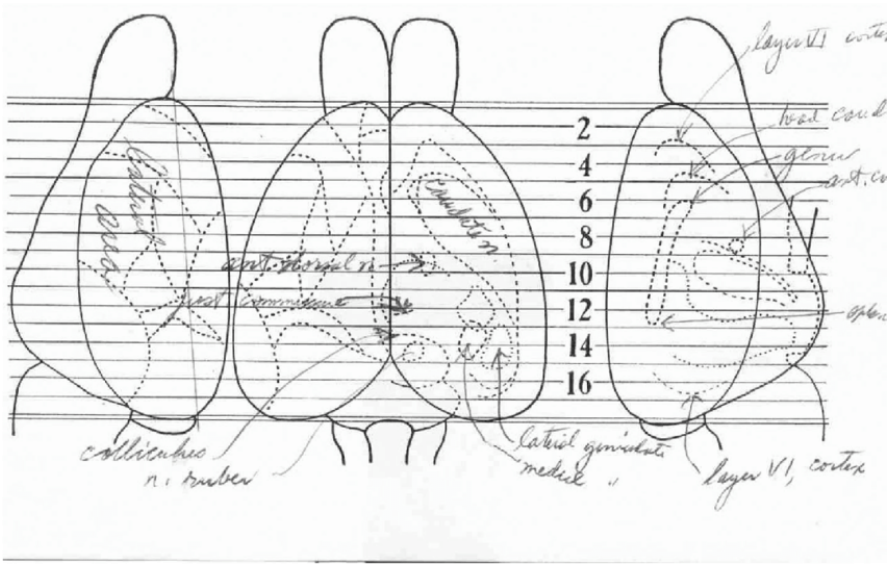

Figure 3.1.1 Lesion localization method. Lesion localization method with Lashley’s handwritten anatomical notes. *Adapted from Nadel & Maurer, 2020 [102].*

Although Lashley was not successful in finding the engram, he and Semon inspired many other scientist to search for it [104-106]. Based on Semon's theories, the engram is currently defined as the enduring physical and chemical changes that were elicited by learning and that underlie new memories [15, 107]. According to this definition, cells are considered to be engrams if: 1) they are activated by a learning experience, 2) they are physically and/or chemically modified by that learning experience, 3) reactivation of these cells results in the retrieval of the original memory, and 4) they are necessary for the retrieval of the original memory [15, 107, 108].

3.1.2 Finding the engram with observational studies.

In the recent decade, the hunt for the engram has intensified due to the development of novel tools that enable scientists to visualize and manipulate individual cells. Many of these tools rely on IEG promoters to visualize neurons that were active during a particular experience. Indeed, cells that were active during a training experience can be labeled using viral or genetic strategies that allow temporally inducible IEG promotors that enable the expression of long-lasting fluorescent markers [109-111]. Cells active during the memory retrieval can subsequently be identified by using IEG immunohistochemistry. The overlapping cells that were both active during training and during memory retrieval are then identified to study engram biology (Figure 3.1.2).

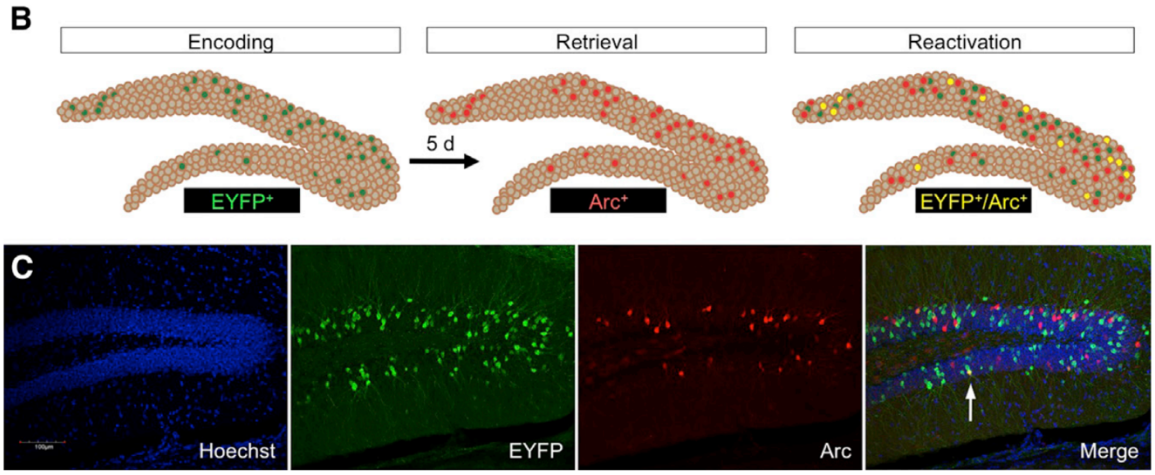

Figure 3.1.2 Indelible labeling of engram cells. Cells that were active during the encoding of an experience are labeled with EYFP. Cells that were active during the retrieval of the experience (the memory) are identified with the IEG Arc. The cells that are active during both experiences are engram cells. *Adapted from Denny et al., 2014 [110].*

One of the earliest studies using these techniques showed that neurons that were active during an auditory fear conditioning task could be labeled in the amygdala. After three days, mice were returned to the training context and active neurons were marked with the IEG *ZIF*268. To identify the engram cells associated with auditory fear conditioning, all cells that were active during training and memory retrieval were quantified. In this study, they showed that approximately 11% of the total cells in the amygdala were active during both experiences and were therefore identified as engram cells [109]. Using similar techniques, engram cells have been observed across different brain regions such as the hippocampus and the cortex, for many different types of experiences [110, 112-114]. Taken together, observational studies like the ones above have provided evidence for the existence of the engrams cells that were described by Semon over a century ago.

3.1.3 Finding the engram with gain-of-function studies.

To show that engram cells are actually necessary for the representation of an experience, various studies have aimed at artificially reactivating engram cells specifically. This has been made possible by combining optogenetic tools with engram labeling techniques (Figure 3.1.3). In the first engram specific gain-of-function study, researchers labeled DG neurons that were active during contextual fear conditioning with the excitatory opsin channelrhodopsin 2 (ChR2). They subsequently showed that artificial reactivation of the labeled DG neurons induced the learning-specific conditioned response [16]. Various studies have now shown that artificial reactivation of engram cells can induce memory expression in a variety of tasks. For example, optogenetic stimulation of fear acquisition neurons was shown to elicit fear in mice, whereas activation of extinction neurons suppressed fear [113]. Similar results have been shown for engram cells outside of the hippocampus, as artificial stimulation of fear engrams in the retrosplenial cortex (RSC) were shown to produce context-specific behavior [115]. Moreover, by combining engram technology with optogenetic reactivation researchers have been able to shed light on the underlying neural circuits of complex matters such as emotional memory, infantile and adult amnesia, and Alzheimer's disease [116-119]. Together, these experiments demonstrate that cells that are activated by learning are able to elicit memory recall once they are reactivated, and that these cells can be considered to be engram cells.

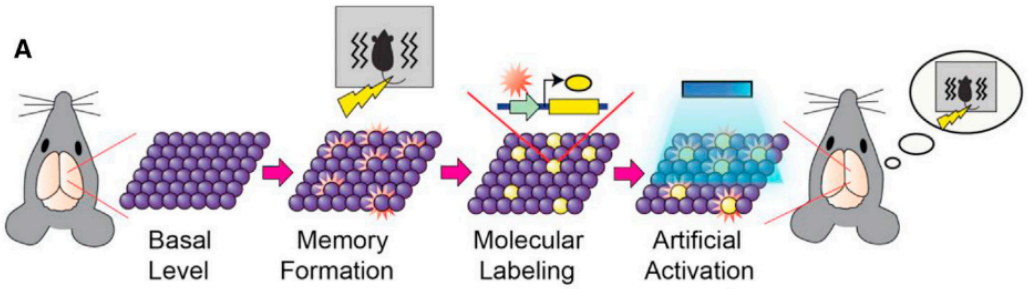

Figure 3.1.3 Artificially reactivating engram cells. Neurons that were active during the formation of fear memory were labeled with ChR2. Using blue light, these neurons are subsequently reactivated in a neutral context. *Adapted from Tonegawa et al., 2015 [108].*

3.1.4 Finding the engram with loss-of-function studies.

Loss-of-function studies rely on similar techniques as the gain-of-function studies described above (Figure 3.1.3). However, these studies aim at inhibiting memory-related neurons to cause memory impairments. Memory engrams have been successfully silenced in a variety of brain regions within the hippocampus and amygdala. For example, neuronal populations that were labeled in the DG or CA3 during fear memory acquisition were shown to cause impaired fear memory recall after optogenetic inhibition [110]. Similar results were found for other hippocampal regions, as memory impairments were found when labeled CA1 engrams were inhibited [120]. These types of studies hold a large translational value, as silencing engrams associated with maladaptive behaviors could prove to be beneficial in general. For example, silencing neurons associated with a cocaine memory was shown to result in reduced cocaine seeking behavior [121]. In general, these loss-of-function studies show that inhibiting memory engram cells leads to the disruption of a specific memory.

3.1.5 Engram labeling strategies.

Viral and genetic strategies that allow for the expression of fluorescent markers have proven to be key in order to label and study engram cells. In the past decade, many different strategies have been developed that allow for the labeling of neurons that were active during a training experience [122]. These strategies can generally be subdivided into two classes: IEG-based strategies and strategies using synthetic promoters (Figure 3.1.4). Both designs can be further subdivided into either doxycycline (dox) or tamoxifen dependent strategies. For instance, the Fos-tTa transgenic mouse is an example of a dox dependent IEG-based strategy. In this mouse, a Fos promoter drives expression of the repressible tetracycline transactivator (tTa), which is inhibited in the presence of dox. In the absence of dox, the tTa will bind to a tetracycline response element (TRE), where it will eventually cause the expression of an effector protein [109].

On the other hand, Robust Activity Marking (RAM) is a good example of a dox dependent viral strategy that uses a synthetic promoter. Here, a small synthetic promoter called PRAM drives the expression of a destabilized tTa, which in the absence of dox will bind to TRE and allow for the expression of an effector protein [123]. Dox dependent strategies have proven to be useful for the labeling of active neurons, however, these strategies have a large labeling window (1-3 days). Alternatively, tamoxifen dependent strategies have much smaller labeling windows (6-24 hours) and allow for permanent labeling of active neurons. The ArcCreER^{T2} and the TRAP2 mice are good examples of well documented tamoxifen dependent IEG-based labeling strategies. In both these lines, CreER^{T2} is knocked into the Fos or Arc translation sites. In the presence of tamoxifen (4-OHT), CreER^{T2} will translocate to the nucleus to recombine floxed alleles, which eventually results in the permanent expression of effector proteins [110, 111]. Finally, E-SARE is a well-known example of a viral strategy that uses a synthetic promoter that is tamoxifen dependent. This synthetic promoter has five repeats of a synaptic-activity responsive element (SARE) that drives CreER^{T2}. In the presence of tamoxifen, CreER^{T2} will translocate to the nucleus, allowing for temporal control and permanent labeling of active neurons [124]. Taken together, these and other strategies have enabled researchers to label and manipulate neurons that were active during a specific experience with high temporal control and specificity.

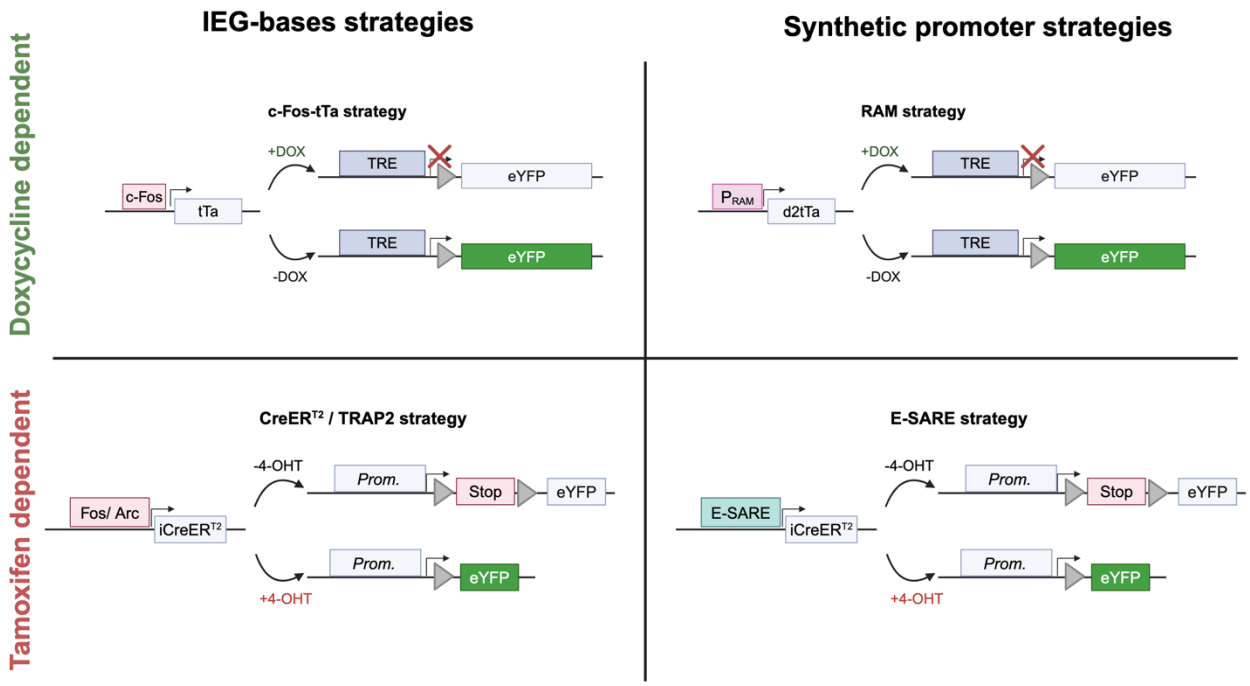

Figure 3.1.4 Engram labeling strategies. To label cells that were active during a particular experience, two strategies can be employed: IEG-based strategies or viral strategies using a synthetic promoter. Moreover, both designs can be further subdivided based on whether they are dependent on doxycycline or tamoxifen.

In this chapter, we set out to identify the engrams cells that are involved in a contextual cold memory. To do so, we created a novel transgenic mouse by combining TRAP2 transgenic mice with a R26R reporter line. This mouse was created to ensure consistent labeling in the hypothalamus. Here, we designed a labeling paradigm that would allow us to identify the cells that were active during the encoding and retrieval of a cold experience. Taken together, this chapter's research question aims at identifying cold-sensitive engrams and determining their influence on whole-body metabolism.

METHODS

3.2.1 Mice

All experiments were performed with TRAP2 x R26R mice. These mice were created by breeding heterozygous TRAP2 mice [111] with homozygous R26R mice [125]. Male mice were used in all experiments. All mice were group-housed in a 12:12-h (07:00-19:00) light-dark colony room at 22°C. Food and water were provided *ad libitum*, and all testing was performed during the light phase. Mice used for experiments were approximately 8-12 weeks of age. All experiments were conducted in accordance with the European Directive 2010/63/EU, under an authorization issued by the Health Products Regulatory Authority Ireland and approved by the Animal Ethics Committee of Trinity College Dublin.

3.2.2 Experimental labeling paradigm

Here, we adapted our previously developed cold training schedule (chapter 1) to enable the labeling of cold-sensitive engrams. Male mice were taken from their home cage each morning and individually housed in the Promethion cages for a maximum of eight hours. On day one and two, mice were placed into the Promethion cages at 21°C to allow them to habituate to the machine. On day three, mice were put into the Promethion cages at 21°C while metabolic and behavioral data were simultaneously recorded in order to establish baseline measurements (Context A). On day four, the cages were changed before the mice were placed inside. Contextual cues were added to the chambers, including wall and floor patterns, brighter lights, different bedding and 3 drops of acetic acid odor (Context B). Once the mice were placed into the cages, the temperature decreased in increments of ~10 degrees per hour. As such, the mice spent a total of 6 hours in the altered context at a temperature of 4°C. To label the neurons that were active during these 6 hours of 4°C cold exposure, mice were injected with tamoxifen five hours after being put in the Promethion cages. Immediately after labeling, all mice were returned to their home cages. Mice subsequently went through two additional training days as previously described. After these training days, mice were returned and kept in their home cages for a two-day break period. Next, on day nine, mice were put back into the Promethion cages without any of the additional cues at 21°C to allow for a second baseline measurement (Context A). Finally, on day ten half of the animals were put back into the cages (Context B) and the other half was kept in their homecage.

3.2.3 4-OHT

To label cold-sensitive engrams in TRAP2 x R26R transgenic animals, we intraperitoneally injected mice with 4-OHT (50 mg/ kg, Santa Cruz). All 4-OHT was freshly prepared on the labeling day in a mix of sunflower seed oil and castor oil (4:1, Sigma-Aldrich) at 10 mg/ml [126].

3.2.4 Brain Harvest

Brains were harvested from mice that went through the above-described labeling paradigm. More specifically, all brains were harvested from either test animals on test day 1 or from control animals that were kept in their home cage. To ensure that the differences seen were due to the differences in conditions and not time of day, all brains were harvested exactly 3 hours after the mice were put inside the Promethion cages. Brains that were harvested from home cage controls were harvested at the exact same time as those harvested from the test animals.

3.2.5 Brain Tissue Preparation

Mice were transcardially perfused with 4% paraformaldehyde (PFA), and brains were fixed in 4% PFA overnight. The next day, brains were transferred into phosphate buffered saline (PBS) and kept at 4°C. They were subsequently sliced in 100 μm coronal sections with a vibratome (Leica VT1200 S) and collected in PBS.

3.2.6 Immunohistochemistry

In order to get clear immunolabeling we utilized the previously described iDISCO-based immunohistochemistry protocol [76, 80]. Sections were rinsed 3 times in 1X phosphate buffered saline (PBS) before subsequently being dehydrated in 50% MeOH/ PBS at room temperature for 2.5 hours. Sections were then rinsed 3 times in 0.2% PBS with TritonX-100 (PBST) and blocked in 0.2% PBST with 10% dimethyl sulfoxide (DMSO) and 6% normal goat serum (NGS) for two hours at room temperature. After blocking, they were washed 3 times in PBS with 0.2% Tween-20 and 10 μg/ml heparin (PTwH). Sections were then incubated with primary antibody chicken polyclonal anti-GFP (1:1,000, Invitrogen, Waltham, MA) and rabbit polyclonal IgG anti-c-Fos (1:1,000, Invitrogen, Waltham, MA) at 4°C on a shaker for 3 days in PTwH with 5% DMSO and 3% NGS. On day 4, sections were washed 3 times in PTwH

and incubated with secondary antibodies Alexa 568 Anti-Rabbit IgG (1:500, Invitrogen, Waltham, MA) and Alexa 488 Anti-Chicken IgG (1:500, Invitrogen, Waltham, MA) overnight at 4°C. The next day, sections were washed three times in PTwH, followed by 3 washes in PBS at room temperature. Finally, sections were stained with DAPI in PBS for 10 minutes followed by a final wash in PBS. Sections were then mounted on superfrost slides using Vectashield-DAPI, cover slipped and sealed.

3.2.7 Confocal Imaging

All images were taken on a confocal scanning microscope (Leica TCS SP8, Leica Microsystems Inc.). Fluorescence from DAPI was detected at 417–488 nm, Alexa Fluor 568 was detected at 595–650 nm, and Alexa Fluor 488 was detected at 500-550nm. Sections were imaged with a dry 20x objective (NA 0.70, working distance 0.5 mm), with a pixel size of 1.14 x 1.14 μm^2, a z step of 3 μm, and a z-stack of approximately 25 μm. Fields of view were stitched together to form tiled images by using an automated stage and the algorithm of the LAS X software.

3.2.8 Cell Counting

After imaging, stitched TIF files were imported into Fiji [127]. Regions of interest (the DG, LHA, MPO and LPO) were subsequently manually drawn and measured for their size in μm^2. Next, $eYFP^+$, c-Fos^+ and co-labeled cells were bilaterally identified and counted throughout the entire z-stack. All cell counts were normalized to their respective areas and plotted as cells per μm^2.

3.2.9 Statistics

All data were analyzed using Prism 10. All data were graphed as means ± Standard errors of the mean (SEM). An alpha level of 0.05 was used as a criterion for statistical significance. The results of figure 3.3.1 were analyzed using unpaired t-tests. Figure 3.3.2 was analyzed with simple linear regressions. Figures 3.3.3 and 3.3.4 were made using Pearson's correlations

3.2.10 Figure design and visualization

Figures and graphical illustrations were created with Biorender (Biorender.com).

RESULTS

3.3.1 Cold-sensitive memory ensembles are located in the DG, LHA, and MPO.

As previously described, engrams have been identified in many different areas of the brain, such as the hippocampus, amygdala and prefrontal cortex for various sensory modalities [74, 110, 115, 116, 118, 128]. Yet, no studies have shown reliable hypothalamic engram labeling. To better understand how cold memories are encoded and retrieved, we aimed at achieving optimal labeling in DG, LHA, MPO, and LPO. To do so, we crossed TRAP2 mice [111] with R26R-STOP-floxed enhanced yellow fluorescent protein (eYFP) transgenic mice [110, 125]. To quantify activated engram cells in multiple brain regions, mice were put through a cold engram labeling protocol (Figure 3.3.1a-b). Here, cold-sensitive engrams were labeled by injecting 4-OHT on cold day 1. Subsequent immunohistochemical analysis revealed consistent labeling in all target areas (Figure 3.3.1c). Next, the number of $eYFP^+$ cells were quantified in the DG, LHA, MPO, and LPO (Figure 3.3.1c-g). Our results show no differences in the number of $eYFP^+$ cells between mice recalling a contextual cold memory at T1 and home cage controls in the DG, LHA, MPO, or LPO, suggesting comparable amounts of labeled cells in both groups (Figure 3.3.1d-g). We then quantified the number of c-Fos^+ cells between the groups (Figure 3.3.1h-l). There was a significant increase in the number of c-Fos^+ cells in mice retrieving the cold in the LHA (Figure 3.3.1j), whereas no significant differences were found in the DG, MPO, or LPO (Figure 3.3.1i, k-l). Finally, we quantified the cells active during both encoding and expression of a cold memory (i.e., ((c-Fos^+eYFP^+)/$eYFP^+$; Figure 3.3.1m). Our results show a significant increase in co-labeling in the DG, LHA and MPO (Figure 3.3.1o-p), but not in the LPO (Figure 3.3.1q) in mice retrieving a cold memory when compared to home cage controls. Together, these data suggest that cold-sensitive memory engrams are located in the DG, LHA, and MPO.

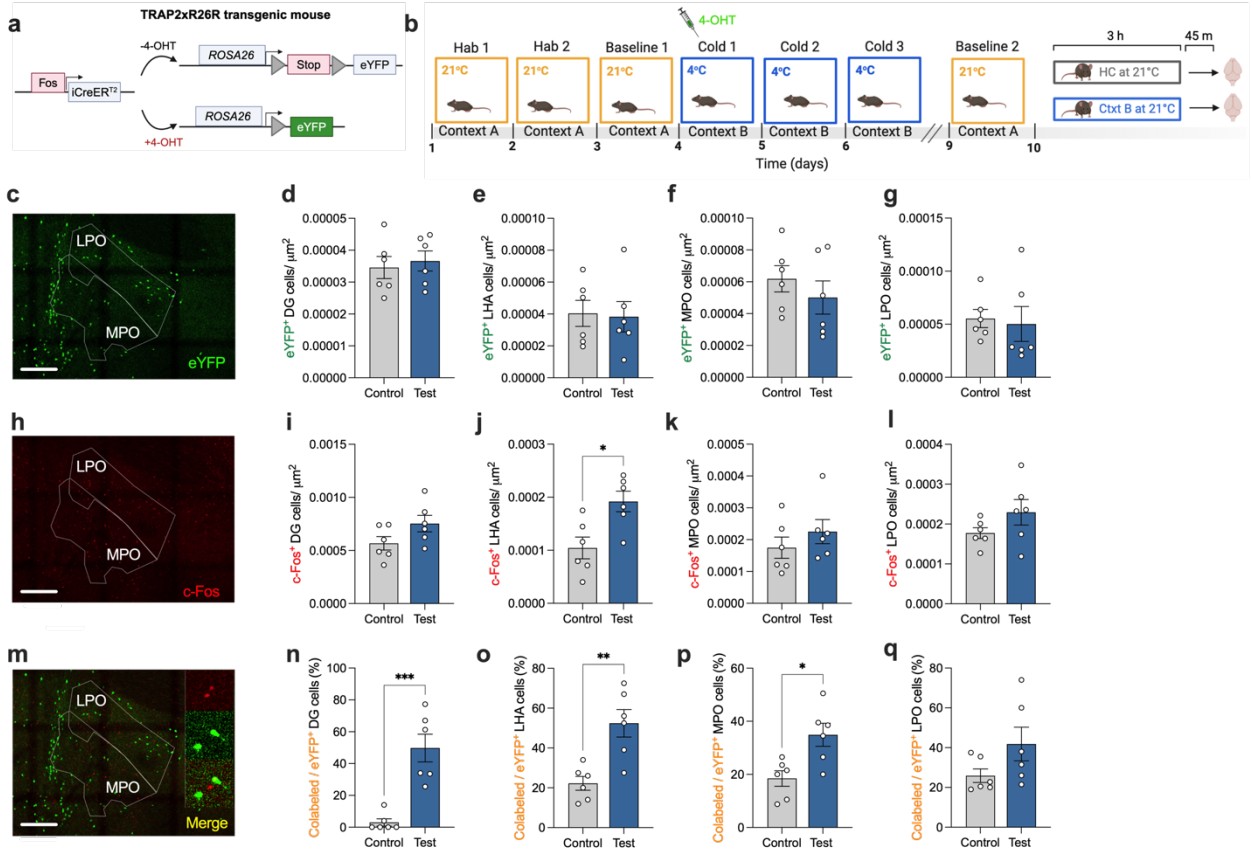

Figure 3.3.1 Putative contextual cold memory engrams labeled in the DG, LHA and MPO. **(a)** Genetic strategy. **(b)** Diagrammatic representation of experimental timeline to label cold-sensitive memory ensembles in TRAP2 x R26R mice, including timeline for tissue collection. **(c)** Representative image of a hypothalamic slice with eYFP$^+$ cells in green. Comparison of eYFP$^+$ neurons normalized to area between the test cohort and home cage control cohort in **(d),** the DG, **(e),** the LHA, **(f),** the MPO and **(g),** the LPO. **(h)** Representative image of c-Fos$^+$ cells in red. Comparison of c-Fos$^+$ neurons normalized to area between the test cohort and home cage control cohort in **(i),** the DG, **(j),** the LHA, **(k),** the MPO and **(l),** the LPO. **(m)** Representative image of eYFP$^+$c-Fos$^+$ colabeled cells with eYFP in green, c-Fos in red and colabeled in yellow. Comparison of colabeled neurons between the test cohort and home cage control cohort in **(n),** the DG, **(o),** the LHA, **(p),** the MPO and **(q),** the LPO.Data shown as mean ± SEM, *n* = 6 mice per group. * p < 0.05, ** p < 0.01, *** p < 0.001. HC, home cage; Ctx, context; h, hour; m, minutes; DG, dentate gyrus; LHA, lateral hypothalamic area; MPO, medial preoptic area; LPO, lateral preoptic area.

3.3.2 Contextual cold engrams correlate with metabolic rates.

Previous studies have shown that correlational analyses can help determine how engram cell activity influences behavioral responses. For example, Reijmers and colleagues showed that the number of engram cells in the lateral amygdala correlated with freezing behavior in mice that underwent fear conditioning [109]. In a similar fashion, we examined how increased reactivation of cold-sensitive engrams affected whole-body metabolism. To do so, we correlated the amount of co-labeled cells in the DG with the metabolic rates that were measured exactly 45 minutes before the brains were harvested (Figure 3.3.2a-b). As such, we were able to correlate cold-sensitive engram cell activity in the DG with VO_2, VCO_2, and EE. We found strong positive correlations between cold engram cell reactivation and metabolic rate at T1 and CL1, but not at BL1 (Figure 3.3.2c-f). These results show that increased cold engram reactivation correlates with increases in whole-body metabolism during both recall and encoding on the original training day.

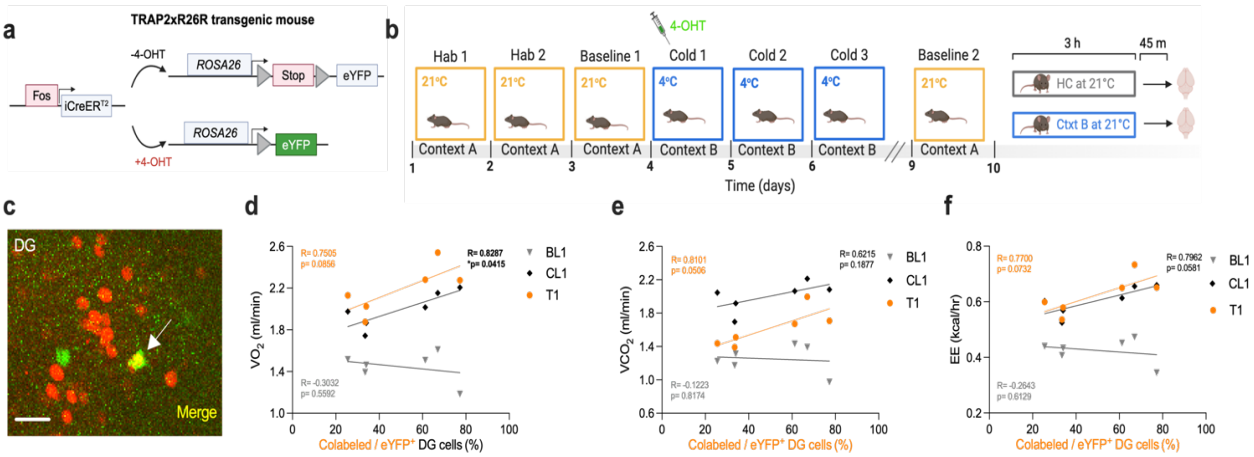

Figure 3.3.2 Cold-sensitive memory ensembles in the DG correlate with metabolic rate. **(a)** Genetic strategy. **(b)** Diagrammatic representation of experimental timeline to label cold-sensitive memory ensembles in TRAP2 x R26R mice, including timeline for tissue collection. **(c)** Representative DG image of eYFP$^+$c-Fos$^+$ colabeled cells with eYFP in green, c-Fos in red and colabeled in yellow. **(d)** Correlation between the percentage of colabeled/ eYFP$^+$ cells in the DG and oxygen consumption at T1, CL1 and BL1. **(e)** Correlation between the percentage of colabeled/ eYFP$^+$ cells in the DG and carbon dioxide production at T1, CL1 and BL1. **(f)** Correlation between the percentage of colabeled/ eYFP$^+$ cells in the DG and energy expenditure at T1, CL1 and BL1. Data shown as mean ± SEM, *n* = 6 mice per group. HC, home cage; Ctx, context; h, hour; m, minutes; DG, dentate gyrus; VO_2, oxygen consumption; BL1, Baseline 1; CL1, Cold 1; T1, test 1; VCO_2, carbon dioxide production; EE, energy expenditure.

3.3.3 The DG and LHA show coordinated engram activity when mice recall the cold.

To further understand how contextual cold memories are stored throughout the brain, we performed correlational analyses of engram reactivation across brain regions. Previous studies have namely shown that correlation heatmaps of engram reactivation can further our understanding of how different memories are stored across multiple regions [74]. Here, we compared coordinated engram activity between animals retrieving a contextual cold memory and home cage control animals. Our analyses revealed a significant positive correlation between the DG and LHA in animals retrieving a cold memory (Figure 3.3.3b), whereas this type of coordinated activity was not found in the home cage control animals (Figure 3.3.3c). Similarly, we find coordinated activity between the MPO and LPO in test animals but not in controls (Figure 3.3.3a-b). In line with our previous c-Fos data, these results suggest that when mice recall the cold, a specific pathway emerges between the DG and LHA, in addition to a connection between the MPO and LPO, and that coordinated hypothalamic activity is essential for contextual cold memories.

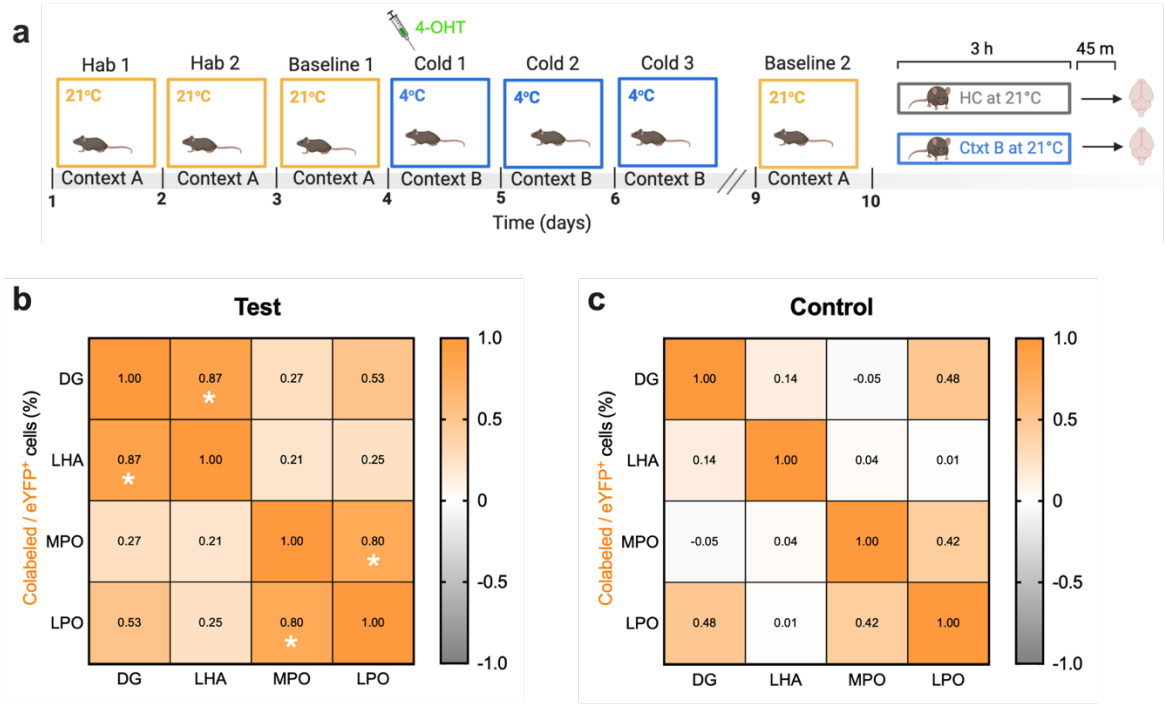

Figure 3.3.3 Coordinated activity between the DG and LHA is essential for contextual cold memories. (a) Diagrammatic representation of experimental timeline to label cold-sensitive memory ensembles in TRAP2 x R26R mice, including timeline for tissue collection. **(b)** Correlation of percentage of colabeled/ eYFP$^+$ cells during the recall of a contextual cold memory on test day. Asterisks represent a significant correlation. **(c)** Correlation of percentage of colabeled/ eYFP$^+$ cells of the home cage control group. Data shown as mean ± SEM, *n* = 6 mice per group. * $p < 0.05$. HC, home cage; Ctx, context; h, hour; m, minutes; DG, dentate gyrus; LHA, lateral hypothalamic area; MPO, medial preoptic area; LPO, lateral preoptic area.

3.3.4 Cold engrams in the DG and LHA specifically correlate with metabolic rates.

As described above, we found that cold-sensitive memory engrams are located in the DG, LHA, and MPO (Figure 3.3.1). Moreover, we show that cold-sensitive memory ensembles in the DG covaried with metabolic rate during T1 and CL1 (Figure 3.3.2). Here, we aimed at determining whether these results were specific to the DG or whether all the areas that were found to hold contextual cold engrams covary with metabolic rates. To investigate this, we created correlation matrices that included engram cell activity from the DG, LHA, MPO and LPO, and the metabolic rates of T1, BL1 and CL1 (Figure 3.3.4a-d). In line with our previous results, we found that cold engrams in the DG correlated with VO_2 and EE during T1 and CL1. However, these correlations were not observed with the cold engram cells found in the LHA, MPO and LPO (Figure 3.3.4b, d). Finally, we found that cold engrams in the DG and LHA both correlated with VCO_2 on T1 specifically (Figure 3.3.4c). These results were specific to the DG and LHA, as these correlations were not found for the MPO or LPO. Moreover, we found that engram activity in general did not correlate with the metabolic rates during BL1 (Figure 3.3.4b-d). Taken together, these data suggest that engram cell reactivation in the DG and LHA specifically contribute to the increased metabolic rates that were observed on T1 and CL1.

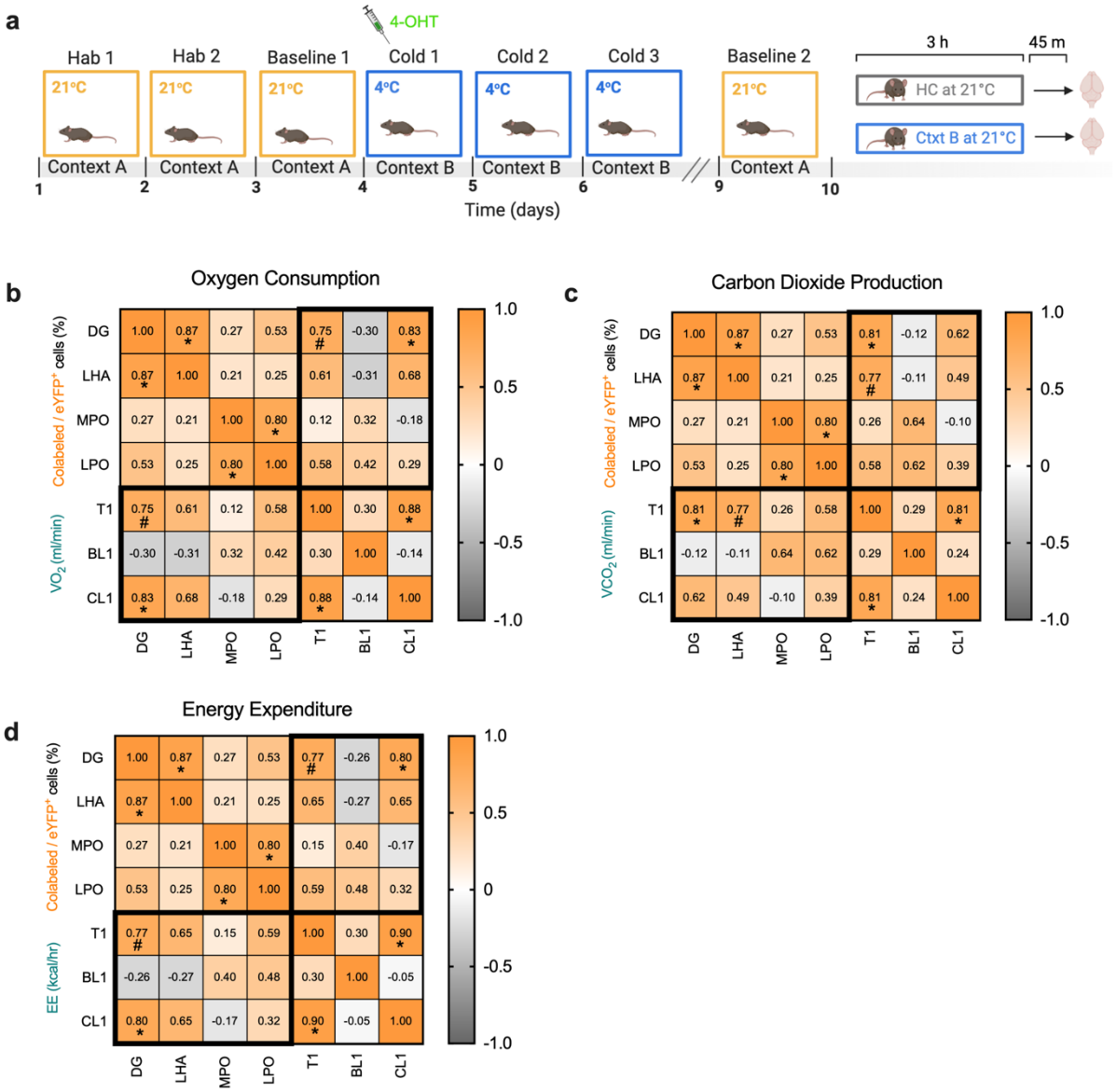

Figure 3.3.4 Correlation matrices of cold engram activity and metabolic rates. **(a)** Diagrammatic representation of experimental timeline to label cold-sensitive memory ensembles in TRAP2 x R26R mice, including timeline for tissue collection. **(b)** Correlation matrix of the percentage of colabeled/ eYFP$^+$ cells during the recall of a contextual cold memory on test day and the amount of oxygen consumed on T1, BL1 and CL1. **(c)** Correlation matrix of the percentage of colabeled/ eYFP$^+$ cells during the recall of a contextual cold memory on test day and the amount of carbon dioxide consumed on T1, BL1 and CL1. **(d)** Correlation matrix of the percentage of colabeled/ eYFP$^+$ cells during the recall of a contextual cold memory on test day and energy expenditure on T1, BL1 and CL1. Data shown as mean ± SEM, *n* = 6 mice per group. * $p < 0.05$, # $p < 0.1$. HC, home cage; Ctx, context; h, hour; m, minutes; DG, dentate gyrus; LHA, lateral hypothalamic area; MPO, medial preoptic area; LPO, lateral preoptic area; BL1, Baseline 1; CL1, Cold 1; T1, test 1; VO_2, oxygen consumption; VCO_2, carbon dioxide production; EE, energy expenditure.

DISCUSSION

In this chapter, we designed a novel transgenic mouse that enabled us to consistently label cold-sensitive engrams in hippocampal and hypothalamic regions. By combining TRAP2 mice with R26R-STOP-floxed eYFP transgenic mice, we were able to visualize and quantify contextual cold engrams in the DG, LHA, MPO and LPO. By combining these mice with a behavioral labeling protocol, we found a significant increase in co-labeling in the DG, LHA and MPO in mice retrieving a cold memory, compared to home cage controls. We also showed that when mice recall the cold, a specific pathway emerges between the DG and LHA, and that coordinated hypothalamic activity is essential for contextual cold memories. Finally, we show that cold-sensitive memory ensembles in the DG and LHA correlate with metabolic rate, suggesting that cold engram cells are involved in whole-body metabolism.

In this study we relied on a tamoxifen dependent tagging strategy to label cold-sensitive engram cells. One big advantage of using a tamoxifen dependent tagging system was the smaller labeling window, compared to the relatively large labeling window that is associated with doxycycline dependent tagging systems. Indeed, previous studies using TRAP2 mice have shown that upon injection of 4-OHT, only the cells that were active 3 hours prior and 3 hours after the injection are labeled [111]. In our behavioral labeling paradigm, once mice were placed into the metabolic chambers on CL1, the temperature decreased in increments of ~10 degrees per hour. As such, the mice spent a total of 6 hours in the altered context at a temperature of 4°C. To label the cells that were active during exposure to 4°C, we injected mice with 4-OHT exactly five hours after being put in the metabolic chambers. Therefore, by using a tamoxifen dependent tagging strategy we were able to tightly control which temperatures were tagged in our behavioral paradigm.

Next, we show that with our novel TRAP2xR26R mouse we were able to label cold-sensitive engrams in a variety of regions. Although consistent labeling was observed in the DG, we found no labeling in other hippocampal areas (i.e. CA3 and CA1). It remains unclear whether these areas do not hold any cold-sensitive engram cells, or whether the chosen genetic strategy does not allow for labeling in these regions specifically. Future studies are necessary, where different behavioral and sensory

modalities are piloted in the TRAP2xR26R mouse to fully establish the potential of this genetic strategy.

In this chapter, we also quantified the number of c-Fos$^+$ cells between groups and found a significant increase in the number of c-Fos$^+$ cells in mice retrieving the cold in the LHA, but not in the DG, MPO, or LPO. These data are in line with the c-Fos results found in chapter two, where we showed that only the LHA had increased c-Fos activity on T1 compared to BL1. We therefore demonstrate that these results could be replicated in our transgenic mouse model. Next, when quantifying the cells that were both active during the encoding and expression of a cold memory, we found a significant increase in co-labeling in the DG. In line with these results, previous studies have shown that contextual engrams are located in the DG [16, 110]. To our knowledge however, we show here for the first time that cold-sensitive engrams are located in the LHA and MPO.

To further understand how contextual cold memories are stored in the murine brain, we performed correlational analyses of engram reactivation activity across brain regions. We found that when mice recall the cold, a specific pathway emerges between the DG and LHA, and that coordinated hypothalamic activity may be important for contextual cold memories. This is in line with previous studies showing that the hypothalamus is important for thermoregulatory responses and with our previous correlational analyses of c-Fos activity in chapter two. Using similar analyses, we also found that that engram cell reactivation in DG and LHA specifically correlates with the increased metabolic rates that were observed on T1 and CL1. This suggests that cold-sensitive engram cells are involved in whole-body metabolism. Up until now, engram cell activity has never been directly correlated with whole-body responses. Indeed, typical engram activity is only correlated with behavioral responses [74, 109]. Future studies are necessary to further explore which body-responses are controlled by engram cells specifically.

In this chapter we aimed at identifying and quantifying cold-sensitive engram cells in multiple brain regions. Moreover, we aimed at understanding whether contextual cold engrams also have an influence on whole-body metabolism. This chapter showed observational evidence that cold-sensitive engrams are located in the hippocampus

and hypothalamus. Based on these results, we designed subsequent gain and loss-of-function studies to further establish whether cold-sensitive engram cells control whole-body metabolism.

Chapter 4:

Artificially manipulating cold engrams alters whole-body metabolism.

INTRODUCTION

4.1.1 The development of optogenetic tools.

In 1979, Francis Crick wrote an article stating that to really understand how the brain works, new ways of thinking about it, combined with novel techniques, would be necessary [129]. Moreover, he suggested that one of the major challenges was the need for tools that allowed for the control of one type of cell in the brain, while leaving others unaltered. Crick speculated that electrodes would not allow for precise targeting of specific cells, nor would they be able to turn neurons on or off. As such, he proposed that light could serve as a control tool, enabling the delivery of precisely timed pulses in different locations of the brain. However, at the time no clear strategy was available to make specific cells respond to light.

Meanwhile in the microbiology field, researchers were working on microorganisms that were known to produce light-gated proteins, known as opsins, which directly regulated the flow of ions across the plasma membrane. Indeed, certain species of algae have opsin proteins that respond to visible light. When illuminated, these opsin protein channels allow electrically charged ions to cross membranes for the extraction of energy from their environments [130]. Different types of opsins with varying light sensitivity and responses to different wavelengths of light have since been discovered (Figure 4.1.1), such as channelrhodopsin (ChR2) and halorhodopsin (NpHR) [131, 132]. Although these opsins were all discovered in the seventies, it took another 30 years before they were introduced into the neuroscience field [133].

In 2005, Boyden and colleagues showed for the first time that upon insertion of an opsin gene, neurons become responsive to light [134]. Moreover, they demonstrated that opsin-based technology allowed light to alter neural processes at the level of single spikes and synaptic events. With that, the field of optogenetics was born, as several additional follow-up studies showed that channelrhodopsin and halorhodopsin could be used to turn neurons on and off in a cell-specific and rapid manner In addition to allowing for temporal control of neurons at a single cell resolution, optogenetics has been shown to be a powerful tool that can be used to control different types of defined cells in freely moving mice [135, 136].

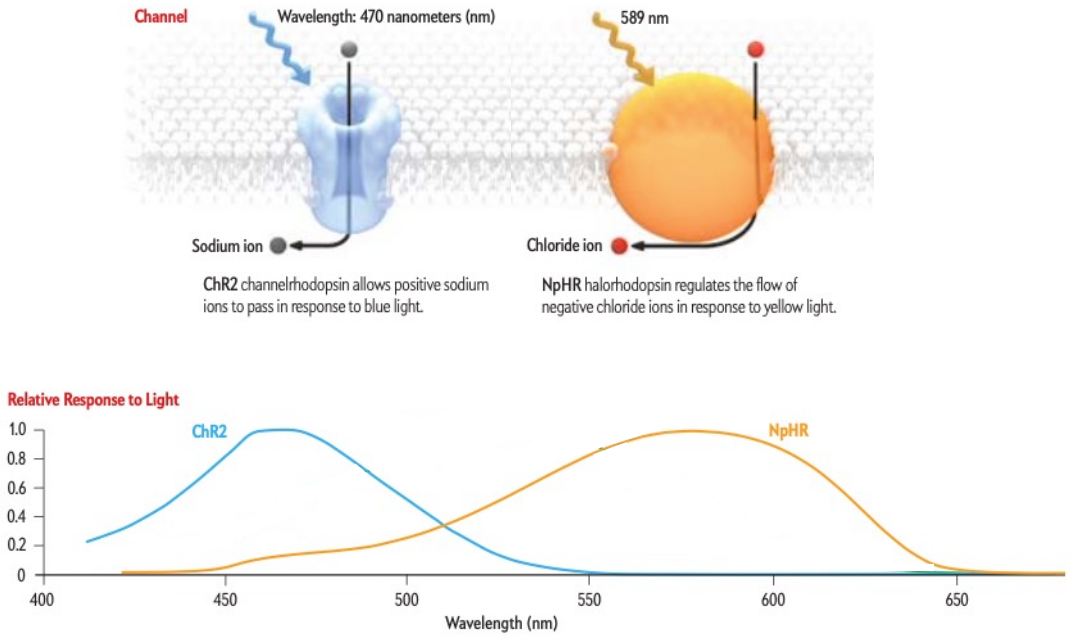

Figure 4.1.1 Light-sensitive proteins and their relative response to light. Channelrhodopsin (ChR2) and halorhodopsin (NpHR) are light-gated proteins that directly regulated the flow of ions across the plasma membrane. They each have varying light sensitivity as ChR2 peaks at 470 nm and NpHR at 589 nm. *Adapted from Deisseroth, 2010 [133].*

4.1.2 Combining optogenetics with engram labeling technology.

Optogenetic tools quickly became a key technique in neuroscience in general and in the memory field specifically. Indeed, these tools advanced the memory field significantly, as researchers could now address more targeted questions with regards to how memories are encoded in the brain. For example, one of the earliest studies combining optogenetics with memory tasks showed that optogenetic inhibition of CA1 neurons blocked the acquisition and retrieval of fear memories [137]. In this study, all excitatory CA1 neurons were inhibited from spiking, resulting in inhibition of 94% of the cells in this area. However, with the development of the previously described engram labeling strategies, subsequent studies were able to combine these labeling strategies with optogenetics to reactivate or inhibit specific ensembles of cells. Indeed, Liu and colleagues were able to label and reactivate a subpopulation of DG cells that were active during the encoding of a memory [16]. This was achieved by targeting the DG of c-fos-tTa transgenic mice with an AAV_9-TRE-ChR2-EYFP virus and an optical fibre implant (Figure 4.1.2). By doing so, they could reactivate specific cells in the DG

that were active during the encoding of a fear memory by shining blue light through the optical fibre. With this set up, they showed that optical stimulation of engram cells induced post-training freezing [138]. Various studies have since shown that different types of memory engrams can be labeled and reactivated in different brain regions [107, 139, 140].

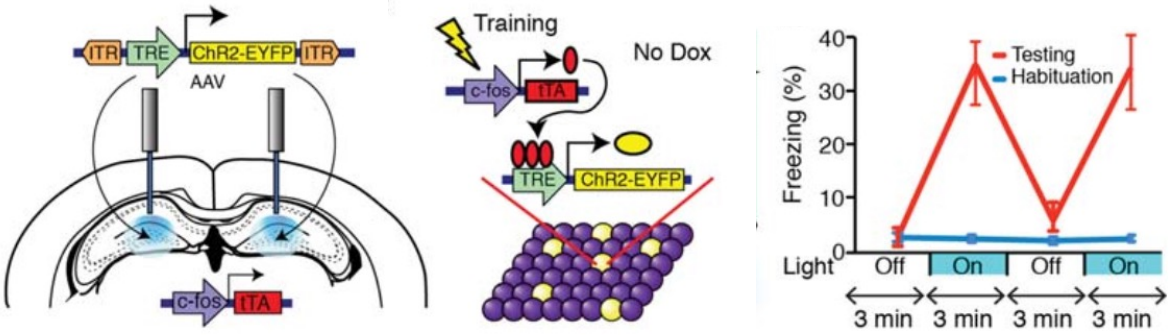

Figure 4.1.2 Optical stimulation of engram cells induces freezing. c-fos-tTa transgenic mice are injected with an AAV_9-TRE-ChR2-EYFP virus and implanted with an optical fibre implant. Only those cells that are active during a certain experience are labeled when doxycycline is removed. Optical stimulation of labeled engram cells results in increased freezing. *Adapted from Liu et al., 2014 [138].*

4.1.3 Optogenetics outside of the brain.

Optogenetics were initially designed to be applied in rodent models for the control of specific neural circuits in the brain. However, recent technological advancements have allowed for the use of optogenetic tools in other organs and tissues. For example, Hsueh and colleagues developed a method for noninvasive optogenetic control of cardiac rhythms in freely moving mice [12]. With this method, they showed that optically induced tachycardia elicited anxiety-like behaviors in risky contexts, suggesting that both the brain and the body are involved in the development of emotional states and aversive behaviors. Similar advancements in optogenetic tools have been reported for the gut, where wireless devices specifically designed for optogenetic control of the gastrointestinal tract have allowed for *in vivo* colonic motility and transit studies [141]. Wireless optogenetic tools have become increasingly popular, as they can be freely implanted in a wide variety of organs. Indeed, to activate adipose tissue thermogenesis without the presence of a cold environmental stimulus, Tajima and colleagues developed a wireless optogenetic device that triggered Ca^{2+}

cycling selectively in brown adipocytes [142]. With this device, they showed that optogenetic stimulation of adipose tissue activated non-shivering thermogenesis and increased whole-body energy expenditure in the absence of cold stimuli. In addition to the manipulation of organ specific processes, various studies have now also shown that these tools can be used to modulate activity in limbs, the spinal cord and other peripheral areas [143]. As such, optogenetic tools have been shown to be useful in manipulating circuits inside and outside of the brain.

4.1.4 Manipulating neurons using pharmacosynthetics

Optogenetic approaches are not the only tools that can be used to study specific brain circuits. Indeed, pharmacogenetics enables the use of designer receptors to selectively modulate neuronal functioning with pharmacological tools [136]. Nowadays, Designer Receptors Exclusively Activated by Designer Drugs (DREADDs) are commonly used to study the function of specific brain cells and regions [144]. DREADDS are G-protein coupled receptors that can be expressed in neurons through viral vectors, and that show little activity in the absence of the ligand clozapine N-oxide (CNO). By including promoters for specific neuronal cell types, these receptors allow for the manipulation of specific cell types *in vivo* through the administration of CNO [145]. For example, available DREADDs include hM3Dq, which increases excitability in neurons, and hM4Di which causes presynaptic inhibition and silencing (Figure 4.1.3). In addition, it has been shown that there are equivalent effects between optogenetic and DREADD techniques, and that both tools are useful to activate and silence neurons [144]. Due to the longer effect duration and bioavailability of CNO and DREADD activity, they display less precise temporal control compared to optogenetic approaches.

DREADDs are now also commonly used to further understand the neuronal circuitry that is involved in different types of memories. For example, Park and colleagues showed that by using DREADDs they could silence a small number of CREB-overexpressing DG neurons 5 minutes after training and disrupt subsequent memory expression [146]. Moreover, studies have shown that engram labeling strategies can be combined with pharmacological tools to inhibit specific neuronal ensembles. Indeed, DREADD inhibition of specific cortical ensembles that were active during fear conditioning was shown to reduce fear expression [147]. As such, DREADDs can be

used to inhibit engrams of specific memories in a variety of regions. DREADDs are therefore powerful tools that can be used to dissect the neural circuitry underlying learning and memory.

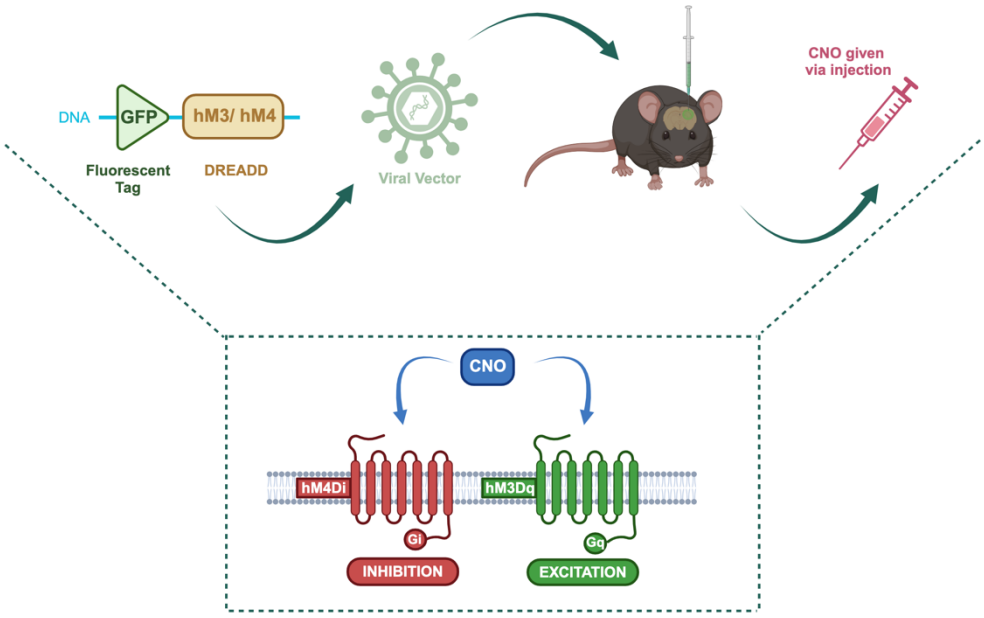

Figure 4.1.3 Overview of inhibitory and excitatory DREADs. DREADDs are receptors that can be expressed in neurons through viral vectors. These receptors are activated if CNO is present in the system. hM4Di DREADDs can be used to inhibit neurons, whereas hM3Dq DREADDs can be used to increase excitability in neurons.

4.1.5 Artificially manipulating thermoregulatory circuitry

To further understand the neural circuitry underlying thermoregulation, studies have used both optogenetic and pharmacogenetic approaches. For example, acute chemogenetic activation of the dorsomedial hypothalamus (DMH) was shown to cause increases in body temperature, BAT temperature, energy expenditure and heart rate [64]. Conversely, chemogenetic inhibition of the DMH decreased body temperature and energy expenditure, suggesting that this area has a clear role in thermoregulatory responses. Similar results were found for the preoptic area of the hypothalamus (POA), where optogenetic reactivation of this area resulted in increased body temperature [148]. Finally, chemogenetic inhibition of the LHA was shown to inhibit behavioral thermoregulatory responses such as nest building and postural extension [23]. The development of optogenetic and chemogenetic tools has majorly contributed to our understanding regarding the underlying circuits of the physiological as well as the behavioral components of thermoregulation. However, up until now no studies

have used these tools to examine how artificial manipulation of cold memories affects thermoregulatory responses.

In this chapter, we set out to artificially manipulate cold-sensitive engrams with optogenetic and chemogenetic tools. We aimed at understanding whether memories control whole-body responses and whether artificial manipulation of cold engrams causes changes in whole-body metabolism. Here, we designed a behavioral timeline that allowed us to label cold-sensitive engrams with ChR2, and optogenetically reactivated these engram cells while simultaneously measuring metabolic rates. To fully understand how cold engrams influence thermoregulatory responses, we also inhibited these engram cells using inhibitory DREADDs. Taken together, this chapter's research question aims at examining whether we can artificially alter whole-body metabolic rates by manipulating cold engrams in the brain.

METHODS

4.2.1 Mice

Optogenetic reactivation experiments were performed with TRAP2 x Ai32 mice. These mice were created by breeding homozygous TRAP2 mice [111] with homozygous Ai32 mice [149]. Additional optogenetic control experiments were performed with c-fos-tTa transgenic mice. These mice were created by breeding WT mice with heterozygous FtTa mice [109]. All chemogenetic experiments were performed with TRAP2 mice. Male mice were used in all experiments. All mice were group-housed in a 12:12-h (07:00-19:00) light-dark colony room at 22°C. Food and water were provided ad libitum, and all testing was performed during the light phase. Mice used for experiments were approximately 8-12 weeks of age. All experiments were conducted in accordance with the European Directive 2010/63/EU, under an authorization issued by the Health Products Regulatory Authority Ireland and approved by the Animal Ethics Committee of Trinity College Dublin.

4.2.2 Optic Fiber Implant Surgeries

Mice that were used in optogenetic experiment were implanted with a custom implant containing two optic fibers (200 mm core diameter; Doric Lenses). The optical fiber implant was lowered above the injection site at -1.75 mm dorsoventral (DV). To secure the implant, an even layer of Metabond (C&B Metabond) was applied and left to dry for 15 minutes. A protective cap was then made from a black polypropylene microcentrifuge tube and secured with dental cement. Animals were then put in a recovery chamber at 29°C until they were fully recovered from the anesthesia before being returned to their home cage. Animals were allowed to recover from surgery ~2-3 weeks before behavioral testing.

4.2.3 Viral Injection Surgeries

For optogenetic experiments, c-fos-tTa transgenic mice were put on a diet containing doxycycline (DOX) 48 hours prior to surgeries. All surgeries were performed when the animals were ~7-8 weeks old. Mice were anesthetized with 500 mg kg-1 avertin and head fixed on a stereotaxic frame. Bilateral craniotomies were performed using a 0.5mm diameter drill at -2.00 mm anteroposterior (AP), and ±1.35 mm mediolateral (ML). Next, 300 µL AAV9-TRE-ChR2-EYFP was injected in each side using a micro syringe pump (UMP3; WPI) and a Hamilton syringe (701LT; Hamilton) at -2.00 mm

anteroposterior (AP), ±1.35 mm mediolateral (ML), and -2.00 mm dorsoventral (DV). Injection speed was performed at 60 nL/min, and the needle was subsequently left on site for an additional 10 minutes after virus delivery to achieve maximum virus spread.

For chemogenetic experiments, TRAP2 mice were injected with 300 µL pAAV-hSyn-DIO-HA-hM4D(Gi)-IRES-mCitrine in each side at -2.00 mm anteroposterior (AP), ±1.35 mm mediolateral (ML), and -2.00 mm dorsoventral (DV). Injection speed was performed at 60 nL/min.

4.2.4 Optogenetic Reactivation Timeline: TRAP2xAi32 Strategy

Here, we adapted our previously developed labeling paradigm (Chapter 3) to enable the reactivation of cold-sensitive engrams. On day one and two, mice with fiber optic implants were attached to a patch cord, placed into the Promethion cages at 21°C, and allowed to habituate 8 hours each day. On day three, mice were put into the Promethion cages at 21°C while metabolic and behavioral data were simultaneously recorded in order to establish baseline measurements (Context A). On day four, contextual cues were added to the chambers, and the mice spent a total of 6 hours in the altered context at a temperature of 4°C. To label the neurons that were active during these 6 hours of 4°C cold exposure, mice were injected with 4-OHT five hours after being put in the Promethion cages. Immediately after labeling, all mice were returned to their home cages. Mice subsequently went through two additional training days as previously described. Optogenetic reactivation was performed a week later in context A (day 13). On the reactivation day, mice were exposed to a 15-minute optogenetic stimulation session that was divided into 3-minute on- and 1-minute off periods (i.e. 3 minutes on, followed by 1 minute off). Optogenetic activation was performed through a 450 nm laser diode fiber light source (Doric LDFLS 450/080). During the light-on epochs, mice received blue light stimulation (20 Hz) with a pulse width of 15ms for the entire 3-minute duration. During the light-off period the mice received no light stimulation. To enable animals to return to baseline, each 15-minute stimulation period was followed by 1 hour of no light stimulation. Mice received a total of 3 rounds of 15-minute stimulation periods. Metabolic rates were measured continuously.

4.2.5 Optogenetic Reactivation Timeline: c-fos-tTa Strategy

To label and reactivate cold engram cells in a second mouse line, we adapted the above-described reactivation timeline to fit with the c-fos-tTa labeling strategy. Here, mice were kept on a DOX diet and run through the same training schedule. To label cells activated by a cold experience, DOX food was substituted by normal food 36h before being exposed to a cold experience on day four. Cold engrams were identified as the cells that expressed ChR2-EYFP as a result of being active during the cold. To close the labeling window, mice were immediately put back on DOX food after the initial cold experience. On the reactivation day, mice were exposed to a 25-minute optogenetic stimulation session that was divided into 5-minute on- and 5-minute off periods. Optogenetic activation was performed through a 450 nm laser diode fibre light source (Doric LDFLS 450/080). During the light-on epochs, mice received blue light stimulation (20 Hz) with a pulse width of 15ms for the entire 5-minute duration. Metabolic rates were measured continuously.

4.2.6 Chemogenetic Inhibition Timeline

To inhibit cold engrams, we used the same labeling timeline as described previously. Briefly, mice went through two habituation days and a baseline measurement day in Context A, at 21°C. On day four, contextual cues were added to the chambers, and the mice spent a total of 6 hours in the altered context at a temperature of 4°C. To label the neurons that were active during these 6 hours of 4°C cold exposure, mice were injected with 4-OHT five hours after being put in the Promethion cages. Immediately after labeling, all mice were returned to their home cages. Mice subsequently went through two additional training days and were subsequently kept in their home cages for a two-day break period. On day nine, mice were put back into the Promethion cages without any of the additional cues at 21°C to allow for a second baseline measurement (Context A). Finally, on day ten half of the mice were injected with CNO (2 mg/ kg, Tocris) and half of the mice were injected with Saline. Mice were kept in their home cage for 30 minutes post injection and were then put into the Promethion cages (Context B, 21°C).

4.2.7 4-OHT

To label cold-sensitive engrams in transgenic animals, we intraperitoneally injected mice with 4-OHT (50 mg/ kg, Santa Cruz). All 4-OHT was freshly prepared on the

labeling day in a mix of sunflower seed oil and castor oil (4:1, Sigma-Aldrich) at 10 mg/ml.

4.2.8 Brain Harvest

Brains were harvested from all mice in order to be able to verify implant and virus location. For optogenetic experiments, all brains were harvested exactly 45 minutes after the last light stimulation ended. For chemogenetic experiments, all brains were harvested exactly 4 hours and 45 minutes after the animals were put into metabolic chambers.

4.2.9 Brain Tissue Preparation and Immunohistochemistry

Brains were prepared and immunolabeled using the same protocols that were described in chapter 3.

4.2.10 Confocal Imaging

In order to check for implant and virus location, all images were taken on a confocal scanning microscope as previously described in Chapter 3. Only the mice that had correct virus and implant locations were kept in subsequent analyses.

4.2.11 Statistics

All data were analyzed using Prism 10. All data were graphed as means ± Standard errors of the mean (SEM). An alpha level of 0.05 was used as a criterion for statistical significance. The results of figures 3.1, 3.2, 3.4 and 3.5 were analyzed using paired t-tests. Figure 3.3 was analyzed with paired t-tests and a two-way ANOVA. Figures 3.6 and 3.7 were analyzed with paired and unpaired t-tests

4.2.12 Figure design and visualization

Figures and graphical illustrations were created with Biorender (Biorender.com).

RESULTS

4.3.1 Optogenetic activation of cold-sensitive engrams increases metabolic rate.

To determine whether cold-sensitive engrams are functionally relevant for whole-body metabolism, we set out to optogenetically reactivate cold engrams in the DG. To do so, we labeled cold-sensitive engrams in the DG on cold day 1, and optogenetically reactivated them in a neutral context (Figure 4.3.1a-d). With this paradigm, we show that optogenetic reactivation of cold-sensitive engrams was sufficient to artificially increase oxygen consumption (Figure 4.3.1e). Moreover, we show that oxygen consumption rates increased when cold-sensitive engrams were stimulated, and that they returned to baseline during the unstimulated periods (Figure 4.3.1f-i). Of note, oxygen consumption only increased during the first two consecutive stimulations, but not during a third stimulation, suggesting an attenuation of whole body-responses or a limitation of optogenetic engram stimulation (Figure 4.3.1h).

In addition to oxygen consumption, we also analyzed energy expenditure and carbon dioxide production to further understand whether optogenetic reactivation of cold engrams altered these metabolic processes. Here, we show that when cold-sensitive engrams were stimulated, both energy expenditure and carbon dioxide production artificially increased (Figure 4.3.2). We also show that similar to oxygen consumption, these rates returned to baseline levels during the unstimulated off periods (Figure 4.3.2c-l). Both energy expenditure and carbon dioxide emission did not increase during the third optogenetic stimulation period, suggesting a similar attenuation of whole body-responses as described above (Figure 4.3.2f, k). Together, these results suggest that optogenetic activation of cold-sensitive engrams increases metabolic rate.

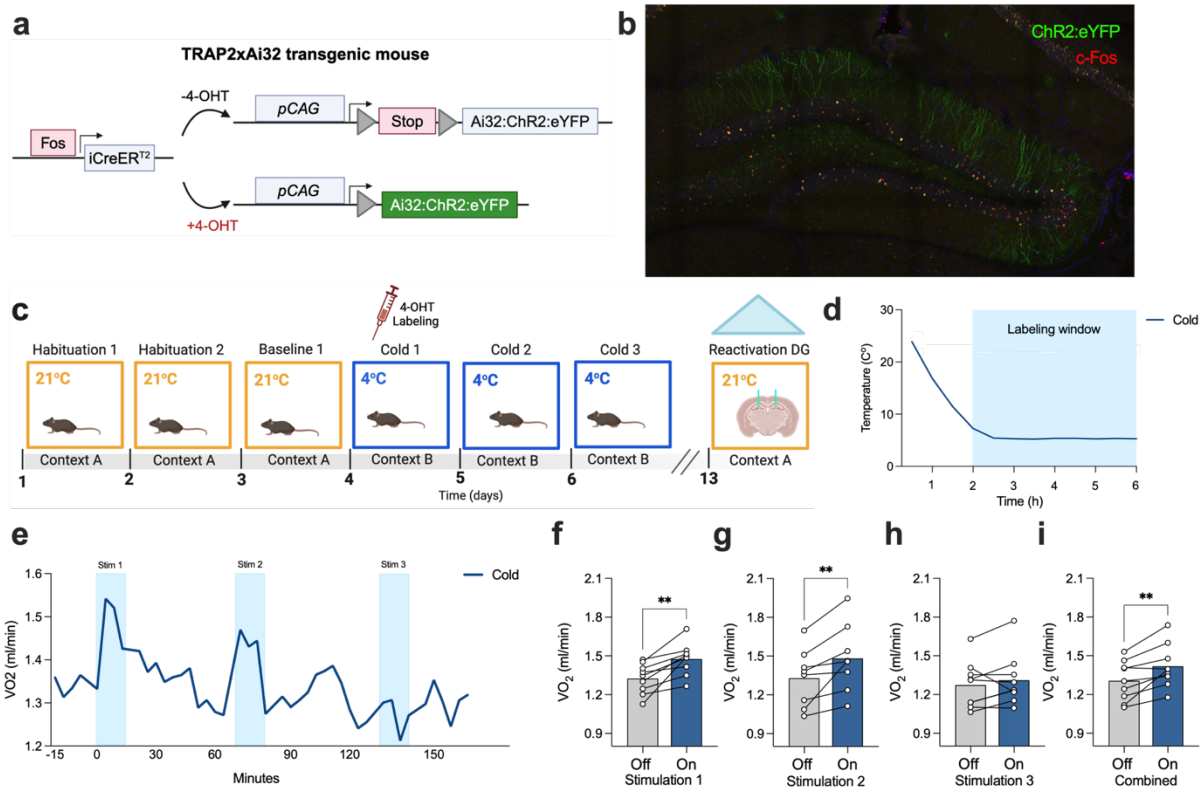

Figure 4.3.1 Artificial optogenetic reactivation of cold-sensitive memory engrams in the DG increases oxygen consumption. **(a)** Genetic strategy **(b)** Representative image of hippocampal slice with c-Fos$^+$ cells (red) and eYFP$^+$ cells (green) **(c)** Diagrammatic representation of experimental timeline to label and reactivate contextual cold memory engrams. **(d)** Environmental temperature during the labeling window on cold day 1. **(e)** Time plot of oxygen consumption during artificial reactivation of cold-sensitive engrams. Blue bars indicate the time the laser was turned on during the 3 stimulation periods. **(f, g, h)** Comparison of oxygen consumption between the on and off epochs during the three stimulations of cold-sensitive cells. **(i)** Comparison of oxygen consumption between the on and off epochs of cold-sensitive cells during all stimulations combined. *n* = 8-9 mice per group. ** p < 0.01. 4-OHT, 4-hydroxytamoxifen; ChR2, Channelrhodopsin; DG, dentate gyrus; VO_2, oxygen consumption; Stim 1, stimulation 1; Stim 2, stimulation 2; Stim 3, stimulation 3.

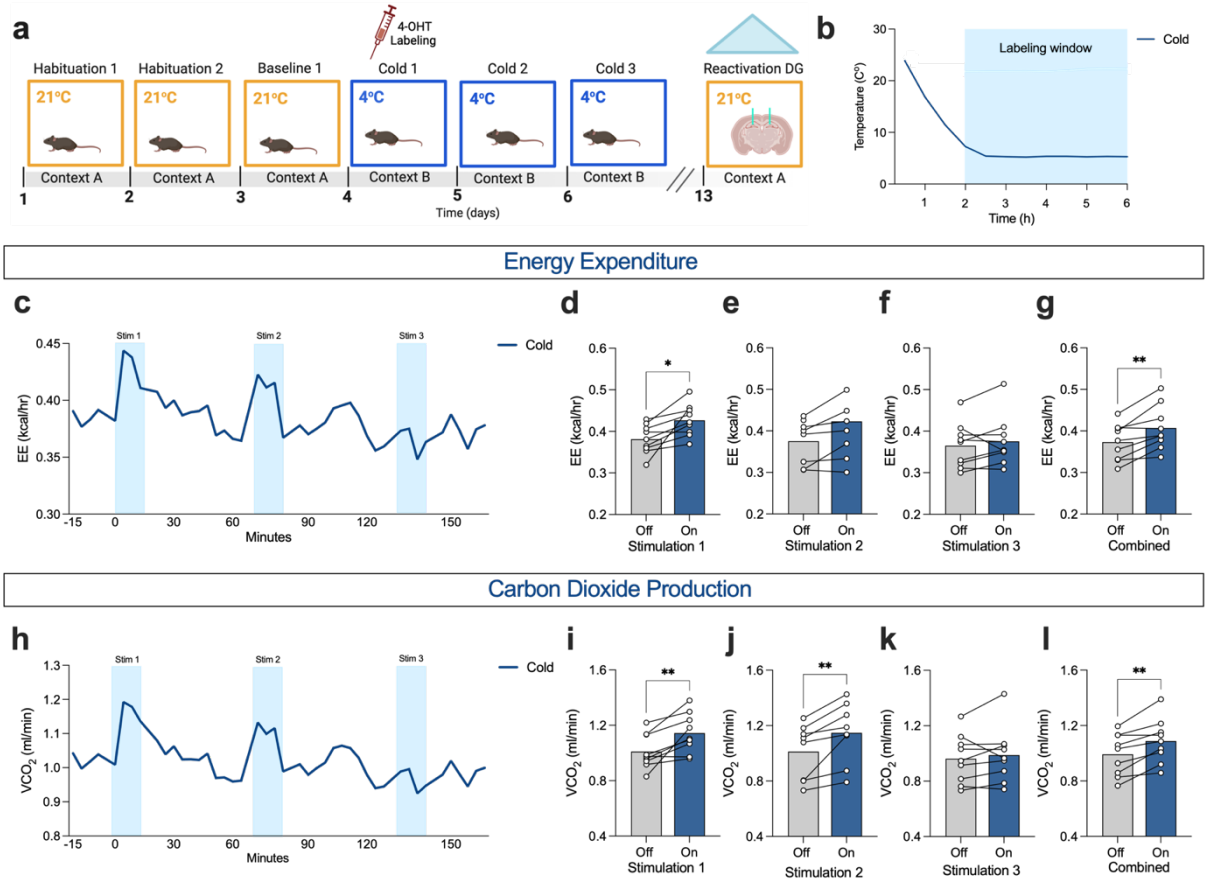

Figure 4.3.2 Artificial optogenetic reactivation of cold-sensitive memory engrams in the DG increases metabolic rate. (a) Diagrammatic representation of experimental timeline to label and reactivate contextual cold memory engrams. **(b)** Environmental temperature during the labeling window on cold day 1. **(c)** Time plot of energy expenditure during artificial reactivation of cold-sensitive engrams. Blue bars indicate the time the laser was turned on during the 3 stimulation periods. **(d, e, f)** Comparison of energy expenditure between the on and off epochs during the three stimulations of cold-sensitive cells. **(g)** Comparison of energy expenditure between the on and off epochs of cold-sensitive cells during all stimulations combined. **(h)** Time plot of carbon dioxide production during artificial reactivation of cold-sensitive engrams. Blue bars indicate the time the laser was turned on during the 3 stimulation periods. **(i, j, k)** Comparison of carbon dioxide production between the on and off epochs during the three stimulations of cold-sensitive cells. **(l)** Comparison of carbon dioxide production between the on and off epochs of cold-sensitive cells during all stimulations combined. *n* = 8-9 mice per group. * $p < 0.05$, ** $p < 0.01$. EE, energy expenditure; Stim 1, stimulation 1; Stim 2, stimulation 2; Stim 3, stimulation 3; VCO_2, carbon dioxide production.

4.3.2 Optogenetic activation of no-cold engrams does not increase metabolic rate.

To confirm that the above-described increases in metabolic rate were due to contextual cold memories, we designed a control experiment where mice were run through the same timeline but were never exposed to the cold (Figure 4.3.3a-b). As such, we labeled no-cold engram cells and optogenetically reactivated them in a neutral context. Our results showed that optogenetically stimulating no-cold engram cells does not increase oxygen consumption (Figure 4.3.3c). There were no significant differences between on and off periods, during any of the three stimulations (Figure 4.3.3d-g). Interestingly, a slight decrease in oxygen consumption was found when the laser was on compared to when it was off (Figure 4.3.3g). Next, we directly compared optogenetic stimulation of cold-sensitive engrams with “no-cold” contextual engrams (Figure 4.3.3h). We show that oxygen consumption significantly increased in the cold labeled group compared to the no-cold labeled group during laser stimulation (Figure 4.3.3i). This difference in metabolic rate during laser activation was not due to pre-existing differences between the cohorts, as no differences were found between the cold and no-cold labeled groups when the laser was off (Figure 4.3.3i). Finally, we show that optogenetically stimulating no-cold engram cells does not increase energy expenditure or carbon dioxide production either, as there were no significant differences in these rates during any of the three stimulations (Figure 4.3.4). Therefore, we conclude that only cold-sensitive engrams control whole-body metabolism, as optogenetic activation of no-cold engrams did not results in increased metabolic rate.

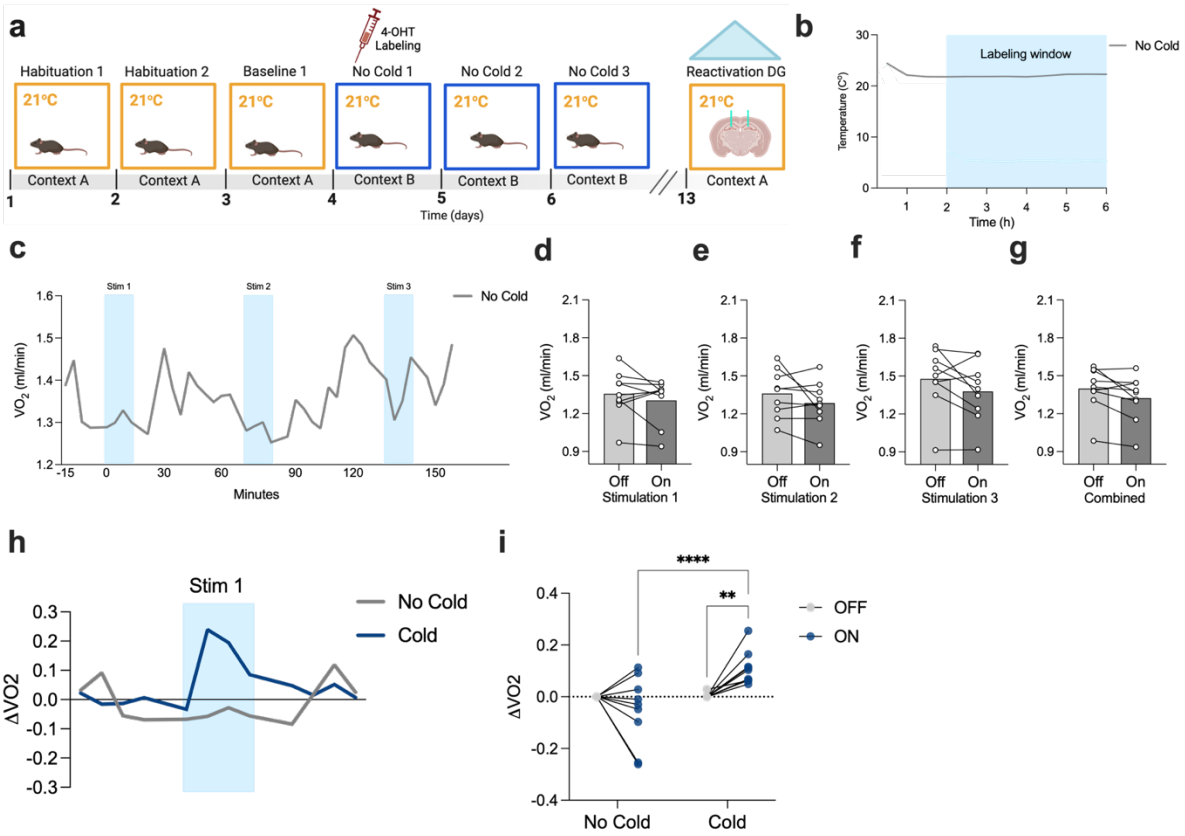

Figure 4.3.3 Artificial optogenetic reactivation of no-cold engrams in the DG does not increase oxygen consumption. (a) Diagrammatic representation of experimental timeline to label and reactivate no cold control engrams. **(b)** Environmental temperature during the labeling window on no cold day 1. **(c)** Time plot of oxygen consumption during artificial reactivation of no cold control engrams. Blue bars indicate the time the laser was turned on during the 3 stimulation periods. **(d, e, f)** Comparison of oxygen consumption between the on and off epochs during the three stimulations of no cold control cells. **(g)** Comparison of oxygen consumption between the on and off epochs of no cold control cells during all stimulations combined. **(h)** Change of oxygen consumption before, during and after stimulating cold-sensitive engram cells and no cold control cells normalized to the initial 20 minutes of recording. **(i)** Comparison of the change in oxygen consumption during on and off epochs between cold-sensitive stimulated cells and no cold control stimulated cells. *n* = 8-9 mice per group. ** $p < 0.01$, **** $p < 0.0001$. 4-OHT, 4-hydroxytamoxifen; DG, dentate gyrus; VO_2, oxygen consumption; Stim 1, stimulation 1; Stim 2, stimulation 2; Stim 3, stimulation 3.

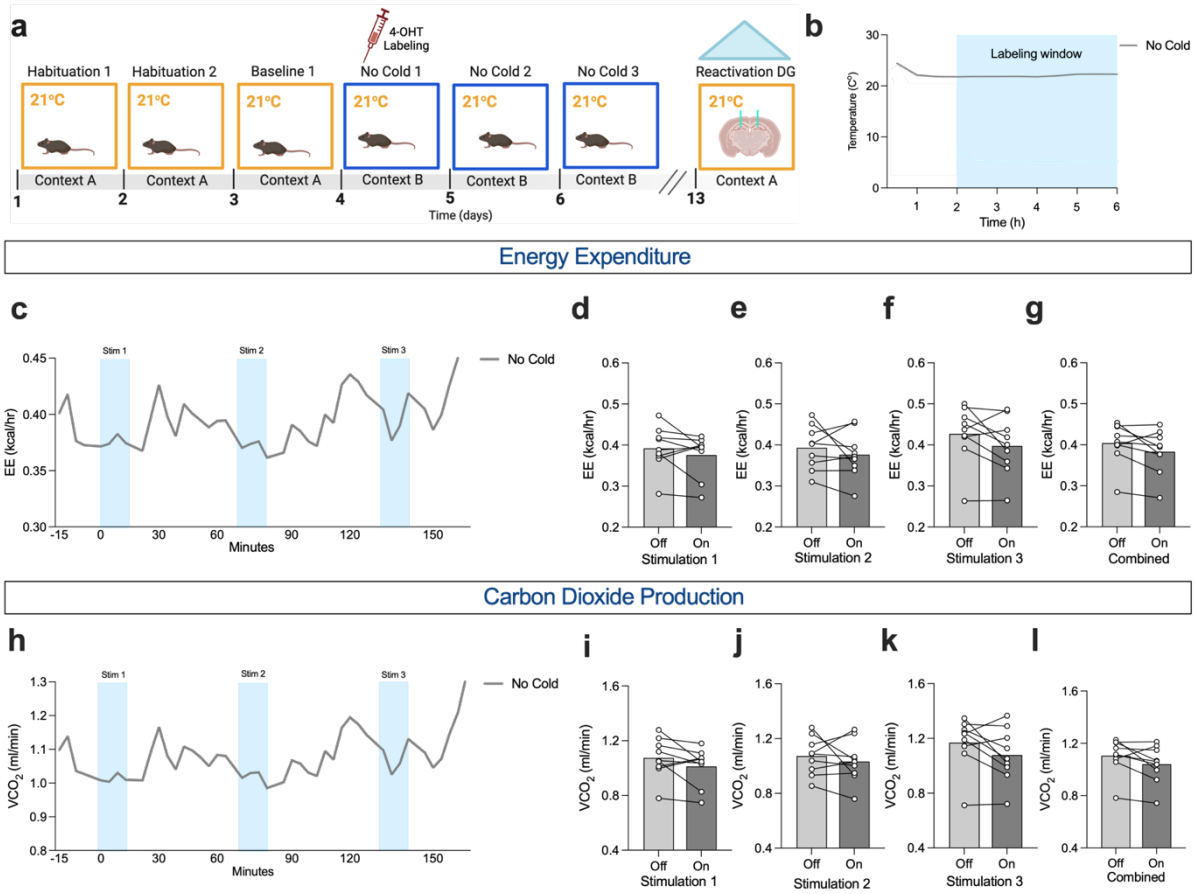

Figure 4.3.4 Artificial optogenetic reactivation of no-cold engrams in the DG does not increase metabolic rates. **(a)** Diagrammatic representation of experimental timeline to label and reactivate no cold control engrams. **(b)** Environmental temperature during the labeling window on no cold day 1. **(c)** Time plot of energy expenditure during artificial reactivation of no cold control engrams. Blue bars indicate the time the laser was turned on during the 3 stimulation periods. **(d, e, f)** Comparison of energy expenditure between the on and off epochs during the three stimulations of no cold control cells. **(g)** Comparison of energy expenditure between the on and off epochs of no cold control cells during all stimulations combined. **(h)** Time plot of carbon dioxide production during artificial reactivation of no cold control engrams. Blue bars indicate the time the laser was turned on during the 3 stimulation periods. **(i, j, k)** Comparison of carbon dioxide production between the on and off epochs during the three stimulations of no cold control cells. **(l)** Comparison of carbon dioxide production between the on and off epochs of no cold control cells during all stimulations combined. 4-OHT, 4-hydroxytamoxifen; DG, dentate gyrus; VO_2, oxygen consumption; Stim 1, stimulation 1; Stim 2, stimulation 2; Stim 3, stimulation 3.

4.3.3 Optogenetic activation of cold engrams increases metabolic rate across lines.

To demonstrate that optogenetic reactivation of cold-sensitive engrams is possible with multiple transgenic mouse lines, we designed an additional experiment where we labeled and reactivated cold-sensitive engram cells using c-Fos-tTa transgenic mice (Figure 4.3.5a). Here, we labeled cold-sensitive engrams in the DG on cold day 1 by removing DOX from the animals diet and subsequently optogenetically reactivated the labeled cells in a neutral context (Figure 4.3.5b). In line with our previous findings, we show that optogenetic activation of cold-sensitive engrams increases metabolic rate, whereas no light controls did not show an increase in metabolic rate (Figure 4.3.5c-h). As such, these results show that cold-sensitive engrams can be artificially reactivated with multiple transgenic mouse lines and with different engram labeling strategies.

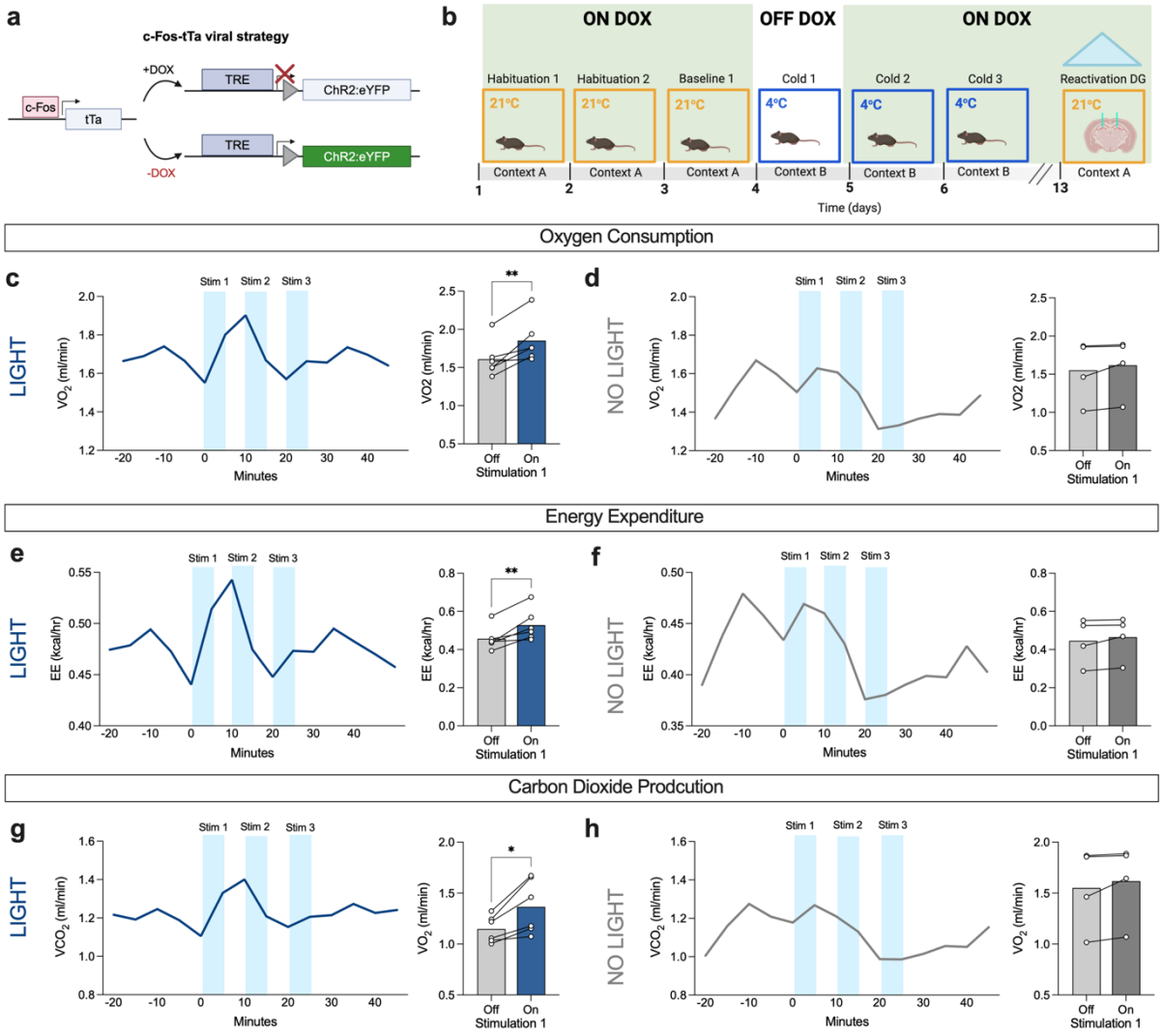

Figure 4.3.5 Artificial reactivation of cold-sensitive engrams in the DG increases metabolic rate in c-Fos tTA mice. (a) Diagrammatic representation of the c-Fos tTA transgenic labeling system for ChR2::GFP expression. **(b)** Diagrammatic representation of experimental timeline to label cold-sensitive memory ensembles using c-Fos tTA mice. Time plot of **(c),** oxygen consumption **(e),** energy expenditure and **(g),** carbon dioxide production during artificial reactivation of cold-sensitive engrams (left), with comparison of oxygen consumption, energy expenditure and carbon dioxide production between the on and off epochs during the first stimulation of cold-sensitive cells (right). Time plot of **(d),** oxygen consumption **(f),** energy expenditure and **(h),** carbon dioxide production during artificial reactivation of no cold control cells (left), with comparison of oxygen consumption, energy expenditure and carbon dioxide production between the on and off epochs during the first stimulation of no cold control cells (right). Blue bars indicate the time the laser was turned on during the 3 stimulation periods. *n* = 4-6 mice per group; * $p < 0.05$, ** $p < 0.01$. ChR2, channelrhodopsin-2; GFP, green fluorescent protein; DOX, doxycycline; VO_2, oxygen consumption; VCO_2, carbon dioxide production; Stim 1, stimulation 1; Stim 2, stimulation 2; Stim 3, stimulation 3.

4.3.4 Chemogenetic inhibition of cold-sensitive engrams prevents the memory associated increases in oxygen consumption.

In the above-described experiments, we set out to determine whether cold-sensitive engrams are functionally relevant for whole-body metabolism, by optogenetically reactivating cold engrams in the DG. To further explore the role of cold-sensitive engram cells, we aimed to chemogenetically inhibit these cells in vivo. To do so, we injected inhibitory DREADDs into the DG of TRAP2 mice (Figure 4.3.6a-b). Next, we labeled cold-sensitive engrams on cold day 1, and chemogenetically inhibited these cells by injecting CNO on test day 1 (Figure 4.3.6c). Here, we show that control animals that are injected with Saline on test day 1 showed increased oxygen consumption rates on test day 1 compared to baseline day 1 (Figure 4.3.6d). This increase in oxygen consumption was found throughout the first two hours, and for the combined total testing time (Figure 4.3.6e-g).

Next, we found that mice injected with CNO on test day 1 no longer show the memory associated increase in oxygen consumption (Figure 4.3.6h). Indeed, we show that the conditioned response is no longer present at any point throughout the testing time (Figure 4.3.6i-k). Finally, we plotted the responses of the Saline and CNO injected mice as the percentage of change in oxygen consumption rates that occurred between test day 1 and baseline day 1 (Figure 4.3.6l-m). When directly comparing the Saline and CNO injected mice, we found a significantly higher percentage of change in the Saline injected mice compared to the CNO injected mice (Figure 4.3.6n). Together, these data suggest that chemogenetic inhibition of cold-sensitive cells in the DG prevents the conditioned whole-body response, as we found no increases in oxygen consumption in mice injected with CNO specifically.

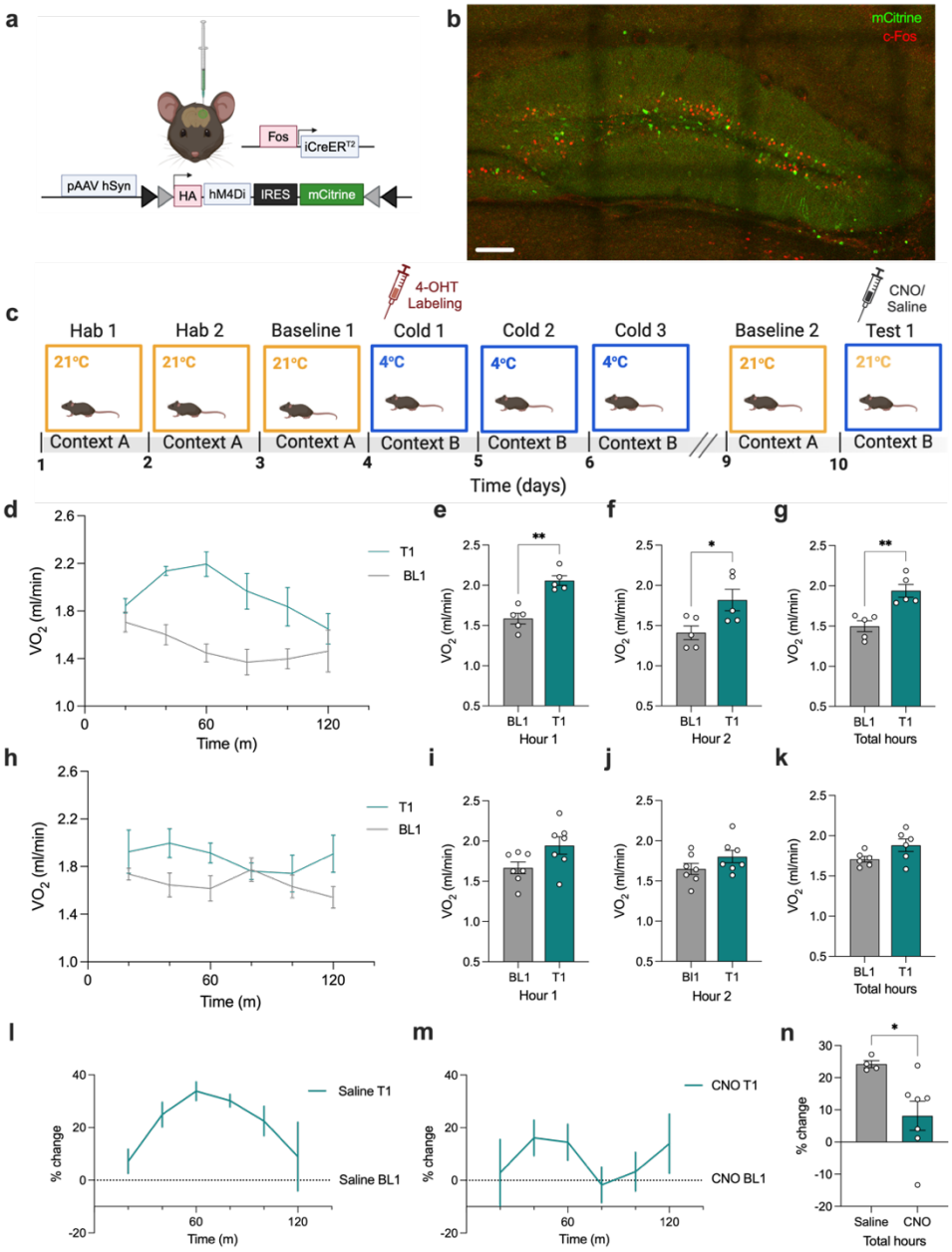

Figure 4.3.6 Chemogenetic inhibition of cold-sensitive engrams in the DG prevents the memory associated increases in oxygen consumption. (a) Genetic strategy **(b)** Representative image of hippocampal slice with c-Fos$^+$ cells (red) and mCitrine$^+$ cells (green) **(c)** Diagrammatic representation of experimental timeline to label and inhibit contextual cold memory engrams. **(d)** Time plot of oxygen consumption of saline injected mice during Baseline 1 and Test 1 **(e, f, g)** Comparison of oxygen consumption of saline injected mice during Baseline 1 and Test day 1 at hour one, hour two and total time averaged. **(h)** Time plot of oxygen consumption of CNO injected mice during Baseline 1 and Test 1 **(i, j, k)** Comparison of oxygen consumption of CNO injected mice during Baseline 1 and Test day 1 at hour one, hour two and total time averaged. **(l)** Time plot of the % change of oxygen consumption on Test 1 compared to Baseline 1 in Saline injected mice. **(m)** Time plot of the % change of oxygen consumption on Test 1 compared to Baseline 1 in CNO injected mice. **(n)** Comparison of the % change of oxygen consumption between Saline and CNO injected mice. *n* = 5-7 mice per group. * $p < 0.05$, ** $p < 0.01$. 4-OHT, 4-hydroxytamoxifen; VO_2, oxygen consumption; T1, test 1; BL1, baseline 1; m, minutes; CNO, clozapine N-oxide.

4.3.5 Chemogenetic inhibition of cold-sensitive engrams prevents the memory associated increases in metabolic rate.

To further establish whether the chemogenetic inhibitory results found above were specific for oxygen consumption rates, we additionally analyzed carbon dioxide production and energy expenditure. Cold-sensitive engrams were labeled on cold day 1, and chemogenetically inhibited on test day 1 with CNO (Figure 4.3.7a). In line with our previous results, we found that Saline injected control animals showed an increase in carbon dioxide production on test day 1, compared to baseline day 1 (Figure 4.3.7b-c). However, this increase was not observed in the CNO injected animals, as no difference in carbon dioxide production was found in these mice between test day 1 and baseline day 1 (Figure 4.3.7d-e). Moreover, direct comparison of the percentage of change between Saline and CNO injected mice revealed a significantly higher percentage of change in carbon dioxide production in Saline injected controls compared to CNO injected mice (Figure 4.3.7f). Similar results were found with regards to energy expenditure, as Saline control mice showed increased energy expenditure on test day 1 compared to baseline day 1, whereas CNO injected animals showed no differences (Figure 4.3.7g-j). Finally, we found that CNO injected mice had a lower percentage of change in energy expenditure compared to Saline injected mice (Figure 4.3.7k). Together, these data show that by inhibiting cold-sensitive cells in the DG, we were able to inhibit contextual cold memories and as a result, prevent the conditioned whole-body responses that were associated with those memories.

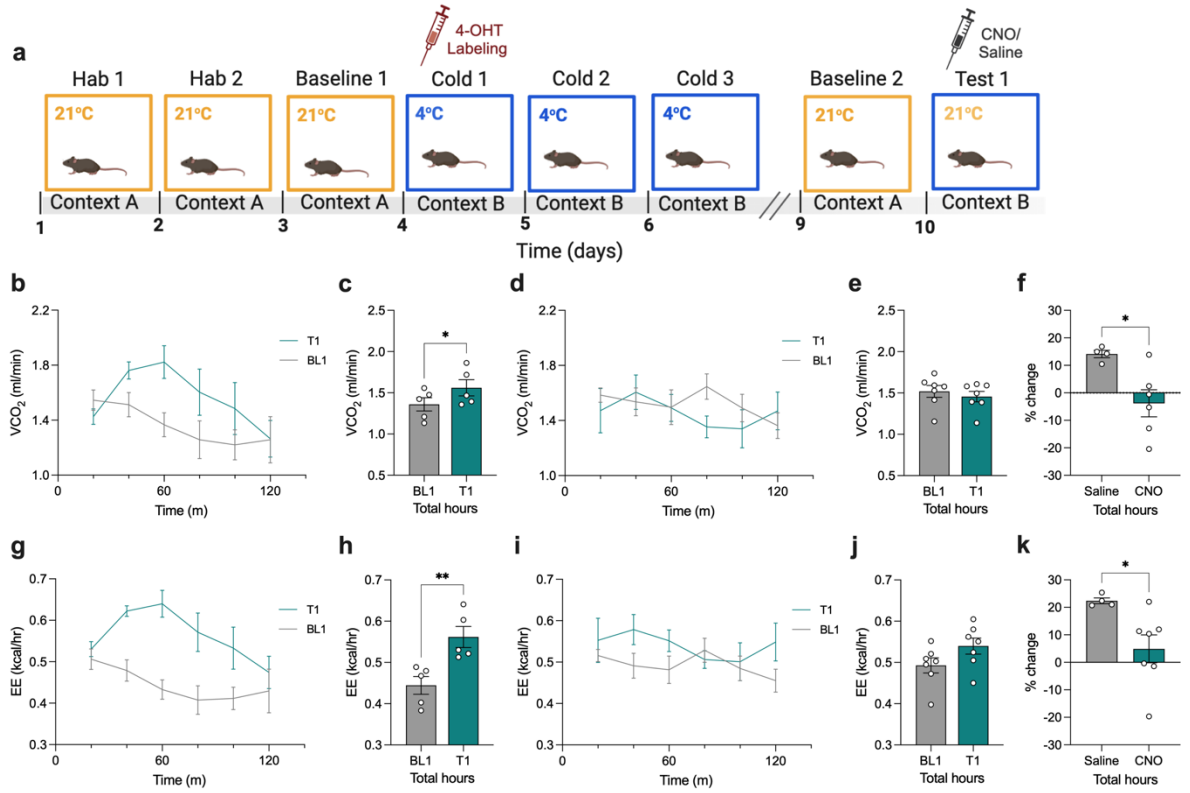

Figure 4.3.7 Chemogenetic inhibition of cold-sensitive engrams in the DG prevents the memory associated increases in metabolic rates. (a) Diagrammatic representation of experimental timeline to label and inhibit contextual cold memory engrams. **(b)** Time plot of carbon dioxide production of saline injected mice during Baseline 1 and Test 1 **(c)** Comparison of carbon dioxide production of saline injected mice during Baseline 1 and Test day 1 for the total time averaged. **(d)** Time plot of carbon dioxide production of CNO injected mice during Baseline 1 and Test 1 **(e)** Comparison of carbon dioxide production of CNO injected mice during Baseline 1 and Test day 1 for the total time averaged. **(f)** Comparison of the % change of carbon dioxide production between Saline and CNO injected mice. **(g)** Time plot of energy expenditure of saline injected mice during Baseline 1 and Test 1 **(h)** Comparison of energy expenditure of saline injected mice during Baseline 1 and Test day 1 for the total time averaged. **(i)** Time plot of energy expenditure of CNO injected mice during Baseline 1 and Test 1 **(j)** Comparison of energy expenditure of CNO injected mice during Baseline 1 and Test day 1 for the total time averaged. **(k)** Comparison of the % change of energy expenditure between Saline and CNO injected mice. *n* = 5-7 mice per group. * $p < 0.05$, ** $p < 0.01$. 4-OHT, 4-hydroxytamoxifen; VCO_2, carbon dioxide production; T1, test 1; BL1, baseline 1; m, minutes; CNO, clozapine N-oxide; EE, energy expenditure.

DISCUSSION

In this chapter, we used optogenetic and chemogenetic tools to artificially manipulate cold-sensitive engrams. By using these techniques, we aimed at investigating whether contextual cold memories controlled whole-body metabolic responses. We showed that we could label cold-sensitive engrams that were active during a cold experience, and that we could artificially reactivate these cells in a neutral context using optogenetics. With this protocol, we showed that optogenetic reactivation of cold-sensitive cells increased whole-body metabolism. Importantly, we showed that cold-sensitive engram cells could be reactivated with multiple transgenic mouse lines and with different engram labeling strategies. Finally, by using chemogenetics, we showed that we could also inhibit cold-sensitive cells and prevent the conditioned whole-body responses that were associated with contextual cold memories.

Previous studies have shown that optogenetic activation of engrams is sufficient to induce a learning-specific conditioned response [16]. In these studies, behavioral responses such as freezing are the most commonly used measure of the conditioned response [15]. To our knowledge, this is the first study that has investigated whether memories in general, and engrams specifically, control whole-body responses such as metabolic rate. In this chapter, we have shown that cold-sensitive engrams, and therefore contextual cold memories, control whole-body metabolism. These results suggest that engram cells not only control behavioral responses, but that they additionally control a variety of whole-body processes. For example, it is likely that fear engrams not only control freezing behaviors, but also bodily processes such as heart rate and the release of specific stress hormones. More studies are needed to investigate how and which bodily processes are controlled by the engram cells of different types of memories.

One big question that remains is whether bodily responses in turn also have an influence on engram cells specifically and memories in general. For example, increasing heart rate by optogenetic activation of cardiac rhythms resulted in enhanced anxiety [12]. It is therefore highly likely that information not only flows from the brain to the body but also vice-versa. With the development of novel optogenetic tools, it is now possible to manipulate circuits outside of the brain in organs such as BAT. With the help of these tools, future studies will be able to determine how bodily

states modulate the storage and formation of memories, and how this relates to engram cells.

We showed that we could artificially manipulate temperature engrams and control whole-body metabolic responses as a result. Interestingly, we found that after optogenetically stimulating cold-sensitive engram cells, an hour-long break was necessary to allow metabolic rates to return to baseline levels. This is in contrast with other engram studies showing that 5-minute breaks are sufficient for behavioral responses to return to baseline. However, our data suggest that complex bodily responses may take longer to return to their original baseline. This is in line with previous studies, where body temperature only returned to baseline levels after a prolonged period of time follow optogenetic reactivation of hypothalamic neurons [148]. We also found that we could only increase metabolic rates during the first two consecutive optogenetic stimulations, but not during a third stimulation. It remains unclear whether this effect is due to an attenuation of whole body-responses, a limitation of optogenetic engram stimulation, or rather competing information from the real temperature experienced by the animal, compared to cold temperature information from the memory. Indeed, future studies are necessary to further explore the limitations of optogenetically stimulating engram cells and their effects on whole-body responses.

In this study we exclusively manipulated cold-sensitive engrams in the DG, as we aimed at understanding whether contextual memories have an influence on bodily processes. However, our previous results have shown that functional connectivity between the hippocampus and the hypothalamus increases during cold retrieval. Moreover, studies have previously shown that reactivation of preoptic hypothalamic neurons results in the alteration of whole-body responses such as heart rate, body temperature and energy expenditure. As such, we hypothesize that the results found in this chapter may in part be due to an underlying network that emerges between the hippocampus and the hypothalamus when we artificially manipulate cold engrams in the DG. However, to fully elucidate the underlying network that is activated when we artificially stimulate cold engrams in the DG, tracing studies are needed to determine whether activation of the DG result in the activation of other hypothalamic regions.

In this chapter we aimed at optogenetically reactivating and chemogenetically inhibiting cold-sensitive engrams. Here, we aimed at understanding whether artificially reactivating cold memories affects whole-body thermoregulatory responses. This chapter showed gain- and loss-of-function evidence that cold-sensitive engrams are located in the DG and that these cells control whole-body metabolic rates. Taken together, our data provides evidence that memories can control peripheral physiological processes beyond the traditionally studied behavioral responses.

Chapter 5:

Natural and artificial reactivation of cold memories upregulates thermogenesis genes in brown adipose tissue.

INTRODUCTION

5.1.1 The homeostatic role of adipose tissue depots.

Adipose tissue is a complex organ that has been found to have profound effects on physiology and pathophysiology. It has been shown to be essential for whole-body metabolism and is now regarded as the endocrine organ at the center of systemic homeostasis [150]. Adipose tissue can be subdivided into two major types: white adipose tissue (WAT) and brown adipose tissue (BAT). WAT plays a predominant role in energy storage and systemic glucose homeostasis [151]. Moreover, WAT is mainly composed of white adipocytes, which consist of a single large lipid droplet with few mitochondria. In contrast, BAT is mainly composed of brown adipocytes, which contain multiple small lipid droplets with a high abundance of mitochondria. The primary function of BAT is thermogenesis, a process that is strongly induced by cold exposure. Both WAT and BAT have been found in humans and rodents, across different body sites (Figure 5.1.1). Indeed, studies have shown that adult humans have metabolically active BAT depots, and that cold exposure results in increases of BAT content in both humans and rodents [150-152].

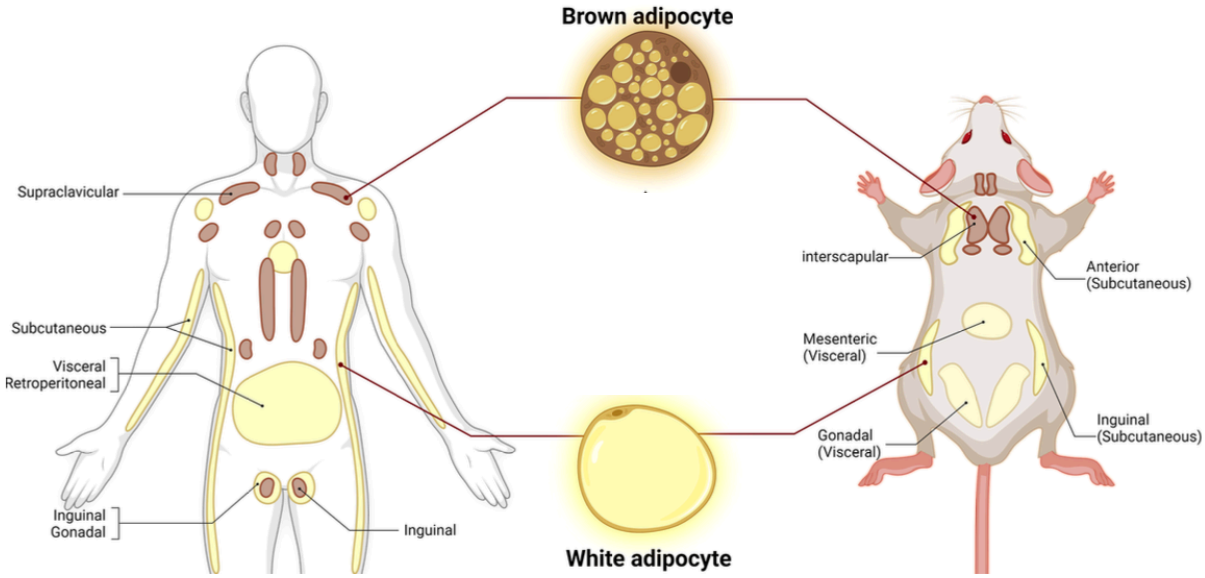

Figure 5.1.1 Adipose tissue in humans and rodents. Both WAT and BAT have been found in multiple locations in humans and rodents. WAT consists of a large lipid droplet with few mitochondria. BAT contains multiple lipid droplets with many mitochondria. *Adapted from Torres Irizarry et al., 2022 [151].*

5.1.2 The BAT thermogenesis pathway.

As described in previous chapters, thermoregulation is the ability of animals to maintain their physiological body temperature within a narrow range. This type of thermogenesis relies predominantly on brown adipocytes in BAT, where mitochondrial respiration is used for heat dissipation. As BAT is highly vascularized, it can transfer dissipated heat to the blood, and therefore maintain body temperature within a set range [153]. External temperature is relayed to BAT via the sympathetic nervous system, through the release of noradrenaline from nerve terminals into the BAT environment [66]. Noradrenaline will subsequently activate the β3-adrenergic receptor (AR-β3) on the surface of adipocytes (Figure 5.1.2), inducing the activation of cyclic adenosine monophosphate (cAMP) signaling cascades [41]. The increased concentrations of intracellular cAMP in adipocytes will induce the phosphorylation and activation of hydrolytic enzymes adipose triglyceride lipase (ATGL), and hormone sensitive lipase (HSL).

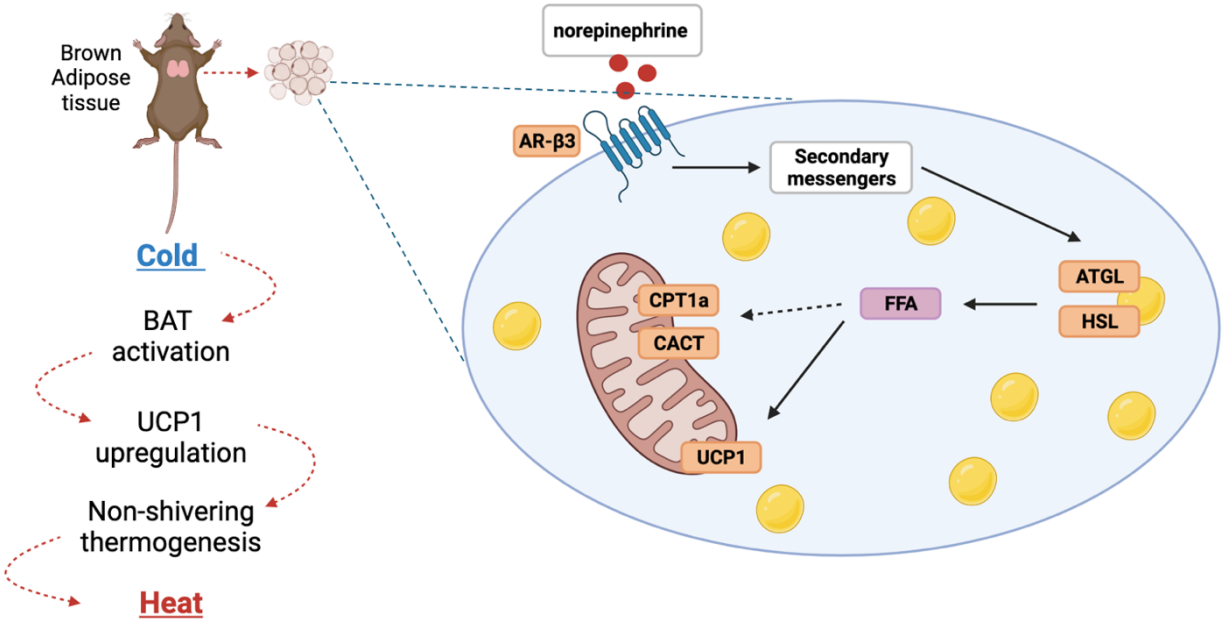

Figure 5.1.2 Brown adipose tissue thermogenesis is important to generate heat. Cold exposure will cause the activation of BAT and the upregulation of UCP-1. This will result in non-shivering thermogenesis and the production of heat. Cold exposure will cause noradrenaline to be released, resulting in the activation of β3-adrenergic receptors. Through secondary messengers, ATGL and HSL will be activated, which will cause them to convert lipid droplets to FFAs. FFAs are converted to fatty acyl-CoA molecules by CPT1 and transported into the mitochondria by CACT. Here, it acts as fuel for UCP1.

Both ATGL and HSL will then convert lipid droplets to free fatty acids (FFAs) and glycerol [154]. FFAs are converted to fatty acyl-CoA molecules, which in turn are converted to acylcarnitines by the enzyme carnitine palmitoyltransferase 1 (CPT1) on the surface of the mitochondrial membrane. Next, the transporter carnitine acyltransferase (CACT) transports the acylcarnitines into the mitochondria where it acts as fuel for the uncoupling protein-1 (UCP-1) on the inner mitochondrial membrane. UCP-1 is then able to create heat by uncoupling the electron transport chain (ETC) from adenosine triphosphate (ATP) generation to allow for heat dissipation [155].

5.1.3 BAT activation after different psychological stressors.

Adipose tissue is considered to act as a regulator of various metabolic and endocrine processes. Indeed, not only has BAT been shown to be key for non-shivering thermogenesis, it has also been shown to regulate appetite, lipid metabolism and glucose homeostasis [151]. More recently, studies have suggested that BAT might be a stress-responsive endocrine organ that is required for an adaptive ‘’fight or flight’’ response. For example, Kataoka and colleagues examined the effect of social defeat stress on the temperature of interscapular BAT (T_{BAT}) in rats. In this study, they showed that when intruder rats were introduced to the cages of resident rats, the intruders were defeated by the residents and the T_{BAT} of the intruders increased as a result of this defeat [156]. The authors therefore suggest that psychological stress potentially activates BAT thermogenesis. However, in this study no data was provided regarding any of the above-described genes that are essential for BAT dependent non-shivering thermogenesis. In a separate study, Qing and colleagues showed that psychological stress resulted in interleukin-6 (IL6) production from brown adipocytes in an AR-β3 dependent manner [157]. However, they also show that no thermogenic programs were involved in this response as they found no differences in UCP-1, despite finding increased AR-β3 activity. Finally, Jovanovic and colleagues showed that exposing male mice to the predator odor trimethylthiazoline (TMT) does not increase BAT temperature [44]. As such, it seems that not all types of psychological stress recruit BAT and that different stressors elicit different responses from this organ. As such, BAT could potentially be considered a stress-responsive endocrine organ, that has several different responses depending on the contextual inputs.

Up until now, no studies have examined whether specific memories can cause the upregulation of genes in organs outside of the brain. As such, in this chapter, we set out to determine whether contextual cold memories control whole-body thermoregulatory responses by examining thermogenic genes in BAT. First, we leveraged our previously designed behavioral timelines to examine how cold exposure influences BAT. We next aimed to establish whether natural retrieval of a cold memory has an effect on thermogenic genes in BAT. To fully understand how cold memories interact with these genes, we additionally labeled cold-sensitive engrams with ChR2, optogenetically reactivated these engram cells and harvested BAT for further analysis. Taken together, this chapter's research question aims at examining whether natural and artificial reactivation of cold memories upregulates thermogenesis genes in BAT.

METHODS

5.2.1 Mice

All experiments except the optogenetic reactivation experiments were performed with C57BL/6J mice. Optogenetic reactivation experiments were performed with TRAP2 x Ai32 mice. Male mice were used in all experiments. All mice were group-housed in a 12:12-h (07:00-19:00) light-dark colony room at 22°C. Food and water were provided *ad libitum*, and all testing was performed during the light phase. Mice used for experiments were approximately 8-12 weeks of age. All experiments were conducted in accordance with the European Directive 2010/63/EU, under an authorization issued by the Health Products Regulatory Authority Ireland and approved by the Animal Ethics Committee of Trinity College Dublin.

5.2.2 Optic Fiber Implant Surgeries

Mice that were used in optogenetic experiments were implanted with a custom fiber optic implant using the same surgical protocol as described in chapter 4.

5.2.3 Cold Training Schedule

For the natural cold recall experiments, the same behavioral paradigm was used as the one described in chapter 1.

5.2.4 Optogenetic Reactivation Timeline

For the artificial cold recall experiments, the same optogenetic settings and behavioral paradigm (TRAP2 x Ai32 strategy) were used as the ones described in chapter 4.

5.2.5 Contextual Fear Conditioning Timeline

Prior to training, mice were handled for 3 consecutive days in order to habituate them to the experimenter. One day prior to the training day, mice were habituated to the arena and allowed to freely explore the context for 10 minutes. The next day, mice underwent a contextual fear conditioning protocol, where they were allowed to explore the arena for the first 3 minutes. After these 3 minutes, half of the mice received 3 foot shocks (0.2 s, 0.75mA) that were spaced by intervals of 1 min, whereas the other half of the mice received no foot shocks. Mice were subsequently returned to their home cage for 45 minutes.

5.2.6 Predator Odor Exposure Timeline

Mice were placed into a vacuum powered 4-chamber olfactory arena, which was replicated from previously published designs [158]. Air entered each corner of the arena at a flow rate of 150ml/minute and was odorized by passing through a bottle containing 20ml of H_2O or 350mM trimethylthiazole. Mice were exposed to the odor for 5 minutes and were then sacrificed for tissue collection.

5.2.7 4-OHT

To label cold-sensitive engrams in transgenic animals, we intraperitoneally injected mice with 4-OHT (50 mg/ kg, Santa Cruz). All 4-OHT was freshly prepared on the labeling day in a mix of sunflower seed oil and castor oil (4:1, Sigma-Aldrich) at 10 mg/ml.

5.2.8 Tissue Harvest

For the natural cold recall experiments, BAT was harvested on Baseline day 1, Cold day 1, Baseline day 2, and Test day 1. To ensure that the differences seen were due to the differences in conditions and not time of day, all tissue was harvested exactly 3 hours after the mice were put inside the Promethion cages. For the artificial cold recall experiments, BAT of mice with cold-sensitive stimulated cells and no cold control stimulated cells was harvested 45 minutes after the last optogenetic stimulation ended. For the contextual fear conditioning experiments, BAT was harvested 45 minutes after the training session ended. Finally, for the predator odor exposure experiments, BAT was harvested exactly one hour after the animals were exposed to the odors.

5.2.9 Brown adipose Tissue Preparation

Mice were euthanized by CO_2 inhalation and adipose tissue was removed by making a careful incision between the shoulder blades. Interscapular brown adipose tissue was subsequently collected, snap frozen in liquid nitrogen, and stored at -80°C.

5.2.10 RNA Extraction and qPCR Analysis

Harvested brown adipose tissue was defrosted at room temperature and transferred to a 2ml tube and stainless-steel beads were added to each individual tube. Next, tissues were homogenized in 1mL trizol reagent in a tissue lyser for 2.5 minutes at 25 pulses per second. 200µL chloroform was subsequently added to each tube, after

which they were inverted and left at room temperature for 3 minutes. All tubes were then centrifuged at 12,000g for 15 minutes, the RNA was transferred into a new tube and 500µL isopropanol was added to precipitate the RNA. All tubes were inverted 10 times and left at room temperature for 10 minutes, before being centrifuged again at 12,000g for 10 minutes. Supernatants were then discarded, and all remaining RNA pellets were washed in 1mL of 25% RNAse free dH20 and 75% ethanol. After being centrifuged at 12,000g for 5 minutes, all supernatants were discarded by inverting the tube. RNA pellets were left to dry at room temperature for 20-30 minutes until they were transparent, after which they were resuspended in 50µl RNAse free water. Finally, RNA was left on ice for 30 min and subsequently put on a heat block at 55°C for 15 minutes. A Nanodrop 2000 UV spectrophotometer (Thermo Fisher Scientific) was used to assess RNA quality and concentration. 20µl of cDNA was subsequently synthesized from 2µg of isolated RNA using a cDNA reverse transcription kit (Biosciences Ltd) in a MiniAmp Thermal Cycler (BD Biosciences). qPCRs were then performed to quantify the relative mRNA expression of genes of interest. Relative mRNA levels were calculated using the ΔΔ cycle threshold (ΔΔCt) method and normalized to corresponding endogenous controls (*Ppib*).

5.2.11 Brain Tissue Preparation and Immunohistochemistry

Brains were harvested from mice that went through the artificial cold recall experiments. All brains were prepared and immunolabeled using the same protocols that were described in chapter 3.

5.2.12 Confocal Imaging

In order to check for implant location, all images were taken on a confocal scanning microscope as previously described in Chapter 3. Only the mice that had the correct implant locations were kept in subsequent analyses.

5.2.13 Statistics

All data were analyzed using Prism 10. All data were graphed as means ± Standard errors of the mean (SEM). An alpha level of 0.05 was used as a criterion for statistical significance. The results of figures 5.3.1, 5.3.2, 5.3.3, 5.3.4 and 5.3.5 were analyzed using unpaired t-tests.

RESULTS

5.3.1 Cold exposure causes an increase in thermogenic gene expression in BAT.

As discussed above, the lipolytic metabolic pathway has been demonstrated to fuel the thermogenic response in brown adipocytes via UCP-1 (Figure 5.3.1a). To determine the effect of cold exposure on the thermogenic genes in this pathway, we harvested BAT from experimental mice that were exposed to a 4°C environment (CL1), and from control mice that were exposed to a 21°C environment (BL1; Figure 5.3.1b). In line with previous studies, we found that mice that were exposed to 4°C had a significant upregulation of *Ucp1* in BAT compared to the controls (Figure 5.3.1c). Moreover, we found an increase in mitochondrial genes *Cpt1*α and *Cact* in cold exposed mice, compared to the 21°C exposed control mice (Figure 5.3.1d-e). To fully examine the effect of cold on the entire thermogenic pathway, we also compared genes associated with fatty acid release from lipid droplets (Figure 5.3.1f-g). We found that *Atgl* significantly increased in mice exposed to 4°C, compared to mice exposed to 21°C (Figure 5.3.1f). Although not significant, we found a similar trend in *Hsl* (Figure 5.3.1g). Finally, we found an increase in *Pgc1*α expression in cold exposed mice compared to controls (Figure 5.3.1h). Together, these findings show that we could replicate existing findings and confirm that cold exposure causes an increase in thermogenic gene expression in BAT.

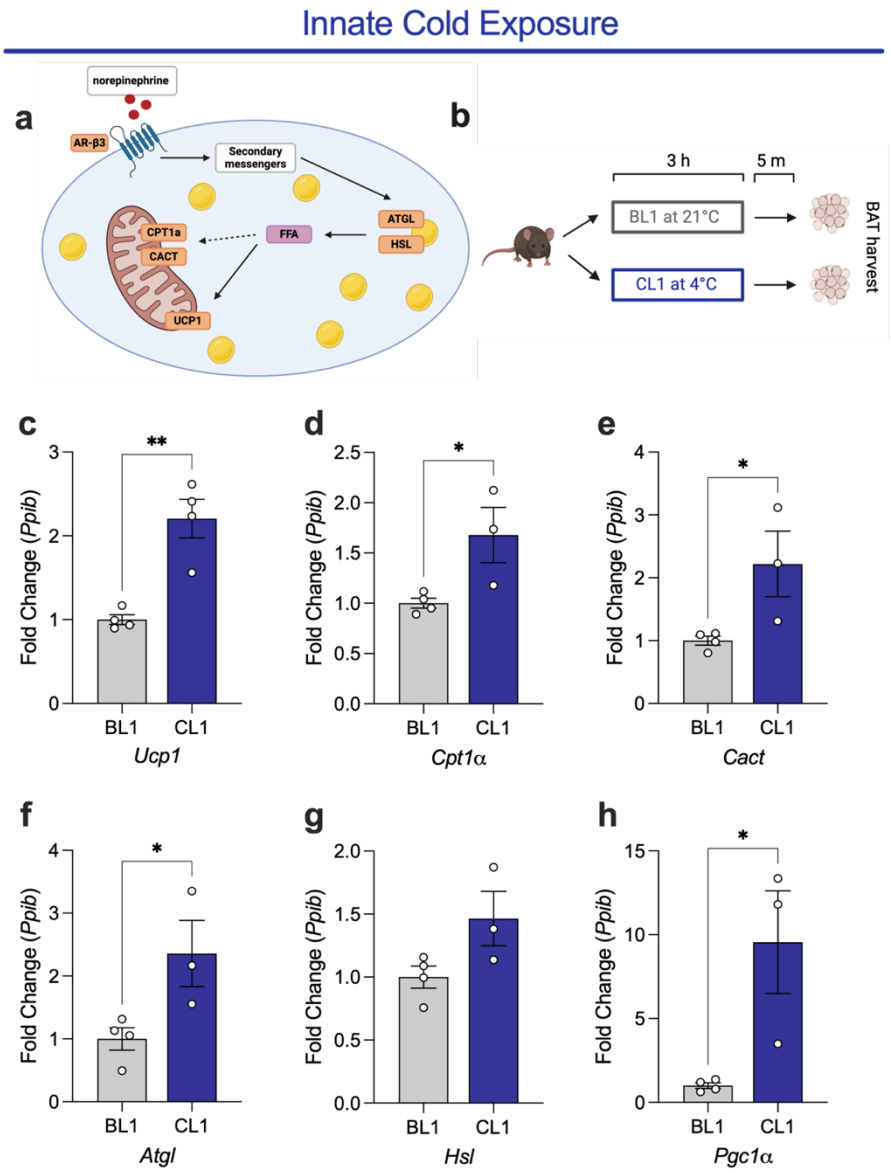

Figure 5.3.1 Innate cold exposure increases lipolytic and thermogenic gene expression in BAT. (a) Diagrammatic representation of the thermogenic pathway in BAT. **(b)** Diagrammatic representation of experimental timeline for tissue collection. Relative expression of lipolysis and thermogenesis genes **(c),** *Ucp1,* **(d),** *Cpt1α,* **(e),** *Cact,* **(f),** *Atgl*, **(g),** *Hsl* and **(h),** *Pgc1α* from the BAT of mice housed during BL1(21°C) compared to cold exposed mice (CL1, 4°C). *n* = 3-4 mice per group. * $p < 0.05$. BAT, brown adipose tissue; FFA, free fatty acid; BL1, baseline 1; CL1, cold 1.

5.3.2 Natural recall of a cold memory increases thermogenic gene expression in BAT.
Our next aim was to understand the relationship between a memory of a cold experience and whole-body metabolic responses. Since the above results showed that a cold experience causes an increase in thermogenic gene expression in BAT, we asked whether a memory of that experience would cause a similar increase. To investigate this, we harvested BAT from mice on BL2 and T1 (Figure 5.3.2a-b). Strikingly, we find that several thermogenic genes are also upregulated in mice during cold recall on T1, compared to control mice on BL2 (Figure 5.3.2c-h). Indeed, we observed an upregulation of *Ucp1* (Figure 5.3.2c), in addition to an increase in mitochondrial genes, *Cpt1*α and *Cact* (Figure 5.3.2d-e) and genes associated with fatty acid release from lipid droplets, such as *Atgl* and *Hsl*, (Figure 5.3.2f-g) and *Pgc1*α (Figure 5.3.2h). Together, these results showed that natural recall of a cold memory is sufficient to upregulate thermogenic genes in BAT.

5.3.3 Artificial reactivation of cold memories increases thermogenic genes in BAT.
Since natural recall of cold memories was sufficient to upregulate thermogenic genes in BAT, we next asked whether we could optogenetically reactivate cold-sensitive engrams to artificially induce a thermogenic response. To answer this, we compared thermogenic gene expression from mice that underwent optogenetic reactivation of cold-sensitive engrams, in comparison to mice with no-cold engram cells (Figure 5.3.3a-b). Our results showed that artificial reactivation of a cold-sensitive engram led to an increase in *Ucp1* and *Cpt1*α expression in BAT, compared to the reactivation of no-cold engram cells (Figure 5.3.3c-d). No differences were found in any other thermogenic genes (Figure 5.3.3e-g). These data suggest that cold-sensitive engram cells control whole-body thermoregulatory responses as reactivation of these engram cells caused an upregulation of certain thermogenesis genes in BAT. Together, these results show that both natural and artificial retrieval of cold memories causes an upregulation of specific thermogenic genes in brown adipocytes.

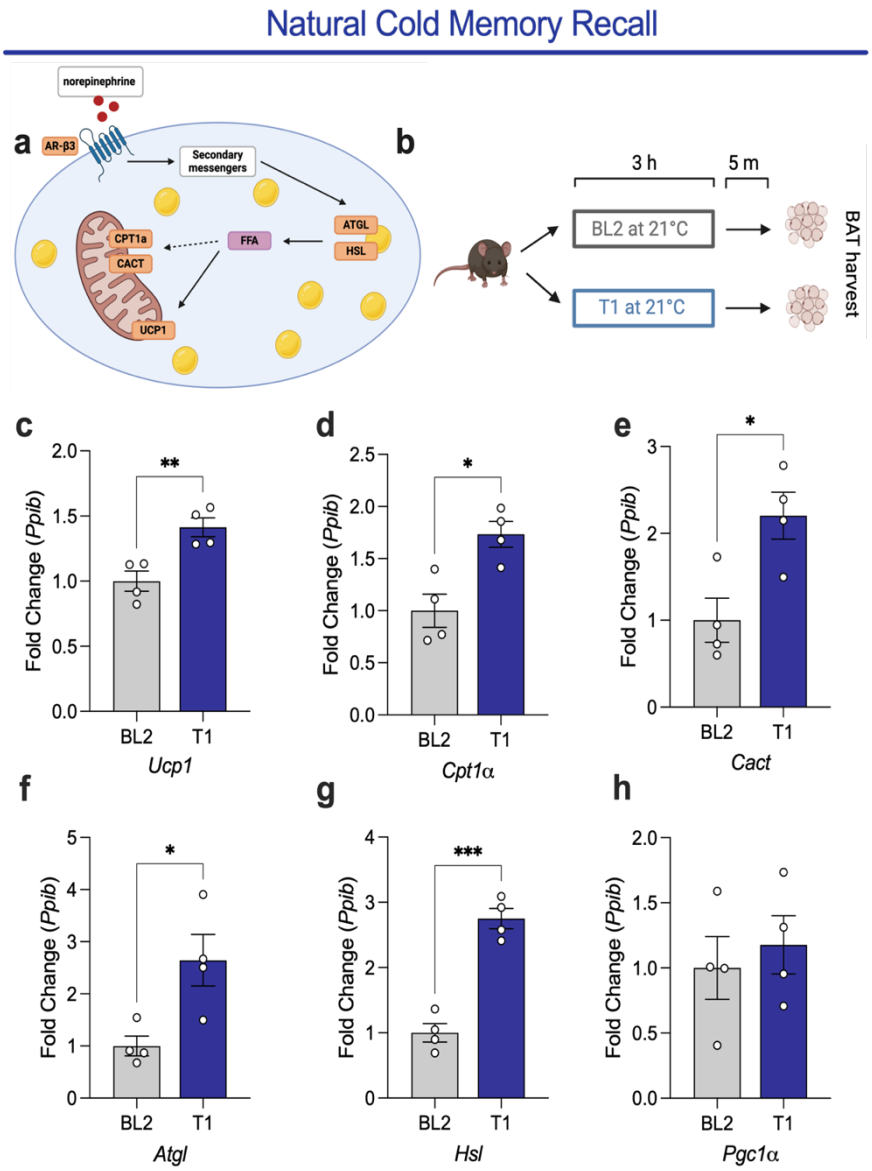

Figure 5.3.2 Natural recall of a cold memory increases lipolytic and thermogenic gene expression in BAT. (a) Diagrammatic representation of the thermogenic pathway in BAT. **(b)** Diagrammatic representation of experimental timeline for tissue collection. Relative expression of lipolysis and thermogenesis genes **(c),** *Ucp1,* **(d),** *Cpt1α,* **(e),** *Cact,* **(f),** *Atgl*, **(g),** *Hsl* and **(h),** *Pgc1α* from the BAT of mice housed during BL2 compared to T1. *n* = 4 mice per group.* p < 0.05, ** p < 0.01, *** p < 0.001. BAT, brown adipose tissue; FFA, free fatty acid; BL2, baseline 2; T1, test 1; h, hour; m, minutes.

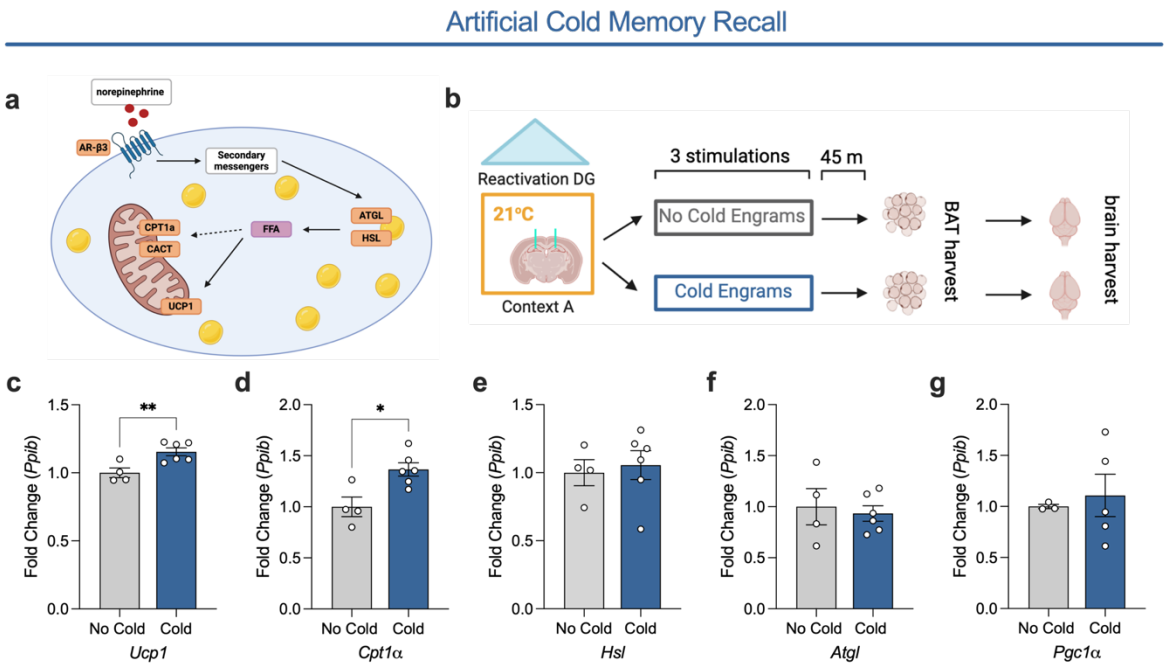

Figure 5.3.3 Artificial reactivation of cold-sensitive memory engrams increases lipolytic and thermogenic gene expression in BAT. (a) Diagrammatic representation of the thermogenic pathway in BAT. **(b)** Diagrammatic representation of optogenetic timeline for cold engram reactivation and tissue collection. Relative expression of lipolysis and thermogenesis genes **(c),** *Ucp1,* **(d),** *Cpt1α,* **(e),** *Hsl,* **(f),** *Atgl*, and **(g),** *Pgc1α* from the BAT of mice with cold-sensitive stimulated cells and no cold control stimulated cells. *n* = 4-6 mice per group.* $p < 0.05$, ** $p < 0.01$. BAT, brown adipose tissue; FFA, free fatty acid; DG, dentate gyrus; m, minutes.

5.3.4 Contextual fear conditioning has no effect on thermogenic genes in BAT.

As previously described, studies have suggested that BAT might be a stress-responsive endocrine organ that is required for an adaptive ‘’fight or flight’’ response. We therefore next asked whether the observed upregulation of thermogenesis genes was specifically due to cold experiences or due to a general stress response. To examine this, we harvested BAT from animals that went through contextual fear conditioning training (Figure 5.3.4a). Here, we compared BAT from animals that received 3 foot shocks with animals that received no foot shocks. Our results showed that there were no differences in any of the examined thermogenesis genes between shocked mice and no shock controls (Figure 5.3.4b-f). Interestingly, we also found no differences in *Il-6* expression between the two groups (Figure 5.3.4g). These results therefore suggest that the previously found increases in thermogenesis genes were not due to a general stress response, as we find that stress caused by fear conditioning does not result in similar increases.

5.3.5 Exposure to a predator odor does not increase thermogenic genes in BAT.

To further confirm that the reported increases in thermogenesis genes were not due to a general ’fight or flight’’ response, we harvested BAT from mice that were exposed to a predator odor (TMT) or to a neutral control odor (H_2O, Figure 5.3.5a). Our results showed that mice exposed to TMT showed no increase in thermogenic gene expression compared to mice that were exposed to H_2O (Figure 5.3.5b-f). Strikingly, we found a significantly decreased expression of *Hsl* in TMT exposed mice compared to H_2O controls (Figure 5.3.5f). Similar to the fear conditioned animals, we found no differences in *Il-6* expression between the two odor groups (Figure 5.3.5g). Together, these experiments showed that thermogenesis genes in BAT are not upregulated due to a stressful experience in general, but that this increase is due to a cold experience specifically.

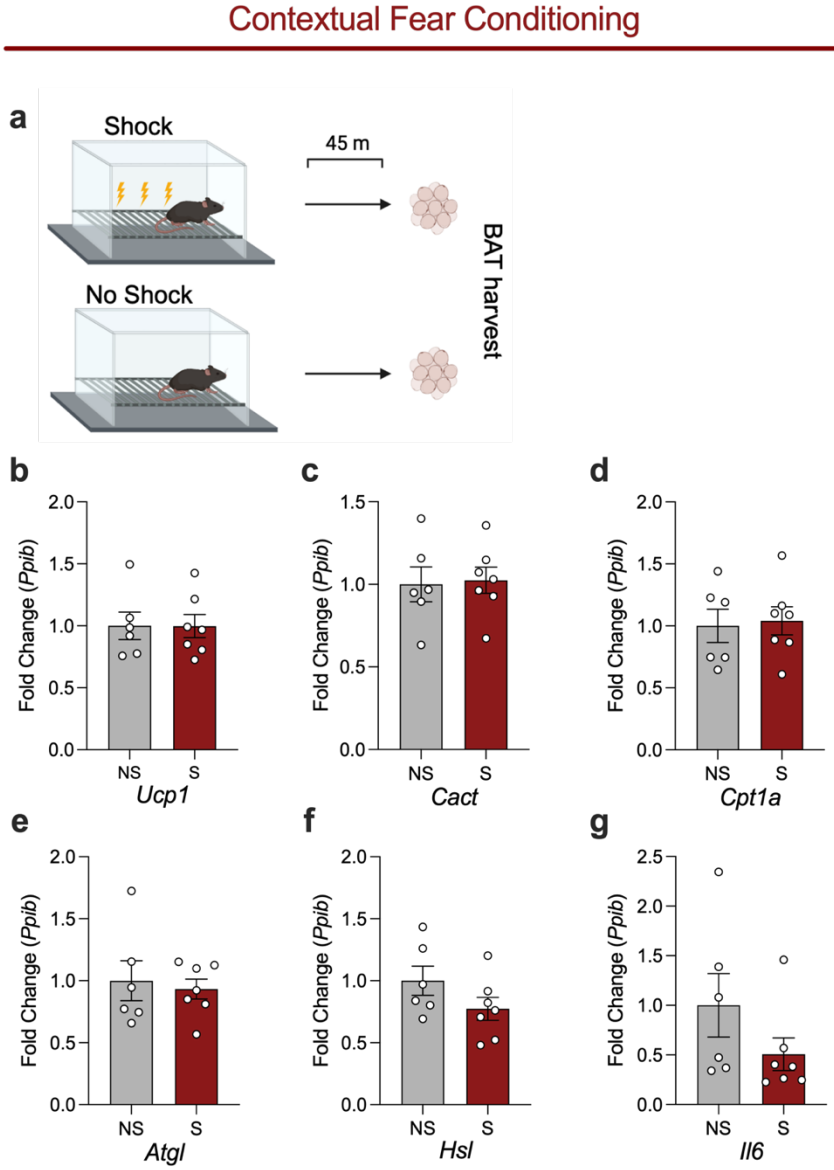

Figure 5.3.4 Contextual fear conditioning does not increase lipolytic and thermogenic gene expression in BAT. (a) Diagrammatic representation of experimental timeline for tissue collection. Relative expression of lipolysis and thermogenesis genes **(b),** *Ucp1,* **(c),** *Cact,* **(d),** *Cpt1α,* **(e),** *Atgl*, **(f),** *Hsl* and **(g),** *Il6* from the BAT of mice that received foot shocks compared to no shock controls. *n* = 6-7 mice per group. BAT, brown adipose tissue; m, minutes; NS, no shock; S, shocked.

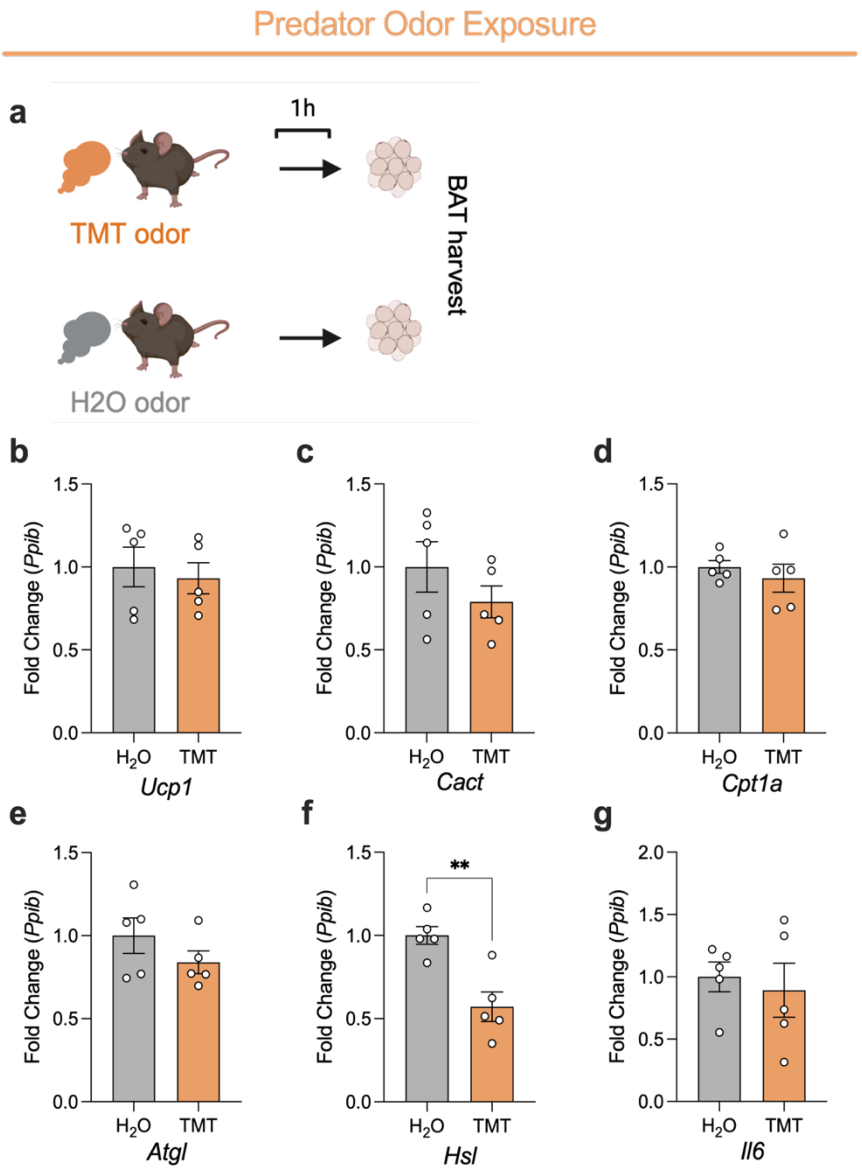

Figure 5.3.5 Predator odor exposure does not increase lipolytic and thermogenic gene expression in BAT. (a) Diagrammatic representation of experimental timeline for tissue collection. Relative expression of lipolysis and thermogenesis genes **(b),** *Ucp1,* **(c),** *Cact,* **(d),** *Cpt1α,* **(e),** *Atgl*, **(f),** *Hsl* and **(g),** *Il6* from the BAT of mice that were exposed to TMT and H_2O exposed controls. *n* = 5 mice per group. TMT, trimethylthiazoline; BAT, brown adipose tissue; h, hour.

DISCUSSION

In this chapter, we aimed to understand whether memories are capable of controlling whole-body metabolic responses. To do so, we leveraged our previously designed behavioral timelines to examine how cold exposure influences thermogenesis in BAT. In line with previous studies, we first showed that innate cold exposure resulted in the upregulation of thermogenesis genes in brown adipocytes. Next, we showed that both natural and artificial retrieval of a contextual cold memory resulted in the upregulation of key thermogenesis genes in BAT. Importantly, we also showed that these increases could not be attributed to a general stress response, as we did not find similar increases in fear conditioned or predator odor exposed mice.

Although clinical studies have shown that memories can have a direct influence on mental state and behavior, it remained unclear whether memories also directly influenced bodily processes. To our knowledge, this is the first study that shows that memories in general, and engrams specifically, control whole-body metabolic responses. Here, we showed that contextual cold memories control metabolic processes in BAT. Although BAT is a key organ involved in thermogenesis, other organs such as the liver and muscle have been shown to contribute to heat generation in cold-exposed rodents [159]. Indeed, the liver is an organ that is important for energy mobilization, providing glucose and packing lipid-rich lipoproteins [160]. Moreover, it has been shown that the liver undergoes a metabolic switch to provide fuel for BAT thermogenesis by producing acylcarnitines [160]. It is likely that in this study we only captured a small fraction of the whole-body response that is triggered by the recall of a cold memory. Future studies are necessary to determine which processes are exactly triggered by the retrieval of a cold memory, in order to fully understand the extent of how engram cells control whole-body responses.

Here, we also showed that by optogenetically reactivating cold-sensitive engrams, we were able to control metabolic processes in BAT. However, we found that only certain thermogenic genes (*Ucp1* and *Cpt1*α) were upregulated. One possible explanation for this is that the optogenetic stimulation protocol used in this study was not long enough to cause an upregulation of lipolysis genes such as *Hsl* and *Atgl*. In contrast, the mitochondrial gene *Cpt1*α might be relying on already circulating lipids to produce fuel

for *Ucp1* to generate heat, considering the role of the liver in generating aclycarnitiens for BAT in cold environments. Additional studies are necessary to determine whether alternative optogenetic reactivation protocols can cause an increase in lipolysis genes, or whether this result holds true regardless of the length of the reactivation period.

In our optogenetic studies, we chose to reactivate cold-sensitive engrams in the DG as we aimed to reactivate contextual cold memories. However, previous studies have shown that the hypothalamus is a key structure that coordinates both the behavioral and autonomic responses that are necessary to maintain homeostasis [64, 148]. Indeed, several hypothalamic regions have also been implicated in the control of thermogenesis in BAT [66]. Based on results from previous chapters, it is likely that the increase in thermogenesis genes in BAT following optogenetic activation of cold-sensitive cells is mediated by hypothalamic regions such as the LHA and the MPO. Indeed, orexigenic neuropeptides have not only been found to be predominantly expressed in the LHA, orexin has also been shown to play a central role in adaptive thermogenesis via its effects on BAT differentiation and function [66, 161]. Future studies are necessary to examine the exact pathway that mediates the increases in BAT genes after optogenetic stimulation of DG cold-sensitive cells. For example, one interesting question that arises is whether the previously observed increases in thermogenesis genes would be absent if one was to chemogenetically inhibit the LHA while simultaneously reactivating cold-sensitive engrams in the DG.

BAT has been found to be a versatile organ that is involved in a variety of metabolic and endocrine processes. Recently it has also been suggested that it might be a stress-responsive organ that is crucial for a ‘’fight or flight’’ response [156, 157]. Here, we show that although BAT could potentially be a stress-responsive organ, the specific genes in the thermogenic pathway studied in this chapter are not uniquely activated by stress. Indeed, our results showed no differences in thermogenic gene expression in fear conditioned or predator odor exposed mice. As such, we showed that these genes are specifically involved in thermoregulatory processes that are activated when an animal is encoding and recalling a cold environment. Together, our data, and previously published data, seem to suggest that different types of stressors elicit different responses from BAT, and that its response is highly dependent on the type of contextual input that it receives.

In this chapter we examined how cold memories in general, and cold-sensitive engrams specifically influenced thermogenic gene expression in brown adipocytes. Taken together, here we showed evidence that both natural and artificial reactivation of a contextual cold memory upregulates thermogenesis genes in BAT. Moreover, it showed that different types of physiological stressors do not increase thermogenesis genes in BAT. As such, this chapter showed additional important evidence that memories can control whole-body metabolic responses that are important for non-shivering thermogenesis.

Overall Discussion

6.1. Cold engrams control whole-body metabolic responses.

In this study, we identified the influence of memory engrams on whole-body responses. We demonstrated that mice increase their metabolic rate and adjust their behavior when recalling a cold environment, indicating that mice can store and recall temperature information (Figure 1). Our findings reveal that the recall of a cold environment increases c-Fos activity in the hippocampus and hypothalamus, which in turn leads to increased functional connectivity between these two structures. We found that cold-sensitive engram cells are located in the DG, LHA and MPO and that artificial reactivation of DG engram cells leads to an increase in whole-body metabolism. Moreover, our results showed that inhibition of cold-sensitive cells in the DG prevents the conditioned whole-body response that was previously associated with cold memories. Notably, our study shows that contextual cold memories control whole-body responses in BAT, by increasing thermogenic genes during cold recall. Together, these data show that cold sensitive engrams control whole-body thermoregulatory responses.

6.2. Engrams are an important part of the body-brain axis.

Many different studies using various methods have shown that complex information is stored in the brain in the form of an engram [162-164]. Indeed, observational studies have provided support for the existence of engrams, whereas gain- and loss-of-function studies have provided evidence that these cells are part of the internal representation of a given experience [15]. Together, these studies have shown that engrams are activated by a learning experience, are physically modified by that learning experience and result in the retrieval of the original memory when reactivated. However, to assess whether reactivation of engram cells results in the retrieval of the original memory, only behavioral measurements such as freezing are typically used as a readout. To our knowledge, this is the first study showing that engrams control more than the traditionally studied behavioral responses. Here, we show that contextual engrams control whole-body metabolic responses, and that remembering a particular event can trigger the bodily processes that were associated with this experience. As such, we provide further evidence that the reactivation of an engram results in the retrieval of the original memory and that both the bodily and behavioral responses associated with that memory are recapitulated.

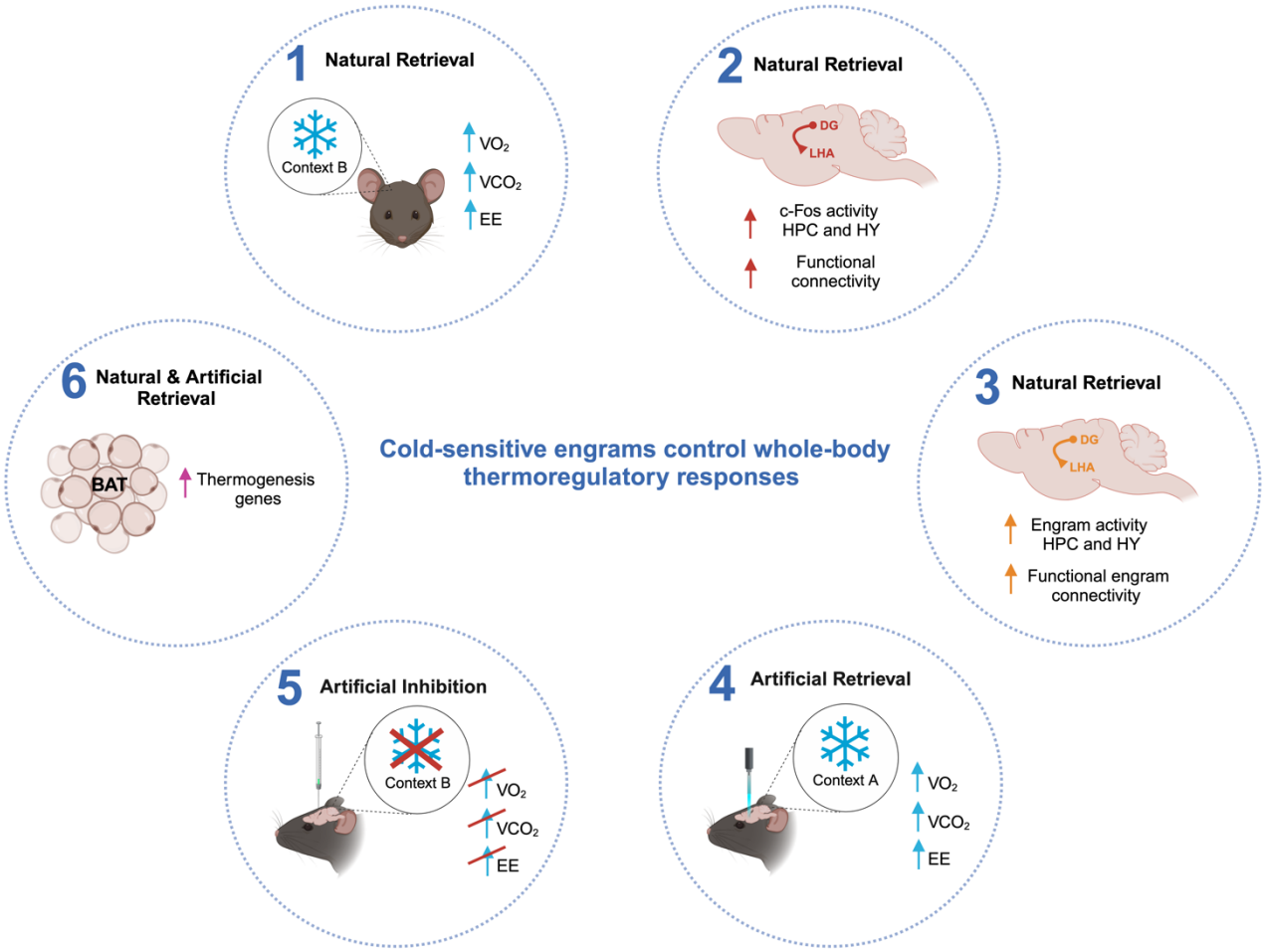

Figure 6.1. Cold-sensitive engrams control whole-body thermoregulatory responses. In this study, we show that natural retrieval of contextual cold memories increases metabolic rates (1), c-Fos activity and connectivity (2), and engram cell activity and connectivity (3). We show that artificial retrieval of a cold memory increases metabolic rates (4), whereas chemogenetic inhibition prevents these increases (5). Finally, we show that natural and artificial retrieval of cold memories increases thermogenesis genes in brown adipocytes (6).

It is plausible that the alterations in bodily responses following the reactivation of engrams are necessary in order for the behavioral responses to follow. For example, when animals retrieve a fear memory, it is likely that bodily responses such as heart rate and adrenaline levels are altered in order for the animal to exhibit the appropriate behavioral response. Indeed, the fight-or-flight response is coined as the immediate physiological reaction that occurs when danger is perceived by an organism. It was originally described by Cannon in 1929 as the neural and physiological mechanisms that are necessary to confront or escape the threat [165]. Based on our results, we hypothesize that memories of salient events can similarly trigger both the neural and

physiological mechanisms that are required for the appropriate behavioral responses to ensue. Evidence supporting this idea comes from clinical data obtained from patients that are diagnosed with PTSD, who re-experience traumatic events in the form of memory flashbacks [166]. These flashbacks are often reported to be accompanied with the physical sensations that were originally experienced during the traumatic event. Therefore, it seems that in these patients, remembering a traumatic event is sufficient to trigger the originally felt bodily sensations, suggesting that memories can indeed trigger whole-body responses.

Our findings support the growing body of evidence which demonstrate that mental state can have an influence on bodily functions in health and disease. Indeed, the rapidly growing field of neuroimmunology has provided increasing evidence on how psychological states can have an impact on physiological processes in the body, and how somatic states can in turn influence the CNS [7, 167]. Here, we showed that engram cells control whole-body thermoregulatory responses, supporting the idea that the brain and the body are interconnected in a reciprocal manner. However, one question that remains is whether bodily responses in turn also have an influence on engram cells specifically and memories in general. For example, it is likely that information not only flows from the brain to the body but also vice-versa. Future studies are necessary to determine how bodily states modulate the storage and formation of memories, and how this relates to engram cells. Moreover, more studies are needed to investigate the bodily responses that are potentially altered by engrams in order to fully understand which processes are under the control of these cells. In the future, this will not only provide us with insights on the impact that memories have during healthy and diseased states, but it will also allow us to identify novel therapeutic targets, in the treatment of psychological disorders or the beneficial effects of positive valence memories.

6.3. Temperature engrams are important for survival.

Previous studies have suggested that animals are capable of learning and remembering temperature information. For example, animals can be trained to adjust their own environment by pressing a bar to receive either a hot or cold air reinforcement [23, 24]. Despite these studies, clear evidence of whether animals form temperature memories was lacking. Moreover, it remained unclear how these types of

memories would be stored and retrieved in the brain. In this study, we report that temperature information is stored in the brain in the form of memories. We show that mice are able to retrieve temperature information regarding a specific environment and adjust their behavior accordingly. Indeed, mice preferred to avoid the cold-paired context when given the choice. To our knowledge, this is the first study that has directly shown that mice are capable of forming memories about the specific temperature of their environment. We hypothesize that the storage of temperature information in the form of memories enables animals to anticipate thermal challenges based on previous experiences. As previously described, thermoregulatory responses can be subdivided into motivated, goal-directed behavioral responses, and autonomic physiological mechanisms. Forming memories regarding the temperature of a given environment would enable animals to adapt their behavioral responses to enhance survivability and allow them to respond in an energy-efficient manner. For example, animals might return to shaded cooler places if they live in an environment with a very hot climate [168]. Although in this study we only focused on cold memories, we hypothesize that animals are also capable of forming memories of a hot environment. Indeed, Osterhout and colleagues showed that sick mice preferred to spend more time in a warmer environment compared to healthy mice [169]. This study suggests that these mice were not only capable of remembering which side of the apparatus was warmer, but that they chose their environment based on their thermoregulatory needs. Finally, our results also provide some insight into how contextual cold memories are stored in the brain. We find that these types of memories are stored in the form of engrams in the hippocampus and hypothalamus, two structures that have been shown to be important for memory and thermoregulation respectively. Additional studies are needed to fully understand how these two structures cooperate in order to orchestrate the wide variety of thermoregulatory responses observed in this study, ideally using viral tracers. Finally, we show here that thermoregulation, an innate type of behavior that all mammals perform, is facilitated by the ability of animals to form context dependent temperature memories. Future studies will be necessary to further examine whether other innate behaviors are also stored in the brain in the form of memories and engram cells.

6.4. The translational value of cold engrams.

The findings described in this study may have important translational implications for potential treatment avenues for metabolic diseases. In humans, BAT has been associated with cardiometabolic health, making it a promising target for future therapies. For example, a recent study showed that pharmacological stimulation of the AR-β3 receptor in BAT in humans resulted in increased metabolic activity in BAT specifically [170]. Humans with more BAT were also shown to have lower prevalence of cardiometabolic diseases, and increased presence of BAT was shown to correlate with lower odds of type-2 diabetes, coronary artery disease, cerebrovascular disease, congestive heart failure and hypertension [171]. Moreover, Stanford and colleagues showed that by transplanting BAT from donor mice into matched recipient mice, they could improve glucose tolerance, insulin sensitivity, body weight and fat mass, and reverse high-fat diet–induced insulin resistance in recipient mice [172]. These studies illustrate that BAT is an important organ that has many implications in a variety of diseases, and therefore is an excellent candidate for novel targeted treatment options in metabolic disease. In this study, we aimed at understanding how the brain affects bodily functions with the ultimate goal of identifying novel therapeutic targets that would enable more targeted treatments for cardiometabolic diseases in the future. For example, here we showed that by stimulating neurons in the brain, we were able to upregulate thermogenesis genes in BAT. With the current technological advancements of optogenetics in humans, this line of research opens interesting avenues for future therapeutic approaches in humans [173].

6.5. Concluding remarks.

In this thesis we tried to illustrate the importance of interdisciplinary research in answering important and contemporary questions in the field of neuroscience. Our study shows that in order to fully understand how the brain functions, it is essential to consider processes happening outside of it. Only by understanding how the brain and the body work in concert, will we be able to identify novel therapeutic targets for the complex and comorbid diseases that are increasingly being diagnosed in our society.

References

1. O'Connor, D.B., J.F. Thayer, and K. Vedhara, *Stress and health: A review of psychobiological processes*. Annual review of psychology, 2021. **72**: p. 663-688.
2. Chan, K.L., et al., *Central regulation of stress-evoked peripheral immune responses*. Nature Reviews Neuroscience, 2023. **24**(10): p. 591-604.
3. Halaris, A., *Inflammation-associated co-morbidity between depression and cardiovascular disease*. Inflammation-associated depression: Evidence, mechanisms and implications, 2017: p. 45-70.
4. Barberio, B., et al., *Prevalence of symptoms of anxiety and depression in patients with inflammatory bowel disease: a systematic review and meta-analysis*. The Lancet Gastroenterology & Hepatology, 2021. **6**(5): p. 359-370.
5. Cathomas, F., et al., *Circulating myeloid-derived MMP8 in stress susceptibility and depression*. Nature, 2024: p. 1-8.
6. Zhu, X., et al., *Somatosensory cortex and central amygdala regulate neuropathic pain-mediated peripheral immune response via vagal projections to the spleen*. Nature Neuroscience, 2024: p. 1-13.
7. Ben-Shaanan, T.L., et al., *Modulation of anti-tumor immunity by the brain's reward system*. Nature communications, 2018. **9**(1): p. 2723.
8. Koren, T., et al., *Insular cortex neurons encode and retrieve specific immune responses*. Cell, 2021. **184**(24): p. 5902-5915. e17.
9. Kayama, T., Y. Ikegaya, and T. Sasaki, *Phasic firing of dopaminergic neurons in the ventral tegmental area triggers peripheral immune responses*. Scientific reports, 2022. **12**(1): p. 1447.
10. Savitz, J. and N.A. Harrison, *Interoception and inflammation in psychiatric disorders*. Biological Psychiatry: Cognitive Neuroscience and Neuroimaging, 2018. **3**(6): p. 514-524.
11. Lange, C.G.E. and W.E. James, *The emotions, Vol. 1*. 1922.
12. Hsueh, B., et al., *Cardiogenic control of affective behavioural state*. Nature, 2023. **615**(7951): p. 292-299.
13. Gentsch, A. and E. Kuehn, *Clinical manifestations of body memories: the impact of past bodily experiences on mental Health*. Brain sciences, 2022. **12**(5): p. 594.
14. Denny, C.A., E. Lebois, and S. Ramirez, *From engrams to pathologies of the brain*. Frontiers in neural circuits, 2017. **11**: p. 23.
15. Josselyn, S.A. and S. Tonegawa, *Memory engrams: Recalling the past and imagining the future*. Science, 2020. **367**(6473): p. eaaw4325.
16. Liu, X., et al., *Optogenetic stimulation of a hippocampal engram activates fear memory recall*. Nature, 2012. **484**(7394): p. 381-385.
17. Ryan, T.J., et al., *Engram cell connectivity: an evolving substrate for information storage*. Current opinion in neurobiology, 2021. **67**: p. 215-225.
18. Morrison, S. and K. Nakamura, *Central mechanisms for thermoregulation*. Annual review of physiology, 2019. **81**: p. 285-308.
19. Liedtke, W.B., *Deconstructing mammalian thermoregulation*. Proceedings of the National Academy of Sciences, 2017. **114**(8): p. 1765-1767.
20. Tan, C.L. and Z.A. Knight, *Regulation of body temperature by the nervous system*. Neuron, 2018. **98**(1): p. 31-48.
21. Fuller, A., R.N. Carter, and D. Mitchell, *Brain and abdominal temperatures at fatigue in rats exercising in the heat*. Journal of Applied Physiology, 1998. **84**(3): p. 877-883.

22. Walters, T., et al., *Exercise in the heat is limited by a critical internal temperature*. Journal of applied physiology, 2000.
23. Jung, S., et al., *A forebrain neural substrate for behavioral thermoregulation*. Neuron, 2022. **110**(2): p. 266-279. e9.
24. Almeida, M.C., R.C.L. Vizin, and D.C. Carrettiero, *Current understanding on the neurophysiology of behavioral thermoregulation*. Temperature, 2015. **2**(4): p. 483-490.
25. Carlton, P.L. and R.A. Marks, *Cold exposure and heat reinforced operant behavior*. Science, 1958. **128**(3335): p. 1344-1344.
26. Terrien, J., M. Perret, and F. Aujard, *Behavioral thermoregulation in mammals: a review*. Frontiers in bioscience, 2011. **16**(4): p. 1428-1444.
27. Morrison, S.F., C.J. Madden, and D. Tupone, *Central neural regulation of brown adipose tissue thermogenesis and energy expenditure*. Cell metabolism, 2014. **19**(5): p. 741-756.
28. Morrison, S.F., C.J. Madden, and D. Tupone, *Central control of brown adipose tissue thermogenesis*. Frontiers in endocrinology, 2012. **3**: p. 17402.
29. Ukropec, J., et al., *UCP1-independent thermogenesis in white adipose tissue of cold-acclimated Ucp1-/-mice*. Journal of Biological Chemistry, 2006. **281**(42): p. 31894-31908.
30. Corrigan, J.K., et al., *A big-data approach to understanding metabolic rate and response to obesity in laboratory mice*. Elife, 2020. **9**: p. e53560.
31. Fischer, A.W., B. Cannon, and J. Nedergaard, *No insulating effect of obesity, neither in mice nor in humans*. American Journal of Physiology-Endocrinology and Metabolism, 2019. **317**(5): p. E952-E953.
32. Bastías-Pérez, M., et al., *Impact of adaptive thermogenesis in mice on the treatment of obesity*. Cells, 2020. **9**(2): p. 316.
33. Ginting, R.P., J.-M. Lee, and M.-W. Lee, *The influence of ambient temperature on adipose tissue homeostasis, metabolic diseases and cancers*. Cells, 2023. **12**(6): p. 881.
34. Celi, F.S., *Human brown adipose tissue plasticity: hormonal and environmental manipulation*. Hormones, metabolism and the benefits of exercise, 2017: p. 1-11.
35. Pavlov, I.P., *Conditioned Reflexes*. 1927.
36. Campo, A., S.C. Nicolis, and J.-L. Deneubourg, *Collective Memory: Transposing Pavlov's Experiment to Robot Swarms*. Applied Sciences, 2021. **11**(6): p. 2632.
37. Kothari, V., et al., *High fat diet induces brain insulin resistance and cognitive impairment in mice*. Biochimica et Biophysica Acta (BBA)-Molecular Basis of Disease, 2017. **1863**(2): p. 499-508.
38. Weir, J.d.V., *New methods for calculating metabolic rate with special reference to protein metabolism*. The Journal of physiology, 1949. **109**(1-2): p. 1.
39. Golden, S.A., et al., *Basal forebrain projections to the lateral habenula modulate aggression reward*. Nature, 2016. **534**(7609): p. 688-692.
40. Cannon, B. and J. Nedergaard, *Brown adipose tissue: function and physiological significance*. Physiological reviews, 2004.
41. Cohen, P. and S. Kajimura, *The cellular and functional complexity of thermogenic fat*. Nature Reviews Molecular Cell Biology, 2021. **22**(6): p. 393-409.

42. Fischer, A.W., B. Cannon, and J. Nedergaard, *Optimal housing temperatures for mice to mimic the thermal environment of humans: an experimental study*. Molecular metabolism, 2018. **7**: p. 161-170.
43. Lal, N.K., et al., *Xiphoid nucleus of the midline thalamus controls cold-induced food seeking*. Nature, 2023. **621**(7977): p. 138-145.
44. Jovanovic, P., et al., *A sex-specific thermogenic neurocircuit induced by predator smell recruiting cholecystokinin neurons in the dorsomedial hypothalamus*. Nature communications, 2023. **14**(1): p. 4937.
45. Minatohara, K., M. Akiyoshi, and H. Okuno, *Role of immediate-early genes in synaptic plasticity and neuronal ensembles underlying the memory trace*. Frontiers in molecular neuroscience, 2016. **8**: p. 78.
46. Cole, A.J., et al., *Rapid increase of an immediate early gene messenger RNA in hippocampal neurons by synaptic NMDA receptor activation*. Nature, 1989. **340**(6233): p. 474-476.
47. Guzowski, J.F., et al., *Environment-specific expression of the immediate-early gene Arc in hippocampal neuronal ensembles*. Nature neuroscience, 1999. **2**(12): p. 1120-1124.
48. Guzowski, J.F., et al., *Experience-dependent gene expression in the rat hippocampus after spatial learning: a comparison of the immediate-early genesArc, c-fos, and zif268*. Journal of Neuroscience, 2001. **21**(14): p. 5089-5098.
49. Sommerlandt, F.M., et al., *Immediate early genes in social insects: a tool to identify brain regions involved in complex behaviors and molecular processes underlying neuroplasticity*. Cellular and molecular life sciences, 2019. **76**: p. 637-651.
50. Lanahan, A. and P. Worley, *Immediate-early genes and synaptic function*. Neurobiology of learning and memory, 1998. **70**(1-2): p. 37-43.
51. Squire, L.R., *Memory and the hippocampus: a synthesis from findings with rats, monkeys, and humans*. Psychological review, 1992. **99**(2): p. 195.
52. Rolls, E.T., *A theory of hippocampal function in memory*. Hippocampus, 1996. **6**(6): p. 601-620.
53. Mancini, A., et al., *Hippocampal neuroplasticity and inflammation: relevance for multiple sclerosis*. Multiple Sclerosis and Demyelinating Disorders, 2017. **2**: p. 1-12.
54. Voss, J.L., et al., *A closer look at the hippocampus and memory*. Trends in cognitive sciences, 2017. **21**(8): p. 577-588.
55. Knierim, J.J., *The hippocampus*. Current Biology, 2015. **25**(23): p. R1116-R1121.
56. Eichenbaum, H., *The role of the hippocampus in navigation is memory*. Journal of neurophysiology, 2017. **117**(4): p. 1785-1796.
57. Preston, A.R. and H. Eichenbaum, *Interplay of hippocampus and prefrontal cortex in memory*. Current biology, 2013. **23**(17): p. R764-R773.
58. Hammel, H., J. Hardy, and M. Fusco, *Thermoregulatory responses to hypothalamic cooling in unanesthetized dogs*. American Journal of Physiology-Legacy Content, 1960. **198**(3): p. 481-486.
59. Wang, T.A., et al., *Thermoregulation via temperature-dependent PGD2 production in mouse preoptic area*. Neuron, 2019. **103**(2): p. 309-322. e7.
60. Almeida, M.C., et al., *Neural substrate of cold-seeking behavior in endotoxin shock*. PloS one, 2006. **1**(1): p. e1.

61. Schulze, G., M. Tetzner, and H. Topolinski, *Operant thermoregulation of rats with anterior hypothalamic lesions*. Naunyn-Schmiedeberg's Archives of Pharmacology, 1981. **318**: p. 43-48.
62. Madden, C.J. and S.F. Morrison, *Excitatory amino acid receptors in the dorsomedial hypothalamus mediate prostaglandin-evoked thermogenesis in brown adipose tissue*. American Journal of Physiology-Regulatory, Integrative and Comparative Physiology, 2004. **286**(2): p. R320-R325.
63. Cao, W.-H., W. Fan, and S. Morrison, *Medullary pathways mediating specific sympathetic responses to activation of dorsomedial hypothalamus*. Neuroscience, 2004. **126**(1): p. 229-240.
64. Piñol, R.A., et al., *B rs3 neurons in the mouse dorsomedial hypothalamus regulate body temperature, energy expenditure, and heart rate, but not food intake*. Nature neuroscience, 2018. **21**(11): p. 1530-1540.
65. Rossi, M.A., *Control of energy homeostasis by the lateral hypothalamic area*. Trends in neurosciences, 2023.
66. Contreras, C., et al., *Traveling from the hypothalamus to the adipose tissue: the thermogenic pathway*. Redox biology, 2017. **12**: p. 854-863.
67. McGaugh, J.L., *Searching for memory in the brain: Confronting the collusion of cells and systems*. Neural Plasticity and Memory: From Genes to Brain Imaging, F. Bermudez-Rattoni, ed.(CRC Press), 2007: p. 1-13.
68. Varshney, L.R., et al., *Structural properties of the Caenorhabditis elegans neuronal network*. PLoS computational biology, 2011. **7**(2): p. e1001066.
69. Oh, S.W., et al., *A mesoscale connectome of the mouse brain*. Nature, 2014. **508**(7495): p. 207-214.
70. Chiang, A.-S., et al., *Three-dimensional reconstruction of brain-wide wiring networks in Drosophila at single-cell resolution*. Current biology, 2011. **21**(1): p. 1-11.
71. Bargmann, C.I. and E. Marder, *From the connectome to brain function*. Nature methods, 2013. **10**(6): p. 483-490.
72. Vetere, G., et al., *Chemogenetic interrogation of a brain-wide fear memory network in mice*. Neuron, 2017. **94**(2): p. 363-374. e4.
73. Dorst, K.E., et al., *Hippocampal engrams generate variable behavioral responses and brain-wide network states*. Journal of Neuroscience, 2024. **44**(2).
74. Santos, S.L., et al., *Propranolol decreases fear expression by modulating fear memory traces*. Biological psychiatry, 2021. **89**(12): p. 1150-1161.
75. Roy, D.S., et al., *Brain-wide mapping reveals that engrams for a single memory are distributed across multiple brain regions*. Nature communications, 2022. **13**(1): p. 1799.
76. Renier, N., et al., *iDISCO: a simple, rapid method to immunolabel large tissue samples for volume imaging*. Cell, 2014. **159**(4): p. 896-910.
77. Chung, K. and K. Deisseroth, *CLARITY for mapping the nervous system*. Nature methods, 2013. **10**(6): p. 508-513.
78. Susaki, E.A., et al., *Advanced CUBIC protocols for whole-brain and whole-body clearing and imaging*. Nature protocols, 2015. **10**(11): p. 1709-1727.
79. Tian, T., Z. Yang, and X. Li, *Tissue clearing technique: Recent progress and biomedical applications*. Journal of anatomy, 2021. **238**(2): p. 489-507.

80. Pavlova, I.P., et al., *Optimization of immunolabeling and clearing techniques for indelibly labeled memory traces*. Hippocampus, 2018. **28**(7): p. 523-535.
81. Tappan, S.J., et al., *Automatic navigation system for the mouse brain*. Journal of Comparative Neurology, 2019. **527**(13): p. 2200-2211.
82. Morrison, S.F. and K. Nakamura, *Central neural pathways for thermoregulation*. Frontiers in bioscience: a journal and virtual library, 2011. **16**: p. 74.
83. Milenkovic, N., et al., *A somatosensory circuit for cooling perception in mice*. Nature neuroscience, 2014. **17**(11): p. 1560-1566.
84. Roozendaal, B., B.S. McEwen, and S. Chattarji, *Stress, memory and the amygdala*. Nature Reviews Neuroscience, 2009. **10**(6): p. 423-433.
85. Walker, D.L., D.J. Toufexis, and M. Davis, *Role of the bed nucleus of the stria terminalis versus the amygdala in fear, stress, and anxiety*. European journal of pharmacology, 2003. **463**(1-3): p. 199-216.
86. Stackmann, M., et al., *A multiple Arc (mArc) tagging system to uncover the organizational principles of multiple memories*. bioRxiv, 2024: p. 2024.02. 01.578410.
87. Kesner, R.P., *A behavioral analysis of dentate gyrus function*. Progress in brain research, 2007. **163**: p. 567-576.
88. Morris, A.M., et al., *The role of the dentate gyrus in the formation of contextual representations*. Hippocampus, 2013. **23**(2): p. 162-168.
89. Hainmueller, T. and M. Bartos, *Dentate gyrus circuits for encoding, retrieval and discrimination of episodic memories*. Nature Reviews Neuroscience, 2020. **21**(3): p. 153-168.
90. Bachtell, R.K., N.O. Tsivkovskaia, and A.E. Ryabinin, *Identification of temperature-sensitive neural circuits in mice using c-Fos expression mapping*. Brain research, 2003. **960**(1-2): p. 157-164.
91. Berthoud, H.-R. and H. Münzberg, *The lateral hypothalamus as integrator of metabolic and environmental needs: from electrical self-stimulation to opto-genetics*. Physiology & behavior, 2011. **104**(1): p. 29-39.
92. Burdakov, D., M.M. Karnani, and A. Gonzalez, *Lateral hypothalamus as a sensor-regulator in respiratory and metabolic control*. Physiology & behavior, 2013. **121**: p. 117-124.
93. Birklein, F., R. Rolke, and W. Müller-Forell, *Isolated insular infarction eliminates contralateral cold, cold pain, and pinprick perception*. Neurology, 2005. **65**(9): p. 1381-1381.
94. Rodgers, K.M., et al., *Auditory, somatosensory, and multisensory insular cortex in the rat*. Cerebral cortex, 2008. **18**(12): p. 2941-2951.
95. Vestergaard, M., et al., *The cellular coding of temperature in the mammalian cortex*. Nature, 2023. **614**(7949): p. 725-731.
96. Squire, L.R., *Memory and brain systems: 1969–2009*. Journal of Neuroscience, 2009. **29**(41): p. 12711-12716.
97. James, W., *The principles of psychology*. Vol. 1. 2007: Cosimo, Inc.
98. Semon, R.W., *Die Mneme als erhaltendes Prinzip im Wechsel des organischen Geschehens*. 1911: Engelmann.
99. Schacter, D., J. Eich, and E. Tulving, *Richard Semon's theory of memory. J. Verbal Learn. Verbal Behav. 17, 721–743*. 1978.

100. Lashley, K.S., *Brain mechanisms and intelligence: A quantitative study of injuries to the brain*. 1929.
101. Lashley, K.S., *Mass action in cerebral function.* Science, 1931. **73**(1888): p. 245-254.
102. Nadel, L. and A. Maurer, *Recalling lashley and reconsolidating hebb.* Hippocampus, 2020. **30**(8): p. 776-793.
103. Lashley, K.S., *In search of the engram*. 1950.
104. Hebb, D.O., *The organization of behavior: A neuropsychological theory*. 2005: Psychology press.
105. Penfield, W. and T. Rasmussen, *The cerebral cortex of man; a clinical study of localization of function*. 1950.
106. Squire, L.R., *Memory systems of the brain: a brief history and current perspective.* Neurobiology of learning and memory, 2004. **82**(3): p. 171-177.
107. Tonegawa, S., et al., *Memory engram cells have come of age.* Neuron, 2015. **87**(5): p. 918-931.
108. Tonegawa, S., et al., *Memory engram storage and retrieval.* Current opinion in neurobiology, 2015. **35**: p. 101-109.
109. Reijmers, L.G., et al., *Localization of a stable neural correlate of associative memory.* Science, 2007. **317**(5842): p. 1230-1233.
110. Denny, C.A., et al., *Hippocampal memory traces are differentially modulated by experience, time, and adult neurogenesis.* Neuron, 2014. **83**(1): p. 189-201.
111. DeNardo, L.A., et al., *Temporal evolution of cortical ensembles promoting remote memory retrieval.* Nature neuroscience, 2019. **22**(3): p. 460-469.
112. Trouche, S., et al., *Fear extinction causes target-specific remodeling of perisomatic inhibitory synapses.* Neuron, 2013. **80**(4): p. 1054-1065.
113. Lacagnina, A.F., et al., *Distinct hippocampal engrams control extinction and relapse of fear memory.* Nature neuroscience, 2019. **22**(5): p. 753-761.
114. O'Leary, J.D., et al., *Natural forgetting reversibly modulates engram expression.* eLife, 2023. **12**.
115. Cowansage, K.K., et al., *Direct reactivation of a coherent neocortical memory of context.* Neuron, 2014. **84**(2): p. 432-441.
116. Redondo, R.L., et al., *Bidirectional switch of the valence associated with a hippocampal contextual memory engram.* Nature, 2014. **513**(7518): p. 426-430.
117. Power, S.D., et al., *Immune activation state modulates infant engram expression across development.* Science Advances, 2023. **9**(45): p. eadg9921.
118. Ryan, T.J., et al., *Engram cells retain memory under retrograde amnesia.* Science, 2015. **348**(6238): p. 1007-1013.
119. Roy, D.S., et al., *Memory retrieval by activating engram cells in mouse models of early Alzheimer's disease.* Nature, 2016. **531**(7595): p. 508-512.
120. Tanaka, K.Z., et al., *Cortical representations are reinstated by the hippocampus during memory retrieval.* Neuron, 2014. **84**(2): p. 347-354.
121. Hsiang, H.-L.L., et al., *Manipulating a "cocaine engram" in mice.* Journal of Neuroscience, 2014. **34**(42): p. 14115-14127.
122. DeNardo, L. and L. Luo, *Genetic strategies to access activated neurons.* Current opinion in neurobiology, 2017. **45**: p. 121-129.
123. Sørensen, A.T., et al., *A robust activity marking system for exploring active neuronal ensembles.* Elife, 2016. **5**: p. e13918.

124. Kawashima, T., et al., *Functional labeling of neurons and their projections using the synthetic activity–dependent promoter E-SARE*. Nature methods, 2013. **10**(9): p. 889-895.
125. Srinivas, S., et al., *Cre reporter strains produced by targeted insertion of EYFP and ECFP into the ROSA26 locus*. BMC developmental biology, 2001. **1**: p. 1-8.
126. Allen, W.E., et al., *Thirst-associated preoptic neurons encode an aversive motivational drive*. Science, 2017. **357**(6356): p. 1149-1155.
127. Schindelin, J., et al., *Fiji: an open-source platform for biological-image analysis*. Nature methods, 2012. **9**(7): p. 676-682.
128. Ramirez, S., et al., *Creating a false memory in the hippocampus*. Science, 2013. **341**(6144): p. 387-391.
129. Crick, F.H., *Thinking about the brain*. Scientific American, 1979. **241**(3): p. 219-233.
130. Oesterhelt, D. and W. Stoeckenius, *Rhodopsin-like protein from the purple membrane of Halobacterium halobium*. Nature new biology, 1971. **233**(39): p. 149-152.
131. Nagel, G., et al., *Channelrhodopsin-1: a light-gated proton channel in green algae*. Science, 2002. **296**(5577): p. 2395-2398.
132. Matsuno-Yagi, A. and Y. Mukohata, *Two possible roles of bacteriorhodopsin; a comparative study of strains of Halobacterium halobium differing in pigmentation*. Biochemical and biophysical research communications, 1977. **78**(1): p. 237-243.
133. Deisseroth, K., *Controlling the brain with light*. Scientific American, 2010. **303**(5): p. 48-55.
134. Boyden, E.S., et al., *Millisecond-timescale, genetically targeted optical control of neural activity*. Nature neuroscience, 2005. **8**(9): p. 1263-1268.
135. Tsai, H.-C., et al., *Phasic firing in dopaminergic neurons is sufficient for behavioral conditioning*. Science, 2009. **324**(5930): p. 1080-1084.
136. Aston-Jones, G. and K. Deisseroth, *Recent advances in optogenetics and pharmacogenetics*. Brain research, 2013. **1511**: p. 1-5.
137. Goshen, I., et al., *Dynamics of retrieval strategies for remote memories*. Cell, 2011. **147**(3): p. 678-689.
138. Liu, X., et al. *Identification and manipulation of memory engram cells*. in *Cold Spring Harbor symposia on quantitative biology*. 2014. Cold Spring Harbor Laboratory Press.
139. Okuyama, T., et al., *Ventral CA1 neurons store social memory*. Science, 2016. **353**(6307): p. 1536-1541.
140. Zhou, Y., et al., *A ventral CA1 to nucleus accumbens core engram circuit mediates conditioned place preference for cocaine*. Nature neuroscience, 2019. **22**(12): p. 1986-1999.
141. Efimov, A.I., et al., *Remote optogenetic control of the enteric nervous system and brain-gut axis in freely-behaving mice enabled by a wireless, battery-free optoelectronic device*. Biosensors and Bioelectronics, 2024. **258**: p. 116298.
142. Tajima, K., et al., *Wireless optogenetics protects against obesity via stimulation of non-canonical fat thermogenesis*. Nature communications, 2020. **11**(1): p. 1730.
143. Montgomery, K.L., et al., *Beyond the brain: Optogenetic control in the spinal cord and peripheral nervous system*. Science translational medicine, 2016. **8**(337): p. 337rv5-337rv5.

144. Roth, B.L., *DREADDs for neuroscientists*. Neuron, 2016. **89**(4): p. 683-694.
145. Armbruster, B.N., et al., *Evolving the lock to fit the key to create a family of G protein-coupled receptors potently activated by an inert ligand*. Proceedings of the National Academy of Sciences, 2007. **104**(12): p. 5163-5168.
146. Park, S., et al., *Neuronal allocation to a hippocampal engram*. Neuropsychopharmacology, 2016. **41**(13): p. 2987-2993.
147. Giannotti, G., et al., *Prefrontal cortex neuronal ensembles encoding fear drive fear expression during long-term memory retrieval*. Scientific reports, 2019. **9**(1): p. 10709.
148. Piñol, R.A., et al., *Preoptic BRS3 neurons increase body temperature and heart rate via multiple pathways*. Cell metabolism, 2021. **33**(7): p. 1389-1403. e6.
149. Madisen, L., et al., *A toolbox of Cre-dependent optogenetic transgenic mice for light-induced activation and silencing*. Nature neuroscience, 2012. **15**(5): p. 793-802.
150. Rosen, E.D. and B.M. Spiegelman, *What we talk about when we talk about fat*. Cell, 2014. **156**(1): p. 20-44.
151. Torres Irizarry, V.C., et al., *Hypothalamic estrogen signaling and adipose tissue metabolism in energy homeostasis*. Frontiers in Endocrinology, 2022. **13**: p. 898139.
152. Cypess, A.M., et al., *Identification and importance of brown adipose tissue in adult humans*. New England journal of medicine, 2009. **360**(15): p. 1509-1517.
153. Foster, D.O. and M.L. Frydman, *Tissue distribution of cold-induced thermogenesis in conscious warm-or cold-acclimated rats reevaluated from changes in tissue blood flow: the dominant role of brown adipose tissue in the replacement of shivering by nonshivering thermogenesis*. Canadian journal of physiology and pharmacology, 1979. **57**(3): p. 257-270.
154. Li, Y., et al., *The molecular brakes of adipose tissue lipolysis*. Frontiers in physiology, 2022. **13**: p. 826314.
155. Ricquier, D., *UCP1, the mitochondrial uncoupling protein of brown adipocyte: a personal contribution and a historical perspective*. Biochimie, 2017. **134**: p. 3-8.
156. Kataoka, N., et al., *Psychological stress activates a dorsomedial hypothalamus-medullary raphe circuit driving brown adipose tissue thermogenesis and hyperthermia*. Cell metabolism, 2014. **20**(2): p. 346-358.
157. Qing, H., et al., *Origin and function of stress-induced IL-6 in murine models*. Cell, 2020. **182**(2): p. 372-387. e14.
158. Root, C.M., et al., *The participation of cortical amygdala in innate, odour-driven behaviour*. Nature, 2014. **515**(7526): p. 269-273.
159. Abumrad, N.A., *The liver as a hub in thermogenesis*. Cell metabolism, 2017. **26**(3): p. 454-455.
160. Simcox, J., et al., *Global analysis of plasma lipids identifies liver-derived acylcarnitines as a fuel source for brown fat thermogenesis*. Cell metabolism, 2017. **26**(3): p. 509-522. e6.
161. Sellayah, D., P. Bharaj, and D. Sikder, *Orexin is required for brown adipose tissue development, differentiation, and function*. Cell metabolism, 2011. **14**(4): p. 478-490.

162. Ortega-de San Luis, C., et al., *Engram cell connectivity as a mechanism for information encoding and memory function*. Current Biology, 2023. **33**(24): p. 5368-5380. e5.
163. Autore, L., et al., *Adaptive expression of engrams by retroactive interference*. Cell reports, 2023. **42**(8).
164. Suthard, R.L., et al., *Engram reactivation mimics cellular signatures of fear*. Cell Reports, 2024. **43**(3).
165. Cannon, W.B., *Bodily changes in pain, hunger, fear, and rage, ed2*. Boston, CH Branford, 1953: p. 20-36.
166. North, C.S., et al., *The evolution of PTSD criteria across editions of DSM*. , 28, 3, 2016. **28**(3): p. 197-208.
167. Haykin, H., et al., *Reward system activation improves recovery from acute myocardial infarction*. Nature Cardiovascular Research, 2024: p. 1-16.
168. Mota-Rojas, D., et al., *Physiological and behavioral mechanisms of thermoregulation in mammals*. Animals, 2021. **11**(6): p. 1733.
169. Osterhout, J.A., et al., *A preoptic neuronal population controls fever and appetite during sickness*. Nature, 2022. **606**(7916): p. 937-944.
170. Cypess, A.M., et al., *Activation of human brown adipose tissue by a β3-adrenergic receptor agonist*. Cell metabolism, 2015. **21**(1): p. 33-38.
171. Becher, T., et al., *Brown adipose tissue is associated with cardiometabolic health*. Nature medicine, 2021. **27**(1): p. 58-65.
172. Stanford, K.I., et al., *Brown adipose tissue regulates glucose homeostasis and insulin sensitivity*. The Journal of clinical investigation, 2012. **123**(1).
173. Harris, A.R. and F. Gilbert, *Restoring vision using optogenetics without being blind to the risks*. Graefe's Archive for Clinical and Experimental Ophthalmology, 2022. **260**(1): p. 41-45.